ISSN 0915-633X

NATIONAL INSTITUTE FOR FUSION SCIENCE

Wrap, Tilt and Stretch of Vorticity Lines around a Strong Straight Vortex Tube in a Simple Shear Flow

G. Kawahara, S. Kida, M. Tanaka and S. Yanase

(Received - Sep.20, 1996)

NIFS-456 Oct. 1996

RESEARCH REPORT
NIFS Series

NAGOYA, JAPAN

Wrap, Tilt and Stretch of Vorticity Lines around a Strong Straight Vortex Tube in a Simple Shear Flow

By GENTA KAWAHARA[1], SHIGEO KIDA[2], MITSURU TANAKA[3] AND SHINICHIRO YANASE[4]

[1] Department of Mechanical Engineering, Ehime University

Matsuyama 790–77, Japan

[2] Theory and Simulation Center, National Institute for Fusion Science

Nagoya 464–01, Japan

[3] Department of Mechanical and System Engineering, Kyoto Institute of Technology

Kyoto 606, Japan

[4] Department of Engineering Sciences, Okayama University

Okayama 700, Japan

Abstract

The mechanism of wrap, tilt and stretch of vorticity lines around a strong straight vortex tube with circulation Γ in a simple shear flow ($\boldsymbol{U} = SX_2\widehat{\boldsymbol{X}}_1$, S being a shear rate) is investigated analytically. An asymptotic expression of the vorticity field is obtained at a large Reynolds number $\Gamma/\nu \gg 1$, ν being the kinematic viscosity of fluid, and during the initial time $S\,t \ll 1$ of evolution as well as $S\,t \ll (\Gamma/\nu)^{\frac{1}{2}}$. The vortex tube, which is inclined from the streamwise (X_1) direction both to the vertical (X_2) and spanwise (X_3) directions, is tilted, stretched and diffused under the action of the uniform shear and viscosity. The simple shear vorticity is, on the other hand, wrapped and stretched around the vortex tube by a swirling motion induced by it to form two spiral vortex layers of high normal vorticity. The magnitude of the normal vorticity increases up to $O\left((\Gamma/\nu)^{\frac{1}{3}}S\right)$ at distance $r = O\left((\Gamma/\nu)^{\frac{1}{3}}(\nu t)^{\frac{1}{2}}\right)$ apart from the vortex tube. The spirals induce axial flows of the same spiral shape with alternate sign in adjacent spirals which in turn tilt the simple shear vorticity toward the axial direction. As a result, the vorticity lines wind helically around the vortex tube accompanied with conversion of vorticity of the simple shear to the axial direction. The axial vorticity increases in time as S^2t, the direction of which is opposite to that of the vortex tube at $r = O\left((\Gamma/\nu)^{\frac{1}{2}}(\nu t)^{\frac{1}{2}}\right)$ where the magnitude is strongest. In the near region $r \lesssim (\Gamma/\nu)^{\frac{1}{4}}(\nu t)^{\frac{1}{2}}$, on the other hand, a viscous cancellation takes place in tightly wrapped vorticity of alternate sign, which leads to the disappearance of the normal vorticity. Only the axial component of the simple shear vorticity is left there which is stretched by the simple shear flow itself. As a consequence, the vortex tube inclined toward the direction of the simple shear vorticity (a cyclonic vortex) is intensified, while the one oriented to the opposite direction (an anti-cyclonic vortex) is weakened. The growth rate of vorticity due to this effect attains a maximum (or minimum) value of $\pm S^2/3^{\frac{3}{2}}$ when the

vortex tube is oriented to the direction of $\widehat{\boldsymbol{X}}_1 + \widehat{\boldsymbol{X}}_2 \mp \widehat{\boldsymbol{X}}_3$. The present asymptotic solutions are expected to be closely related to the flow structures around intense vortex tubes observed in various kinds of turbulence such as helically winding of vorticity lines around a vortex tube, the dominance of cyclonic vortex tubes, the appearance of opposite-signed vorticity around streamwise vortices and a zig-zag arrangement of streamwise vortices in homogeneous isotropic turbulence, homogeneous shear turbulence and near-wall turbulence.

1. Introduction

Tube-like vortical structures of concentrated high vorticity have been commonly observed in many turbulent flow fields. In homogeneous isotropic turbulence, there exist strong coherent elongated vortices in a weaker background vorticity, and a relatively large portion of turbulence kinetic energy is dissipated around them (Siggia 1981; Kerr 1985; Hosokawa & Yamamoto 1989; She, Jackson & Orszag 1990; Ruetsch & Maxey 1991; Vincent & Meneguzzi 1991; Douady, Couder & Brachet 1991; Kida & Ohkitani 1992; Jiménez *et al.* 1993; Kida 1993). In homogeneous shear turbulence, Kida & Tanaka (1992, 1994) showed the presence of longitudinal vortex tubes which induce an intense Reynolds shear stress, and clarified their generation and development processes. In near-wall turbulence, it was found that streamwise vortex tubes play a central role in the production of turbulence kinetic energy (Robinson, Kline & Spalart 1988; Brooke & Hanratty 1993; Bernard, Thomas & Handler 1993). In near-wall turbulence streamwise vortices are closely related to the generation of high skin-friction (Choi, Moin & Kim 1993; Kravchenko, Choi & Moin 1993). Another example of tube-like concentrated vortices is libs observed in a turbulent mixing layer (see Hussain 1986). These observations make us to believe that tube-like vortices may be one of the key ingredients of coherent structures which give a significant contribution to the production and dissipation of turbulence kinetic energy. They are also expected to control heat, mass and momentum transfers. Clarification of the dynamics of vortex tubes would lead to a new concept useful for understanding and controlling turbulence phenomena.

In time-evolution of tube-like structures their interactions with a background turbulence field are considered to play a significant role. It is understood at least conceptually that

a background turbulence stretches and rotates vortex tubes as well as deforms their shape and that the vortex tubes, on the other hand, wrap and stretch the background vorticity lines. We must admit, however, that the knowledge of the actual dynamical process in these interactions is still poor. There have been a lot of efforts devoted to this subject. Moore (1985) investigated dynamics of a diffusing straight vortex tube perfectly aligned with a simple shear flow. He derived a large-Reynolds-number asymptotic solution to show that excessive vorticity wrapping enhances viscous cancellation to expell the shear flow vorticity near the vortex tube. In their asymptotic analysis of a strong vortex tube subjected to a uniform non-axisymmetric irrotational strain, Moffatt, Kida & Ohkitani (1994) found that at large Reynolds numbers, a stretched vortex tube can survive for a long time even when two of the principal rates of strain are positive. Recently, Jiménez, Moffatt & Vasco (1996) applied Moffatt, Kida & Ohkitani's (1994) asymptotic theory to dynamics of a two-dimensional diffusing vortex tube in an imposed weak strain. They showed a good agreement between the results of their theory and a numerical simulation of two-dimensional turbulence.

In this paper, we study vorticity dynamics, especially vortex wrapping, tilting and stretching, around a strong straight vortex tube in a simple shear flow ($\boldsymbol{U} = SX_2\widehat{\boldsymbol{X}}_1$, S being a shear rate). A vortex filament of circulation Γ is set at an initial instant being inclined from the streamwise (X_1) direction both to the vertical (X_2) and spanwise (X_3) directions. The vortex filament is tilted, stretched and diffused under the action of the uniform shear and viscosity. An asymptotic analysis is performed at a large Reynolds number $\Gamma/\nu \gg 1$, ν being the kinematic viscosity of fluid, and at the initial time $St \ll 1$ of evolution. The problem to be considered here includes the ones treated by Moore (1985) and by Jiménez, Moffatt & Vasco (1996) as special cases.

In §2, we derive the equations of motion of a vortex tube in a simple shear flow in a coordinate system rotating with the central axis of the vortex tube under the assumption that the vorticity and induced velocity of the vortex tube are uniform along its axis. Asymptotic solutions are presented for $\Gamma/\nu \gg 1$ and $St \ll 1$ by extending Moore's (1985) and Moffatt, Kida & Ohkitani's (1994) methods in §3 (details of analysis for higher order are described in Appendices A and B). In §4, we provide a physical interpretation of the asymptotic solutions to explore structures of the vorticity field. Section 5 is devoted to concluding remarks. The main symbols to be employed in this paper are listed in Table 1.

2. Formulation

We consider the motion of a straight vortex tube in a simple shear flow with uniform pressure P (see figure 1). Let the coordinate system $OX_1X_2X_3$ be at rest, the X_1-axis being aligned with the shear flow direction. The uniform shear velocity $\boldsymbol{U}$ is taken to depend only on X_2, i.e., $\boldsymbol{U} = SX_2\widehat{\boldsymbol{X}}_1$, where $S\,(>0)$ denotes the shear rate, which is constant in time, and $\widehat{\boldsymbol{X}}_i$ is the unit vector in the X_i-direction $(i = 1, 2, 3)$. In this configuration the uniform shear vorticity is given by $\nabla \times \boldsymbol{U} = -S\widehat{\boldsymbol{X}}_3$, which is anti-parallel to the X_3-axis. Hereafter, we call X_1, X_2 and X_3 the streamwise, the vertical and the spanwise coordinates, respectively.

The vortex tube is inclined both vertically and horizontally from the streamwise direction. It will be tilted and stretched by the uniform shear. The origin O is located on the central axis of the vortex tube, so that it is a stagnation point of the flow. We suppose that the vortex tube is of infinite extent, and its vorticity and induced velocity are uniform along its axis.

2.1. *Structural coordinate system*

We formulate the problem in a rotating coordinate system $Ox_1x_2x_3$ as shown in figure 2. Rotating the stationary coordinate system $OX_1X_2X_3$ by an angle of β around the X_1-axis, we set the new X_3-direction as the x_3-axis. Next, we further rotate $OX_1X_2X_3$ by an angle of α around the x_3-axis (new X_3-axis), and then the new X_1- and X_2-directions are set as the x_1- and x_2-coordinates, respectively. Rotation angles, α and β, are taken so that the resulting x_1-axis may coincide with the central axis of the vortex tube. The vorticity of the vortex tube is taken to be pointed to the positive x_1-direction. Hereafter, we call $Ox_1x_2x_3$ the structural coordinate system, x_1 the axial coordinate and (x_2, x_3) the normal plane. Flow symmetry allows us to take α and β in the range of $0 \leq \alpha < \pi$ and $-\frac{1}{2}\pi \leq \beta \leq \frac{1}{2}\pi$ without loss of generality. In the case of $\alpha = 0$, the vortex tube is aligned with the streamwise direction. When $\alpha <$ (or $>$) $\frac{1}{2}\pi$, it is inclined downstream (or upstream). In the cases of $\beta = \pm\frac{1}{2}\pi$, the tube axis is located on the horizontal plane $X_2 = 0$. When $\beta <$ (or $>$) 0, the spanwise vorticity component of the vortex tube is negative (or positive). Hereafter, a vortex tube for $\beta <$ (or $>$) 0 is referred to as a cyclonic (or anti-cyclonic) vortex.

Two vectors, (V_1, V_2, V_3) in $OX_1X_2X_3$ and (v_1, v_2, v_3) in $Ox_1x_2x_3$, are connected by relation

$$V_i = M_{ij} v_j \quad (i = 1, 2, 3), \tag{2.1}$$

where

$$\{M_{ij}\} = \begin{pmatrix} \cos\alpha & -\sin\alpha & 0 \\ \sin\alpha\cos\beta & \cos\alpha\cos\beta & -\sin\beta \\ \sin\alpha\sin\beta & \cos\alpha\sin\beta & \cos\beta \end{pmatrix} \quad (i, j = 1, 2, 3) \tag{2.2}$$

is a transformation matrix which represents a system rotation. Here and subsequently, the sum-

mation convention is employed for repeated subscrips. Similarly, the unit vectors representing the axes in the two coordinate systems are related by

$$\widehat{\boldsymbol{X}}_i = M_{ij}\widehat{\boldsymbol{x}}_j \quad (i = 1, 2, 3). \tag{2.3}$$

As the vortex tube evolves, the structural coordinate system $Ox_1x_2x_3$ rotates around some axis which passes through the origin O. It follows from the definition of α and β that the angular velocity of a system rotation $\boldsymbol{\Omega}$ is given by

$$\boldsymbol{\Omega} = (\mathrm{d}_t\beta)\,\widehat{\boldsymbol{X}}_1 + (\mathrm{d}_t\alpha)\,\widehat{\boldsymbol{x}}_3. \tag{2.4}$$

By making use of (2.2) and (2.3), we can express each component of the angular velocity vector in $Ox_1x_2x_3$ as

$$\Omega_1 = (\mathrm{d}_t\beta)\cos\alpha, \quad \Omega_2 = -(\mathrm{d}_t\beta)\sin\alpha, \quad \Omega_3 = \mathrm{d}_t\alpha. \tag{2.5}$$

2.2. Angular velocity of structural coordinate system

The motion of an incompressible viscous fluid of uniform mass density (taken as unity) is described by the Navier–Stokes equation, or equivalently the vorticity equation, which are respectively written in the structural coordinate system $Ox_1x_2x_3$ as †

$$\partial_t\boldsymbol{u} + [(\boldsymbol{u} - \boldsymbol{\Omega}\times\boldsymbol{x})\cdot\nabla]\boldsymbol{u} = \boldsymbol{u}\times\boldsymbol{\Omega} - \nabla p + \nu\nabla^2\boldsymbol{u}, \tag{2.6}$$

$$\partial_t\boldsymbol{\omega} + [(\boldsymbol{u} - \boldsymbol{\Omega}\times\boldsymbol{x})\cdot\nabla]\boldsymbol{\omega} = \boldsymbol{\omega}\times\boldsymbol{\Omega} + (\boldsymbol{\omega}\cdot\nabla)\boldsymbol{u} + \nu\nabla^2\boldsymbol{\omega}, \tag{2.7}$$

where $\boldsymbol{u}(x_1, x_2, x_3, t)$ is the velocity field relative to the stationary coordinate system, $\boldsymbol{\omega} = \nabla\times\boldsymbol{u}$ is the vorticity, p is the pressure and ∇ is the gradient operator in the structural coordinate

†Recall that a time-derivative of a vector field $\boldsymbol{A}$ in a stationary coordinate system is replaced as $\partial_t\boldsymbol{A} \to \partial_t\boldsymbol{A} - [(\boldsymbol{\Omega}\times\boldsymbol{x})\cdot\nabla]\boldsymbol{A} + \boldsymbol{\Omega}\times\boldsymbol{A}$ in the structural coordinate system.

system. The continuity equation is written as

$$\nabla \cdot \boldsymbol{u} = 0. \tag{2.8}$$

Now let us decompose the velocity, the vorticity and the pressure fields into contributions from the simple shear flow and the fluctuation field as

$$\boldsymbol{u} = \boldsymbol{U} + \boldsymbol{u}', \quad \boldsymbol{\omega} = \nabla \times \boldsymbol{U} + \boldsymbol{\omega}', \quad p = P + p'. \tag{2.9}$$

Then, the time-evolutions of the fluctuation velocity and vorticity are described by

$$\partial_t \boldsymbol{u}' + [(\boldsymbol{u}' + \overline{\boldsymbol{u}}) \cdot \nabla]\boldsymbol{u}' = \boldsymbol{u}' \times \boldsymbol{\Omega} - (\boldsymbol{u}' \cdot \nabla)\boldsymbol{U} - \nabla p' + \nu \nabla^2 \boldsymbol{u}', \tag{2.10}$$

$$\partial_t \boldsymbol{\omega}' + [(\boldsymbol{u}' + \overline{\boldsymbol{u}}) \cdot \nabla]\boldsymbol{\omega}' = \boldsymbol{\omega}' \times \boldsymbol{\Omega} + (\boldsymbol{\omega}' \cdot \nabla)\boldsymbol{U} + [(\boldsymbol{\omega}' + \nabla \times \boldsymbol{U}) \cdot \nabla]\boldsymbol{u}' + \nu \nabla^2 \boldsymbol{\omega}', \tag{2.11}$$

$$\nabla \cdot \boldsymbol{u}' = 0, \tag{2.12}$$

$$\boldsymbol{\omega}' = \nabla \times \boldsymbol{u}', \tag{2.13}$$

where

$$\overline{\boldsymbol{u}} = \boldsymbol{U} - \boldsymbol{\Omega} \times x \tag{2.14}$$

is the simple shear velocity relative to the structral coordinate system. The simple shear velocity and vorticity are respectively written as

$$\boldsymbol{U} = S X_2 \widehat{\boldsymbol{X}}_1 = S M_{1i} M_{2j} x_j \widehat{\boldsymbol{x}}_i, \tag{2.15}$$

$$\nabla \times \boldsymbol{U} = -S \widehat{\boldsymbol{X}}_3 = -S M_{3i} \widehat{\boldsymbol{x}}_i. \tag{2.16}$$

Notice that in general the coordinate x_1 appears explicitly in $\overline{u}_2$ and $\overline{u}_3$. If we require, however, that $\boldsymbol{u}'$ and $\boldsymbol{\omega}'$ are *uniform* in the x_1-direction, it follows from (2.10) and (2.11) that $\overline{u}_2$ and $\overline{u}_3$ are independent of x_1. Then we have

$$\Omega_2 = 0, \quad \Omega_3 = -S \sin^2 \alpha \cos \beta. \tag{2.17}$$

The second and third equations of (2.5) then give

$$(\mathrm{d}_t\beta)\sin\alpha = 0, \tag{2.18}$$

$$\mathrm{d}_t\alpha = -S\sin^2\alpha\cos\beta. \tag{2.19}$$

Equations (2.18) and (2.19) have a trivial solution $\alpha \equiv 0$ for any arbitrary β. Except for this trivial case, (2.18) requires that

$$\mathrm{d}_t\beta = 0. \tag{2.20}$$

In the case of $\alpha \equiv 0$, the vortex axis (x_1-axis) is identical with the X_1-axis, and any rotation around this axis does not change the orientation of it, so that we can take β to be constant in time t. Hence, we can assume that β is constant in any case. The first equation of (2.5) then yields

$$\Omega_1 = 0. \tag{2.21}$$

Equations (2.17) and (2.21) tell us that $\boldsymbol{\Omega}$ has only the x_3-component. By integrating (2.19), we obtain

$$\cot\alpha = \cot\alpha_0 + S\,t\cos\beta \tag{2.22}$$

with α_0 denoting the initial value of α at $t = 0$. It follows from (2.22) that $\alpha \to 0$ as $\alpha_0 \to 0$. Thus, the trivial solution ($\alpha \equiv 0$) is included in (2.22). These considerations lead us to the conclusion that a vortex tube rotates on a plane inclined to the spanwise direction at an angle of β which is invariant in time, and angle α from the streamwise direction approaches zero according to (2.22) as time progresses. This implies that the central axis of the vortex tube, the velocity and vorticity of which are uniform along it, must be passively convected by the uniform shear flow (see figure 3). Note that in the special cases of $\alpha = 0$ or $\beta = \pm\frac{1}{2}\pi$, the vortex tube is not inclined vertically and is stationary.

2.3. *Basic equations*

Suppose now that the fluctuation fields ω', $\boldsymbol{u}'$ and p' are independent of x_1, i.e., $\partial_1 = 0$. We then obtain closed equations for ω_1' and u_1' from (2.10) and (2.11) as

$$\begin{aligned} \partial_t \omega_1' - \frac{\partial(\psi, \omega_1')}{\partial(x_2, x_3)} &- S(\gamma(t)x_2 + \lambda(t)x_3)\partial_2 \omega_1' \\ &= S\gamma(t)\omega_1' + S\xi(t)\partial_3 u_1' + \nu\nabla_\perp^2 \omega_1', \end{aligned} \tag{2.23}$$

$$\begin{aligned} \partial_t u_1' - \frac{\partial(\psi, u_1')}{\partial(x_2, x_3)} &- S(\gamma(t)x_2 + \lambda(t)x_3)\partial_2 u_1' \\ &= -S\gamma(t)u_1' - S(\cos\alpha \sin\beta\, \partial_2 + \cos\beta\, \partial_3)\psi + \nu\nabla_\perp^2 u_1', \end{aligned} \tag{2.24}$$

where ψ ($u_2' = \partial_3\psi$, $u_3' = -\partial_2\psi$) is the streamfunction, which is related to ω_1' via

$$\nabla_\perp^2 \psi = -\omega_1', \tag{2.25}$$

and

$$\gamma(t) = \frac{\partial_1 U_1}{S} = \cos\alpha \sin\alpha \cos\beta, \tag{2.26}$$

$$\lambda(t) = \frac{(\nabla \times \boldsymbol{U}) \cdot \hat{\boldsymbol{x}}_1}{S} = -\sin\alpha \sin\beta, \tag{2.27}$$

$$\xi(t) = \frac{2\Omega_3}{S} = -2\sin^2\alpha \cos\beta \ \ (\leq 0) \tag{2.28}$$

(cf. (2.15)—(2.17)). Here, $\nabla_\perp^2 = \partial_2^2 + \partial_3^2$ is a two-dimensional Laplacian operator. Note that $\gamma(t)$ represents the axial rate of strain of the simple shear flow, $\lambda(t)$ the axial component of the simple shear vorticity, and $\xi(t)$ the vorticity corresponding to the angular velocity of the structural coordinate system, all of which are normalized by the simple shear rate. Note also that the nonlinear stretching-and-tilting terms $\omega_j'\partial_j u_1'$ have disappeared from (2.23) because the flow field is uniform along the vortex tube. Once (2.23) and (2.24) are solved, we can calculate

the other two fluctuation vorticity components through

$$\omega_2' = \partial_3 u_1', \quad \omega_3' = -\partial_2 u_1'. \tag{2.29}$$

The second and third terms on the left-hand sides of (2.23) and (2.24) represent the advection by the fluctuation velocity and the simple shear, respectively. On the right-hand side of (2.23), the first term represents the vorticity stretching via the simple shear, while the second is the production of the axial (x_1) component of the fluctuation vorticity via the tilting by the velocity fluctuation of the vorticity associated with the system rotation which has only the x_3-component. This second term is also interpreted as a sum of the three contributions; the tilting of the x_2-component of the fluctuation vorticity through the simple shear, $\omega_2' \partial_2 U_1 = S \cos^2\alpha \cos\beta \, \partial_3 u_1'$, the tilting of the x_3-component of the simple shear vorticity via the velocity fluctuation, $-S M_{33} \partial_3 u_1' = -S \cos\beta \, \partial_3 u_1'$, and the effect of frame rotation, $(\boldsymbol{\omega}' \times \boldsymbol{\Omega}) \cdot \hat{\boldsymbol{x}}_1 = -S \sin^2\alpha \cos\beta \, \partial_3 u_1'$. If $\beta = \pm\frac{1}{2}\pi$, all of these three contributions vanish. If $\alpha = 0$, the tiltings of the fluctuation vorticity and the simple shear vorticity cancel out, and the effect of frame rotation vanishes. Thus, in these two special cases, the production term on the right-hand side of (2.23) disappears. Except for these cases, the effect of the tilting of the simple shear vorticity is important in production of the axial vorticity. Note that this term is negative (or positive) according as $\omega_2' = \partial_3 u_1' >$ (or $<$) 0. On the right-hand side of (2.24), the first two terms originate from the advection of the simple shear velocity by the velocity fluctuation and the frame rotation.

2.4. *Transformed equations*

For the convenience of analytical treatment, we introduce plane polar coordinates (r, θ) with $x_2 = r\cos\theta$ and $x_3 = r\sin\theta$, and employ Lundgren's (1982) transformation of radial coordinate and time as

$$R = A(t)^{\frac{1}{2}} r, \quad T = \int_0^t A(s)\,\mathrm{d}s, \tag{2.30}$$

where

$$A(t) = \exp\left(S\int_0^t \gamma(s)\,\mathrm{d}s\right) \tag{2.31}$$

represents the stretch factor along the vortex tube. In the present case, it follows from (2.22) and (2.26) that

$$A(t) = \frac{\sin\alpha_0}{\sin\alpha} \tag{2.32}$$

for $\alpha \neq 0$ and $\beta \neq \pm\frac{1}{2}\pi$, and then we have

$$T = \frac{\sin\alpha_0}{2S\cos\beta}\left[\cot\alpha\,\mathrm{cosec}\,\alpha - \cot\alpha_0\,\mathrm{cosec}\,\alpha_0 + \ln\left(\frac{\cot\alpha + \mathrm{cosec}\,\alpha}{\cot\alpha_0 + \mathrm{cosec}\,\alpha_0}\right)\right]. \tag{2.33}$$

If $\alpha = 0$ or $\beta = \pm\frac{1}{2}\pi$, then $\gamma(t) \equiv 0$ and $A(t) \equiv 1$, and thus we have $R = r$ and $T = t$. Since $A(t) > 0$ for $t \geq 0$, T increases monotonically with time t. For $t \ll 1$ it changes as

$$T = t + \tfrac{1}{2}S\cos\alpha_0\sin\alpha_0\cos\beta\; t^2 + \cdots, \tag{2.34}$$

and for $t \gg 1$ it behaves asymptotically as

$$T = t^2\left[\tfrac{1}{2}S\sin\alpha_0\cos\beta + \cos\alpha_0\,\frac{1}{t} + O\left(\frac{\ln t}{t^2}\right)\right]. \tag{2.35}$$

The variations of A and T are plotted against time t for $\alpha_0 = \frac{1}{4}\pi$ and for three values of β in figures 4 and 5, respectively.

Equation (2.24) has a particular solution

$$u'_{1p} = -S\cos\beta\, x_2 + S\cos\alpha\sin\beta\, x_3 \quad (\equiv -Sr\,\mathrm{Real}\,[\mathrm{i}f_\infty(t)\mathrm{e}^{-\mathrm{i}\theta}],\ \text{say}), \tag{2.36}$$

which will turn out to play a key role in vorticity dynamics near the vortex core (see §3.4), where

$$f_\infty(t) = -\cos\alpha\sin\beta - \mathrm{i}\cos\beta = -D(t)\mathrm{e}^{\mathrm{i}\varphi(t)} \tag{2.37}$$

with

$$D(t) = (\cos^2\alpha\sin^2\beta + \cos^2\beta)^{\frac{1}{2}}, \quad \varphi(t) = \arctan\left(\frac{\cos\beta}{\cos\alpha\sin\beta}\right) \quad (0 \le \varphi(t) \le \pi). \tag{2.38}$$

Note that $\partial_3 u'_{1p} = S\cos\alpha\sin\beta = SM_{32}$ and $-\partial_2 u'_{1p} = S\cos\beta = SM_{33}$, i.e., the vorticity associated with this particular solution is equal to minus the component normal to the vortex tube of the simple shear vorticity. If we introduce a new dependent variable u''_1 by

$$u'_1 = u'_{1p} + u''_1 \tag{2.39}$$

and substitute it into (2.24), we can eliminate the inhomogeneous term on the right-hand side of (2.24). Then, $\partial_3 u''_1$ and $-\partial_2 u''_1$ are equal to the x_2- and x_3-components of the total vorticity, respectively, i.e., $\omega_2 = \partial_3 u''_1$ and $\omega_3 = -\partial_2 u''_1$.

Equations (2.23) and (2.24) are now transformed into closed equations for new dependent variables[†]

$$\omega(R,\theta,T) = \omega'_1(r,\theta,t)/A(t) = -\nabla_R^2\psi, \quad Ru(R,\theta,T) = A(t)u''_1(r,\theta,t) \tag{2.40}$$

as

$$-\frac{1}{R}\frac{\partial(\psi,\omega)}{\partial(R,\theta)} + (\partial_T - \nu\nabla_R^2)\omega = SL_1\omega + SL_2 u + \frac{2S^2\gamma(t)\lambda(t)}{A(t)^2}, \tag{2.41}$$

$$-\frac{1}{R}\frac{\partial(\psi,Ru)}{\partial(R,\theta)} + (\partial_T - \nu\nabla_R^2)Ru = SL_1 Ru, \tag{2.42}$$

[†]Notice that the axial velocity is expressed by Ru not by u.

where

$$\nabla_R^2 = \partial_R^2 + \frac{1}{R}\partial_R + \frac{1}{R^2}\partial_\theta^2 \tag{2.43}$$

is the two-dimensional Laplacian operator, and

$$L_1 = \frac{1}{2A(t)}[\gamma(t)(-\sin 2\theta\,\partial_\theta + R\cos 2\theta\,\partial_R) + \lambda(t)(\cos 2\theta\,\partial_\theta + R\sin 2\theta\,\partial_R - \partial_\theta)], \tag{2.44}$$

$$L_2 = \frac{\xi(t)}{A(t)^{\frac{5}{2}}}[\cos\theta\,\partial_\theta + \sin\theta\,(R\partial_R + 1)] \tag{2.45}$$

are first-order differential operators. The components of the total vorticity are expressed in terms of ω and u as

$$\omega_1 = S\lambda(t) + A(t)\omega, \tag{2.46}$$

$$\omega_2 = A(t)^{-\frac{1}{2}}[\cos\theta\,\partial_\theta + \sin\theta\,(R\partial_R + 1)]u, \tag{2.47}$$

$$\omega_3 = A(t)^{-\frac{1}{2}}[\sin\theta\,\partial_\theta - \cos\theta\,(R\partial_R + 1)]u. \tag{2.48}$$

The right-hand sides of (2.41) and (2.42) represent the effects of the simple shear on the fluctuation fields. The first terms $SL_1\omega$ and SL_1Ru represent respectively the deformation of the spatial distribution of ω and u in the normal (x_2, x_3)-plane by the simple shear. The last two terms on the right-hand side of (2.41) represent the coupling effect of the axial vorticity and velocity, that is, the second term on the right-hand side of (2.23), which is composed of the tilting of the x_2-component of the fluctuation vorticity by the simple shear, the tilting of the x_3-component of the simple shear vorticity via the velocity fluctuation, and the effect of the frame rotation. The last term is the contribution from particular solution (2.36). Note that if a vortex tube was not inclined vertically ($\alpha = 0$ or $\beta = \pm\frac{1}{2}\pi$), the second and third terms would vanish, so that ω would be decoupled from u. In these special cases the problem is much simplified. Pearson & Abernathy (1984) and Moore (1985) studied the time-evolution

of a diffusing vortex tube perfectly aligned with a simple shear ($\alpha = 0$), and recently Jiménez, Moffatt & Vasco (1996) examined the structure of a two-dimensional diffusing vortex tube in an imposed weak strain ($\alpha = \frac{1}{2}\pi$ and $\beta = \pm\frac{1}{2}\pi$). The present analysis includes both of them.

3. Asymptotic analysis at $Re \gg 1$ and $ST \ll 1$

In this section, we consider an early stage of time-evolution of a strong straight vortex tube. A straight vortex filament with circulation Γ is put in a simple shear flow at an initial instant $T = 0$. That is, the fluctuation vorticity is concentrated on a straight line $R = 0$, i.e.

$$\omega|_{T=0} = \frac{\Gamma\delta(R)}{\pi R}, \tag{3.1}$$

and the fluctuation axial velocity along the filament is null, $u_1' = 0$, so that, from (2.36)—(2.40),

$$u|_{T=0} = S\,\mathrm{Real}\,[\mathrm{i}f_0\mathrm{e}^{-\mathrm{i}\theta}], \tag{3.2}$$

where

$$f_0 = -\cos\alpha_0\sin\beta - \mathrm{i}\cos\beta = -D_0\mathrm{e}^{\mathrm{i}\varphi_0} \tag{3.3}$$

with

$$D_0 = (\cos^2\alpha_0\sin^2\beta + \cos^2\beta)^{\frac{1}{2}}, \quad \varphi_0 = \arctan\left(\frac{\cos\beta}{\cos\alpha_0\sin\beta}\right) \ (0 \le \varphi_0 \le \pi). \tag{3.4}$$

Note that φ_0 represents an initial angle from the x_2-axis to a projection of the X_3-axis on the normal (x_2, x_3)-plane (see (2.2) and (2.3)).[†] In the case of $\alpha_0 < \frac{1}{2}\pi$, φ_0 is greater than, equal to or less than $\frac{1}{2}\pi$ according as the vortex tube is cyclonic, neutral or anti-cyclonic.

[†]When $\alpha_0 = \frac{1}{2}\pi$ and $\beta = \pm\frac{1}{2}\pi$, the X_3-axis is normal to the (x_2, x_3)-plane, so that the x_1-axis (central axis of the vortex tube) is anti-parallel or parallel to the simple shear vorticity. In this case, $f_0 = 0$ ($u_{1p}' = 0$), and thus $f(\eta) \equiv 0$ (see §3.4). This implies that $u_1' \equiv 0$.

Here, we define Reynolds number by

$$Re = \frac{\Gamma}{2\pi\nu}, \tag{3.5}$$

and denote the reciprocal of it as

$$\epsilon = \frac{1}{2\pi Re} = \frac{\nu}{\Gamma}. \tag{3.6}$$

In the following, an asymptotic analysis will be performed at a large Reynolds number ($Re \gg 1$, $\epsilon \ll 1$) and at an early time of evolution ($ST \ll 1$).

3.1. Non-dimensionalization

We use shear rate S and kinematic viscosity ν in order to non-dimensionalize the variables in (2.41) and (2.42). A characteristic time-scale is then taken to be $1/S$, and a length-scale is $(\nu/S)^{\frac{1}{2}}$. Therefore, the axial velocity Ru is scaled by $(\nu S)^{\frac{1}{2}}$, and u itself is scaled by S. The vorticity ω and the streamfunction ψ are scaled respectively by $\epsilon^{-1}S$ $(= \Gamma S/\nu)$ and by $\epsilon^{-1}\nu$ $(= \Gamma)$ so that the dimensionless vortex strength and streamfunction may be independent of Γ at $T = 0$. The scaling units employed here are tabulated in Table 2.

By rewriting (2.41) and (2.42) with the dimensionless variables using the same notation for them as the originals, we obtain

$$-\frac{1}{R}\frac{\partial(\psi,\omega)}{\partial(R,\theta)} + \epsilon(\partial_T - \nabla_R^2)\omega = \epsilon L_1\omega + \epsilon^2 L_2 u + \epsilon^2\frac{2\gamma(t)\lambda(t)}{A(t)^2}, \tag{3.7}$$

$$-\frac{1}{R}\frac{\partial(\psi,Ru)}{\partial(R,\theta)} + \epsilon(\partial_T - \nabla_R^2)Ru = \epsilon L_1 Ru, \tag{3.8}$$

where L_1, L_2, $\gamma(t)$, $\lambda(t)$, $\xi(t)$ and $A(t)$ are given by the same expressions as before.†

†Dimensionless variables are used only in Section 3 but for §3.1.

3.2. Early-time approximation

Consider the early period of time-evolution of a strong vortex tube which starts with a straight filament. We anticipate that viscous diffusion (i.e., the left-hand sides of (3.7) and (3.8)) has primary effects on dynamics of the vortex tube and that the simple shear (i.e., the right-hand sides of (3.7) and (3.8)) plays secondary roles. We then seek solutions to (3.7) and (3.8) in the form as

$$\omega = \omega^{(0)} + \omega^{(1)} + \omega^{(2)} + \cdots, \tag{3.9}$$

$$\psi = \psi^{(0)} + \psi^{(1)} + \psi^{(2)} + \cdots, \tag{3.10}$$

$$u = u^{(0)} + u^{(1)} + u^{(2)} + \cdots, \tag{3.11}$$

where

$$\omega^{(j)} = -\nabla_R^2 \psi^{(j)} \quad (j = 0, 1, 2, \cdots). \tag{3.12}$$

It is assumed that $\omega^{(0)}$ and $\psi^{(0)}$ represent a diffusing strong vortex tube, and that $Ru^{(0)}$ represents the deformation of the velocity field from the simple shear flow by the vortex tube. Then, $\omega^{(j)}$ and $\psi^{(j)}$ $(j = 1, 2, \cdots)$ describe successively the higher-order interactions between the vortex tube and the simple shear. We shall take account of the effects of the simple shear one by one via $\omega^{(j)}$ and $\psi^{(j)}$ $(j = 1, 2, \cdots)$. Substituting (3.9)—(3.11) into (3.7) and (3.8), we have, at the leading order,

$$-\frac{1}{R}\frac{\partial(\psi^{(0)}, \omega^{(0)})}{\partial(R, \theta)} + \epsilon(\partial_T - \nabla_R^2)\omega^{(0)} = 0, \tag{3.13}$$

$$-\frac{1}{R}\frac{\partial(\psi^{(0)}, Ru^{(0)})}{\partial(R, \theta)} + \epsilon(\partial_T - \nabla_R^2)Ru^{(0)} = 0. \tag{3.14}$$

The next higher-order equations for vorticity are written as

$$-\frac{1}{R}\left[\frac{\partial(\psi^{(0)}, \omega^{(1)})}{\partial(R, \theta)} + \frac{\partial(\psi^{(1)}, \omega^{(0)})}{\partial(R, \theta)}\right] + \epsilon(\partial_T - \nabla_R^2)\omega^{(1)} = \epsilon L_1 \omega^{(0)} + \epsilon^2 L_2 u^{(0)} + \epsilon^2 \frac{2\gamma(t)\lambda(t)}{A(t)^2}, \tag{3.15}$$

and so on. These equations are supplemented by the initial and boundary conditions as

$$\omega^{(0)}|_{T=0} = \frac{\delta(R)}{\pi R}, \quad \omega^{(0)}|_{R=\infty} = 0, \tag{3.16}$$

$$\omega^{(1)}|_{T=0} = \omega^{(2)}|_{T=0} = \cdots = 0, \quad \omega^{(1)}|_{R=\infty} = \omega^{(2)}|_{R=\infty} = \cdots = 0, \tag{3.17}$$

$$\partial_R \psi^{(0)}|_{R=\infty} = \partial_R \psi^{(1)}|_{R=\infty} = \partial_R \psi^{(2)}|_{R=\infty} = \cdots = 0, \tag{3.18}$$

$$u^{(0)}|_{T=0} = u^{(0)}|_{R=\infty} = \mathrm{Real}\,[\mathrm{i} f_0 \mathrm{e}^{-\mathrm{i}\theta}], \tag{3.19}$$

$$u^{(1)}|_{T=0} = u^{(2)}|_{T=0} = \cdots = 0, \tag{3.20}$$

$$\left.\begin{aligned} u^{(1)}|_{R=\infty} &= T\,\mathrm{Real}\left[\mathrm{d}_T\left(A(t)^{\frac{1}{2}} f_\infty(t)\right)|_{T=0} \mathrm{i}\mathrm{e}^{-\mathrm{i}\theta}\right], \\ u^{(2)}|_{R=\infty} &= \tfrac{1}{2} T^2\,\mathrm{Real}\left[\mathrm{d}_T^2\left(A(t)^{\frac{1}{2}} f_\infty(t)\right)|_{T=0} \mathrm{i}\mathrm{e}^{-\mathrm{i}\theta}\right], \end{aligned}\right\} \tag{3.21}$$

and so on, where the conditions for $u^{(j)}|_{R=\infty}$ $(j = 0, 1, 2, \cdots)$ have been obtained by an expansion of (scaled) particular solution (2.36), $-A(t)u'_{1p}/R$. In addition, $\omega^{(j)}$ $(j = 1, 2, \cdots)$, $\psi^{(k)}$ and $R\,u^{(k)}$ $(k = 0, 1, 2, \cdots)$ are assumed to be regular at $R = 0$. The initial condition, on the other hand, has been derived from (3.1) and (3.2). It has been also assumed that the fluctuation parts of the velocity and the axial vorticity may decay at infinity. An additive constant in the streamfunction will be taken to be zero since it does not affect the flow. Solutions are determined successively starting from leading-order equation (3.13), which will be made in the following three subsections.

3.3. Axial vorticity

We first consider the leading-order solutions. Under initial and boundary conditions (3.16), the solution of (3.13) is uniquely determined as

$$\omega^{(0)} = \frac{1}{4\pi T} \mathrm{e}^{-\eta^2}, \tag{3.22}$$

where

$$\eta = \frac{R}{2T^{\frac{1}{2}}} \tag{3.23}$$

is a similarity variable. Substitution of (3.22) into (3.12) for $j = 0$ leads to

$$\psi^{(0)} = -\frac{1}{2\pi}\int_0^\eta \frac{1-\mathrm{e}^{-s^2}}{s}\,\mathrm{d}s, \tag{3.24}$$

which is regular at $\eta = 0$ and satisfies (3.18).

It follows that for $\alpha < \frac{1}{2}\pi$ ($\gamma(t) > 0$) the leading-order axial vorticity $A(t)\omega^{(0)}$ represents a diffusing and stretching vortex tube under the action of viscosity and the axial stress of the simple shear. For $\alpha > \frac{1}{2}\pi$ ($\gamma(t) < 0$), on the other hand, it represents a diffusing and compressing vortex tube.

3.4. Axial velocity and normal vorticity

Next we consider the axial velocity deformed by the vortex tube. We seek a solution to (3.14) written in a separation-of-variable form in similarity variable η and angular coordinate θ as

$$u^{(0)} = \mathrm{Real}\,[\mathrm{i}f(\eta)\mathrm{e}^{-\mathrm{i}\theta}]. \tag{3.25}$$

By substituting (3.25) into (3.14), we obtain

$$f'' + \left(2\eta + \frac{3}{\eta}\right)f' + \mathrm{i}Re\frac{1-\mathrm{e}^{-\eta^2}}{\eta^2}f = 0. \tag{3.26}$$

Hereafter in this section, the prime is used to denote differentiation with respect to η. Boundary conditions to be imposed are that $Rf(\eta)$ is regular at $\eta = 0$ and that $f(\infty) = f_0$ $(= -D_0\mathrm{e}^{\mathrm{i}\varphi_0})$ (see (3.19)). The asymptotic expansion of the solution to (3.26) for large and small values of η can be easily calculated. For $\eta \gg Re^{\frac{1}{2}}$, we have

$$f(\eta) = -D_0\mathrm{e}^{\mathrm{i}\varphi_0}\left[1 + \frac{\mathrm{i}Re}{4\eta^2} - \frac{Re^2}{32\eta^4} - \frac{(\mathrm{i}Re+8)Re^2}{384\eta^6} + \cdots\right] + O(\mathrm{e}^{-\eta^2}), \tag{3.27}$$

while, for $\eta \ll Re^{-\frac{1}{2}}$, we have

$$f(\eta) = c_0 \left[1 - \frac{\mathrm{i}Re}{8}\eta^2 + \left(\frac{\mathrm{i}Re}{24} - \frac{Re^2}{192} \right) \eta^4 + \cdots \right], \tag{3.28}$$

where c_0 is a constant, which will be determined by the asymptotic condition $f(\infty) = -D_0 \mathrm{e}^{\mathrm{i}\varphi_0}$ (see below).

Equation (3.26) is identical with the one obtained by Moore (1985) who analyzed the dynamics of a diffusing vortex tube perfectly aligned with a simple shear flow, which corresponds to the present case of $\alpha = 0$. He has presented the asymptotic solution to (3.26) for $Re \gg 1$ using the WKB (Wentzel-Kramers-Brillouin) method. Here, following his method, we derive an asymptotic solution to our problem for $Re \gg 1$ ($\epsilon \ll 1$).

In order to apply the WKB method, it is convenient to eliminate the first-order-derivative terms in (3.26). To do so we introduce a new dependent variable $g(\eta)$ by

$$f(\eta) = \eta^{-\frac{3}{2}} \mathrm{e}^{-\frac{1}{2}\eta^2} g(\eta). \tag{3.29}$$

Substitution of (3.29) into (3.26) leads to

$$g'' + \left[\mathrm{i}ReH(\eta) - \eta^2 - 4 - \frac{3}{4\eta^2} \right] g = 0, \tag{3.30}$$

where

$$H(\eta) = \frac{1 - \mathrm{e}^{-\eta^2}}{\eta^2}. \tag{3.31}$$

In the following we consider three regions of values of η separately, that is, $\eta = O(Re^{-\frac{1}{2}})$, $O(1)$ and $O(Re^{\frac{1}{4}})$.

First, suppose that $\eta = O(Re^{-\frac{1}{2}})$ and put $\eta = Re^{-\frac{1}{2}}\zeta$. Then (3.30) is written as

$$g'' + \left[\mathrm{i} - \frac{3}{4\zeta^2} + O(Re^{-1}) \right] g = 0, \tag{3.32}$$

which is valid for $\zeta \ll Re^{\frac{1}{2}}$ (i.e. for $\eta \ll 1$). This equation has a solution

$$g = c_1 \zeta^{\frac{1}{2}} J_1(\mathrm{e}^{\frac{1}{4}\pi \mathrm{i}} \zeta) + O(Re^{-1}), \tag{3.33}$$

which is regular at $\zeta = 0$. Here, c_1 is a constant and J_1 is the Bessel function of the first kind. For $\zeta \ll 1$ solution (3.33) is expanded as

$$g = \tfrac{1}{2} c_1 \, \mathrm{e}^{\frac{1}{4}\pi \mathrm{i}} \zeta^{\frac{3}{2}} \left(1 - \frac{\mathrm{i}}{8}\zeta^2 - \frac{1}{192}\zeta^4 + \cdots\right), \tag{3.34}$$

and for $\zeta \gg 1$ it is written , in the leading order, as

$$g \approx \frac{c_1}{(2\pi)^{\frac{1}{2}}} \left[\mathrm{e}^{\frac{5}{8}\pi \mathrm{i}} \exp(\mathrm{e}^{-\frac{1}{4}\pi \mathrm{i}} \zeta) + \mathrm{e}^{-\frac{7}{8}\pi \mathrm{i}} \exp(\mathrm{e}^{\frac{3}{4}\pi \mathrm{i}} \zeta)\right]. \tag{3.35}$$

By requring that (3.34) may coincide with (3.28), we obtain, using definition (3.29) of g, that

$$c_0 = \tfrac{1}{2} c_1 \, \mathrm{e}^{\frac{1}{4}\pi \mathrm{i}} Re^{\frac{3}{4}}. \tag{3.36}$$

Next, in the region of $\eta = O(1)$, equation (3.30) is written as

$$g'' + Re \left[\mathrm{i}H(\eta) + O(Re^{-1})\right] g = 0, \tag{3.37}$$

which is valid for $\eta \ll Re^{\frac{1}{2}}$. We then apply the WKB approximation to obtain

$$g = H(\eta)^{-\frac{1}{4}} \left[c_2 \exp\left(Re^{\frac{1}{2}} n(\eta)\right) + c_3 \exp\left(-Re^{\frac{1}{2}} n(\eta)\right)\right] + O(Re^{-1}), \tag{3.38}$$

where c_2 and c_3 are new constants, and

$$n(\eta) = \mathrm{e}^{-\frac{1}{4}\pi \mathrm{i}} \int_0^\eta H(s)^{\frac{1}{2}} \, \mathrm{d}s. \tag{3.39}$$

The asymptotic forms of (3.38) for small and large values of η are respectively written as

$$g \approx c_2 \exp(\mathrm{e}^{-\frac{1}{4}\pi \mathrm{i}} Re^{\frac{1}{2}} \eta) + c_3 \exp(\mathrm{e}^{\frac{3}{4}\pi \mathrm{i}} Re^{\frac{1}{2}} \eta) \quad \text{for} \quad \eta \ll 1 \tag{3.40}$$

and

$$g \approx \eta^{\frac{1}{2}} \left[c_2 \exp\left(\mathrm{e}^{-\frac{1}{4}\pi \mathrm{i}} Re^{\frac{1}{2}} (\ln \eta + \mu) \right) + c_3 \exp\left(\mathrm{e}^{\frac{3}{4}\pi \mathrm{i}} Re^{\frac{1}{2}} (\ln \eta + \mu) \right) \right] \quad \text{for } \eta \gg 1, \tag{3.41}$$

where

$$\mu = \int_0^1 H(s)^{\frac{1}{2}} \, \mathrm{d}s + \int_1^\infty \left[H(s)^{\frac{1}{2}} - \frac{1}{s} \right] \mathrm{d}s. \tag{3.42}$$

Matching conditions of (3.40) with (3.35) give

$$c_1 = c_2 (2\pi)^{\frac{1}{2}} \mathrm{e}^{-\frac{5}{8}\pi \mathrm{i}}, \tag{3.43}$$

$$c_3 = \frac{c_1}{(2\pi)^{\frac{1}{2}}} \mathrm{e}^{-\frac{7}{8}\pi \mathrm{i}}. \tag{3.44}$$

In the third region of $\eta = O(Re^{\frac{1}{4}})$, we put $\eta = Re^{\frac{1}{4}} \chi$ to obtain

$$g'' + Re \left[\frac{\mathrm{i}}{\chi^2} - \chi^2 - 4Re^{-\frac{1}{2}} + O(Re^{-1}) \right] g = 0, \tag{3.45}$$

which is valid for $Re^{-\frac{1}{2}} \ll \chi \ll Re^{\frac{1}{2}}$ (i.e. for $Re^{-\frac{1}{4}} \ll \eta \ll Re^{\frac{3}{4}}$). We again apply the WKB approximation to (3.45) and find[†]

$$\begin{aligned} g = {} & \mathrm{e}^{-\frac{1}{4}\pi \mathrm{i}} \chi^{\frac{1}{2}} (\chi^4 - \mathrm{i})^{-\frac{1}{4}} \left[c_4 \left(\chi^2 + (\chi^4 - \mathrm{i})^{\frac{1}{2}} \right) \exp\left(Re^{\frac{1}{2}} \sigma(\chi) \right) \right. \\ & \left. + c_5 \left(\chi^2 + (\chi^4 - \mathrm{i})^{\frac{1}{2}} \right)^{-1} \exp\left(-Re^{\frac{1}{2}} \sigma(\chi) \right) \right] + O(Re^{-1}), \end{aligned} \tag{3.46}$$

where

$$\sigma(\chi) = \tfrac{1}{2} \mathrm{e}^{\frac{1}{4}\pi \mathrm{i}} \left[\mathrm{e}^{-\frac{1}{4}\pi \mathrm{i}} (\chi^4 - \mathrm{i})^{\frac{1}{2}} - \arctan\left(\mathrm{e}^{-\frac{1}{4}\pi \mathrm{i}} (\chi^4 - \mathrm{i})^{\frac{1}{2}} \right) + \tfrac{1}{2}\pi \right]. \tag{3.47}$$

[†]There are typographic errors in the WKB solution given by Moore (1985) in his eq. (3.12). The two linearly independent solutions constructed by the WKB method should be

$$\chi^{\frac{1}{2}} (\chi^4 - \mathrm{i})^{-\frac{1}{4}} \left(\chi^2 + (\chi^4 - \mathrm{i})^{\frac{1}{2}} \right)^{\pm 1} \mathrm{e}^{\pm Re^{\frac{1}{2}} \sigma}.$$

For small values of χ, the function σ can be expressed asymptotically as

$$\sigma = \mathrm{e}^{-\frac{1}{4}\pi\mathrm{i}} \ln \chi + \rho + O(\chi^4), \tag{3.48}$$

where

$$\rho = \tfrac{1}{2}\mathrm{e}^{\frac{3}{4}\pi\mathrm{i}} \ln 2 + 2^{-\frac{3}{2}} \left[\tfrac{1}{4}\pi + 1 + \mathrm{i}\left(\tfrac{1}{4}\pi - 1\right)\right]. \tag{3.49}$$

For large χ, on the other hand, σ has the expansion

$$\sigma = \tfrac{1}{2}\chi^2 + \frac{\mathrm{i}}{4\chi^2} - \frac{1}{48\chi^6} + \cdots. \tag{3.50}$$

Hence, (3.46) is written as

$$\begin{aligned} g \approx \chi^{\frac{1}{2}} \Big[& c_4 \mathrm{e}^{-\frac{3}{8}\pi\mathrm{i}} \exp(\mathrm{e}^{-\frac{1}{4}\pi\mathrm{i}} Re^{\frac{1}{2}} \ln \chi + Re^{\frac{1}{2}}\rho) \\ & + c_5 \mathrm{e}^{\frac{1}{8}\pi\mathrm{i}} \exp(\mathrm{e}^{\frac{3}{4}\pi\mathrm{i}} Re^{\frac{1}{2}} \ln \chi - Re^{\frac{1}{2}}\rho)\Big] \quad \text{for } \chi \ll 1, \end{aligned} \tag{3.51}$$

and

$$g \approx 2c_4 \mathrm{e}^{-\frac{1}{4}\pi\mathrm{i}} \chi^{\frac{3}{2}} \exp\left(\tfrac{1}{2} Re^{\frac{1}{2}} \chi^2\right) \quad \text{for } \chi \gg 1. \tag{3.52}$$

By matching (3.51) with (3.41), we find

$$c_2 = c_4 \mathrm{e}^{-\frac{3}{8}\pi\mathrm{i}} Re^{-\frac{1}{8}} \kappa(Re), \tag{3.53}$$

$$c_5 = c_3 \mathrm{e}^{-\frac{1}{8}\pi\mathrm{i}} Re^{\frac{1}{8}} \kappa(Re), \tag{3.54}$$

where

$$\kappa(Re) = \exp\left(Re^{\frac{1}{2}}(\mathrm{e}^{\frac{3}{4}\pi\mathrm{i}} \ln Re^{\frac{1}{4}} + \mathrm{e}^{\frac{3}{4}\pi\mathrm{i}}\mu + \rho)\right). \tag{3.55}$$

Finally, we extend the third region to infinity so that boundary condition $f(\infty) = f_0$ ($= -D_0 \mathrm{e}^{\mathrm{i}\varphi_0}$) can be applied to determine constant c_4. We compare (3.52) with the boundary condition using definition (3.29) of g to obtain

$$c_4 = -\tfrac{1}{2} D_0 \mathrm{e}^{\mathrm{i}(\varphi_0 + \frac{1}{4}\pi)} Re^{\frac{3}{8}}. \tag{3.56}$$

Constants, c_2, c_1, c_0, c_3 and c_5 are determined in turn through (3.53), (3.43), (3.36), (3.44) and (3.54). The results are that

$$c_0 = -\tfrac{1}{2}(\tfrac{1}{2}\pi)^{\frac{1}{2}} D_0 \mathrm{e}^{\mathrm{i}(\varphi_0 - \frac{1}{2}\pi)} Re\kappa(Re), \tag{3.57}$$

$$c_1 = -(\tfrac{1}{2}\pi)^{\frac{1}{2}} D_0 \mathrm{e}^{\mathrm{i}(\varphi_0 - \frac{3}{4}\pi)} Re^{\frac{1}{4}}\kappa(Re), \tag{3.58}$$

$$c_2 = -\tfrac{1}{2} D_0 \mathrm{e}^{\mathrm{i}(\varphi_0 - \frac{1}{8}\pi)} Re^{\frac{1}{4}}\kappa(Re), \tag{3.59}$$

$$c_3 = -\tfrac{1}{2} D_0 \mathrm{e}^{\mathrm{i}(\varphi_0 - \frac{13}{8}\pi)} Re^{\frac{1}{4}}\kappa(Re), \tag{3.60}$$

$$c_5 = \tfrac{1}{2} D_0 \mathrm{e}^{\mathrm{i}(\varphi_0 - \frac{7}{4}\pi)} Re^{\frac{3}{8}}\kappa(Re)^2. \tag{3.61}$$

When $\alpha_0 = \frac{1}{2}\pi$ and $\beta = \pm\frac{1}{2}\pi$, then $D_0 = 0$ and $u'_{1p} = 0$ (see a footnote below (3.4)) and therefore all of the above constants vanish. Hence, in this case it is concluded that $f(\eta) \equiv 0$, and thus $u''_1 \equiv 0$ and $u'_1 \equiv 0$. In this special situation the central axis of the vortex tube is parallel or anti-parallel to the simple shear vorticity. Except for this trivial case, (3.55) implies that $|\kappa|$ is exponentially small as $Re \to \infty$, and so are $|c_0|$, $|c_1|$, $|c_2|$, $|c_3|$ and $|c_5|$.

Now we come back to consider the behaviour of $f(\eta)$. Since c_1, c_2 and c_3 are exponentially small constants, solutions (3.33) and (3.38) become very small as $Re \to \infty$. Hence, in the region of $\eta \lesssim 1$, $|f|$ is very small for $Re \gg 1$. Next, in the region of $\eta = Re^{\frac{1}{4}}\chi$ ($\chi = O(1)$), the dominant contributor to solution (3.46) is the first term since c_5 is an exponentially small constant. Then, (3.29), (3.46) and (3.56) give

$$f = -\tfrac{1}{2} D_0 \mathrm{e}^{\mathrm{i}\varphi_0} \chi^{-1} (\chi^4 - \mathrm{i})^{-\frac{1}{4}} \left(\chi^2 + (\chi^4 - \mathrm{i})^{\frac{1}{2}}\right) \exp\left(Re^{\frac{1}{2}}(\sigma - \tfrac{1}{2}\chi^2)\right). \tag{3.62}$$

Since the real part of the argument, $\sigma - \frac{1}{2}\chi^2$, in the exponential function is shown numerically to be negative (see figure 6), $|f|$ is also very small for $Re \gg 1$ in the region of $\eta = O(Re^{\frac{1}{4}})$ ($\chi = O(1)$). These considerations lead us to the conclusion that $|f|$ (and so Ru and u''_1)

decreases to zero exponentially as $Re \to \infty$ up to the region of $\eta = O(Re^{\frac{1}{4}})$. This implies that $u_1' \approx u_{1p}'$ at $\eta \lesssim Re^{\frac{1}{4}}$ (see (2.39)). In other words, that is, the fluctuation axial velocity is well described in terms of particular solution (2.36). To examine the functional form of $f(\eta)$ in the region of $\eta \gg Re^{\frac{1}{4}}$ ($\chi \gg 1$) we expand (3.62) in a series of inverse powers of χ, by making use of (3.50), to obtain, in terms of original variable η, that

$$f(\eta) \approx -D_0 \mathrm{e}^{\mathrm{i}\varphi_0} \exp\left(\frac{\mathrm{i}Re}{4\eta^2} - \frac{Re^2}{48\eta^6}\right), \tag{3.63}$$

and that

$$f'(\eta) \approx D_0 \mathrm{e}^{\mathrm{i}\varphi_0} \frac{\mathrm{i}Re}{2\eta^3} \exp\left(\frac{\mathrm{i}Re}{4\eta^2} - \frac{Re^2}{48\eta^6}\right). \tag{3.64}$$

In figure 7 we plot $f(\eta)/(-D_0 \mathrm{e}^{\mathrm{i}\varphi_0})$ expressed by asymptotic solution (3.63) (dashed curve) at $Re = 1\,000$ together with a numerical solution (solid curve) of (3.26) solved by a shooting method, where thick and thin curves denote the real and imaginary parts, resprectively. The agreement between the two solutions is excellent except for relatively small values of η. The region of disagreement should be shrinked as Re increases. In order to see the Reynolds number dependence we plot $f(\eta)$ for two different Reynolds numbers in two different scales in figures 8. It oscillates more and more frequently with increasing Reynolds number. The solution itself scales as $Re^{\frac{1}{2}}$ at large η, while the envelope goes with $Re^{\frac{1}{3}}$.

We next consider the vorticity component normal to the vortex tube. By using (2.47), (2.48) and (3.25), the normal components of the total vorticity $\boldsymbol{\omega} = \nabla \times \boldsymbol{U} + \boldsymbol{\omega}'$ can be expressed in terms of $f(\eta)$ as

$$\omega_2 = A(t)^{-\frac{1}{2}} \mathrm{Real}\left[f + \tfrac{1}{2}\eta f' - \tfrac{1}{2}\eta f' \mathrm{e}^{-\mathrm{i}2\theta}\right], \tag{3.65}$$

$$\omega_3 = A(t)^{-\frac{1}{2}} \mathrm{Imag}\left[f + \tfrac{1}{2}\eta f' + \tfrac{1}{2}\eta f' \mathrm{e}^{-\mathrm{i}2\theta}\right]. \tag{3.66}$$

If we use asymptotic forms (3.63) and (3.64), then (3.65) and (3.66) become

$$\omega_2 = -A(t)^{-\frac{1}{2}} D_0 \left[\cos\left(\frac{Re}{4\eta^2} + \varphi_0\right) + \frac{Re}{2\eta^2} \cos\left(\frac{Re}{4\eta^2} + \varphi_0 - \theta\right) \sin\theta \right] \exp\left(-\frac{Re^2}{48\eta^6}\right), \quad (3.67)$$

$$\omega_3 = -A(t)^{-\frac{1}{2}} D_0 \left[\sin\left(\frac{Re}{4\eta^2} + \varphi_0\right) - \frac{Re}{2\eta^2} \cos\left(\frac{Re}{4\eta^2} + \varphi_0 - \theta\right) \cos\theta \right] \exp\left(-\frac{Re^2}{48\eta^6}\right). \quad (3.68)$$

In figure 9 shown are the spatial distribution of normal vorticity $(\omega_2^2 + \omega_3^2)^{\frac{1}{2}}$ and the projected vorticity lines on the normal (x_2, x_3)-plane, which were obtained from (3.67) and (3.68), at $Re = 1\,000$. Figures (a), (b) and (c) represent the cyclonic ($\alpha_0 = \arctan\sqrt{2}$, $\beta = -\frac{1}{4}\pi$), neutral ($\alpha_0 = \frac{1}{4}\pi$, $\beta = 0$), and anti-cyclonic ($\alpha_0 = \arctan\sqrt{2}$, $\beta = \frac{1}{4}\pi$) cases, in which the vortex tube is oriented to the direction of $\widehat{\boldsymbol{X}}_1 + \widehat{\boldsymbol{X}}_2 - \widehat{\boldsymbol{X}}_3$, $\widehat{\boldsymbol{X}}_1 + \widehat{\boldsymbol{X}}_2$, and $\widehat{\boldsymbol{X}}_1 + \widehat{\boldsymbol{X}}_2 + \widehat{\boldsymbol{X}}_3$, respectively. Here, the relative magnitude of the normal vorticity is repsesented by colour: the red is the highest ($7S$) and the blue is the lowest (i.e. zero). It can be seen that the vortex tube wraps and stretches vorticity lines around it to form two spiral vortex layers of high normal vorticity oriented alternately to opposite directions. One of the most interesting features of the spirals is that the x_2-component of normal vorticity takes positive values in the outermost spiral layers of strong vorticity. It changes the sign every time it makes a half turn along the spirals. An important consequence of this change of sign will be discussed in §4.3.

In the near region ($\eta \lesssim Re^{\frac{1}{4}}$), however, the excessive wrapping narrows the spacing of the spiral layers and enhances the viscous diffusion to cancel out their opposite-signed vorticities, which leads to disappearance of the normal vorticity around the vortex tube and to selective stretch-and-intensification of a cyclonic vortex tube (see §4.2).

The circumferential vorticity component ω_θ, which dominates the radial component (see vorticity lines in figure 9), is expressed as

$$\omega_\theta = -\omega_2 \sin\theta + \omega_3 \cos\theta = -A(t)^{-\frac{1}{2}} \mathrm{Real}\left[\mathrm{i}(\eta f)' \mathrm{e}^{-\mathrm{i}\theta}\right], \quad (3.69)$$

which takes local maximum and minimum,

$$\left.\begin{matrix}\omega_{\theta max}\\ \omega_{\theta min}\end{matrix}\right\} = \pm A(t)^{-\frac{1}{2}}|(\eta f)'| \quad \text{at} \quad \left.\begin{matrix}\theta_{max}\\ \theta_{min}\end{matrix}\right\} = \arg[(\eta f)'] \mp \tfrac{1}{2}\pi. \tag{3.70}$$

This implies that two spiral vortex layers of high normal vorticities of opposite signs of ω_θ are arranged alternately. It follows from (3.63) and (3.64) that

$$(\eta f)' \approx -D_0 \mathrm{e}^{\mathrm{i}\varphi_0}\left(1 - \frac{\mathrm{i}Re}{2\eta^2}\right)\exp\left(\frac{\mathrm{i}Re}{4\eta^2} - \frac{Re^2}{48\eta^6}\right), \tag{3.71}$$

and then the magnitude and phase of which are, respectively, written as

$$|(\eta f)'| \approx D_0 \frac{Re}{2\eta^2}\left(1 + \frac{4\eta^4}{Re^2}\right)^{\frac{1}{2}} \exp\left(-\frac{Re^2}{48\eta^6}\right), \tag{3.72}$$

$$\arg[(\eta f)'] \approx \frac{Re}{4\eta^2} + \arctan\left(\frac{2\eta^2}{Re}\right) + \varphi_0 + \tfrac{1}{2}\pi. \tag{3.73}$$

In figure 10 we plot $(\eta f)' Re^{-\frac{1}{3}}/(-D_0 \mathrm{e}^{\mathrm{i}\varphi_0})$ at $Re = 1\,000$, where solid and dashed curves represent the real and imaginary parts respectively, and thin solid lines $\pm|(\eta f)'|$. We can see that magnitude $|(\eta f)'|$ has a single maximum of $0.903 D_0 Re^{\frac{1}{3}}$ at $\eta = 2^{-\frac{2}{3}} Re^{\frac{1}{3}}$ (Moore 1985). It is exponentially small at $\eta \ll Re^{\frac{1}{3}}$, while it approaches a constant $D_0 = (\cos^2\alpha_0 \sin^2\beta + \cos^2\beta)^{\frac{1}{2}}$, which is the magnitude of the normal component of the simple shear vorticity, as η increases. The phase, $\arg[(\eta f)']$, is infinity at $\eta = 0$ and decreases up to $\eta = (\frac{1}{2}Re)^{\frac{1}{2}}$ at which it takes a minimum value of $\frac{1}{2} + \frac{3}{4}\pi + \varphi_0$, and thereafter it increases monotonically to approach $\pi + \varphi_0$ at $\eta \to \infty$. Therefore, the spiral form of the layer actually terminates around $\eta = (\frac{1}{2}Re)^{\frac{1}{2}}$ since beyond this point both θ_{max} and θ_{min} change only by $\frac{1}{4}\pi - \frac{1}{2} \approx 0.29$ in the opposite direction.

The distance between adjacent layers of the two spirals is estimated as follows. Let η_+ and η_- be successive locations for a fixed value of θ of $\omega_{\theta max}$ and $\omega_{\theta min}$, respectively, and let $\Delta\eta = \eta_- - \eta_+$ be their spacing. Then, it follows from (3.70) and (3.73) that

$$\frac{Re}{\eta_+^2} - \frac{Re}{\eta_-^2} = Re\frac{(\eta_+ + \eta_-)}{\eta_+^2\eta_-^2}\Delta\eta = 4\pi - 4\arctan\left(\frac{2\eta_+^2}{Re}\right) + 4\arctan\left(\frac{2\eta_-^2}{Re}\right), \tag{3.74}$$

and therefore we have

$$\Delta\eta = O\left(\frac{\eta^3}{Re}\right) \tag{3.75}$$

as long as $\eta < (\frac{1}{2}Re)^{\frac{1}{2}}$. The spacing between adjacent spiral layers is $O(1)$ at $\eta = O(Re^{\frac{1}{3}})$.† It is greater than $O(1)$ at $O(Re^{\frac{1}{3}}) < \eta \left(< (\frac{1}{2}Re)^{\frac{1}{2}}\right)$. For $Re^{\frac{1}{3}} \gg \eta \ (\gg Re^{\frac{1}{4}})$, the spacing become very small as $Re \to \infty$.

3.5. Higher-order axial vorticity

In this subsection we consider solutions to higher-order equation (3.15) for the axial vorticity. In order to get an explicit analytical solution, we restrict ourselves at early-time evolution ($T \ll 1$). Since time T does not explicitly appear in the leading-order streamfunction (3.24), the first-order streamfunction and the corresponding axial vorticity may be expanded respectively as

$$\psi^{(1)}(R,\theta,T) = T\psi^{(1,1)}(\eta,\theta) + T^2\psi^{(1,2)}(\eta,\theta) + \cdots, \tag{3.76}$$

$$\omega^{(1)}(R,\theta,T) = \omega^{(1,0)}(\eta,\theta) + T\omega^{(1,1)}(\eta,\theta) + \cdots, \tag{3.77}$$

where

$$\omega^{(1,j-1)} = -\tfrac{1}{4}\nabla_\eta^2\psi^{(1,j)} \quad (j = 1, 2, \cdots) \tag{3.78}$$

with

$$\nabla_\eta^2 = \partial_\eta^2 + \frac{1}{\eta}\partial_\eta + \frac{1}{\eta^2}\partial_\theta^2. \tag{3.79}$$

For small values of T, the time-dependent factors, γ/A, λ/A and $\xi/A^{\frac{5}{2}}$ in linear operators L_1 and L_2 (see (2.44) and (2.45)) are expanded in power series of T, using $\alpha = \alpha_0 - T\,\sin^2\alpha_0\cos\beta + \cdots$,

†In dimensional variables, the location of the maximum normal vorticity is $O\left(Re^{\frac{1}{3}}(\nu T)^{\frac{1}{2}}\right)$ and the spacing of the spirals is $O\left((\nu T)^{\frac{1}{2}}\right)$ (see §4.4 and figure 19).

as

$$\frac{\gamma}{A} = \frac{\cos\alpha\sin^2\alpha\sin\beta}{\sin\alpha_0} = \gamma_0 + \gamma_1 T + \cdots, \tag{3.80}$$

$$\frac{\lambda}{A} = -\frac{\sin^2\alpha\sin\beta}{\sin\alpha_0} = \lambda_0 + \lambda_1 T + \cdots, \tag{3.81}$$

$$\frac{\xi}{A^{\frac{5}{2}}} = -\frac{2\sin^{\frac{9}{2}}\alpha\cos\beta}{\sin^{\frac{5}{2}}\alpha_0} = \xi_0 + \xi_1 T + \cdots, \tag{3.82}$$

where

$$\gamma_0 = \gamma|_{T=0} = \cos\alpha_0\sin\alpha_0\cos\beta, \quad \gamma_1 = \sin^2\alpha_0(1-3\cos^2\alpha_0)\cos^2\beta, \tag{3.83}$$

$$\lambda_0 = \lambda|_{T=0} = -\sin\alpha_0\sin\beta, \quad \lambda_1 = 2\cos\alpha_0\sin^2\alpha_0\cos\beta\sin\beta, \tag{3.84}$$

$$\xi_0 = \xi|_{T=0} = -2\sin^2\alpha_0\cos\beta, \quad \xi_1 = -9\cos\alpha_0\sin^3\alpha_0\cos^2\beta. \tag{3.85}$$

Substituting (3.76), (3.77) and (3.80)—(3.82) into (3.15), and equating T^{-1}-order terms, we obtain

$$-\frac{1}{4\eta}\left[\frac{\partial(\psi^{(0)},\omega^{(1,0)})}{\partial(\eta,\theta)} + \frac{\partial(\psi^{(1,1)},\omega^{(0,0)})}{\partial(\eta,\theta)}\right] - \epsilon\tfrac{1}{2}\eta\partial_\eta\omega^{(1,0)} - \epsilon\tfrac{1}{4}\nabla_\eta^2\omega^{(1,0)} = \epsilon L_{10}\omega^{(0,0)}, \tag{3.86}$$

where

$$L_{10} = \tfrac{1}{2}[\gamma_0(-\sin 2\theta\,\partial_\theta + \eta\cos 2\theta\,\partial_\eta) + \lambda_0(\cos 2\theta\,\partial_\theta + \eta\sin 2\theta\,\partial_\eta - \partial_\theta)] \tag{3.87}$$

and

$$\omega^{(0,0)}(\eta) = T\omega^{(0)}(\eta) = \frac{1}{4\pi}\mathrm{e}^{-\eta^2}. \tag{3.88}$$

At T^0-order of (3.15), we have

$$-\frac{1}{4\eta}\left[\frac{\partial(\psi^{(0)},\omega^{(1,1)})}{\partial(\eta,\theta)} + \frac{\partial(\psi^{(1,2)},\omega^{(0,0)})}{\partial(\eta,\theta)}\right] + \epsilon(1-\tfrac{1}{2}\eta\partial_\eta)\omega^{(1,1)} - \epsilon\tfrac{1}{4}\nabla_\eta^2\omega^{(1,1)}$$
$$= \epsilon L_{11}\omega^{(0,0)} + \epsilon^2 L_{20}u^{(0)} + \epsilon^2 2\gamma_0\lambda_0, \tag{3.89}$$

where

$$L_{11} = \tfrac{1}{2}[\gamma_1(-\sin 2\theta\,\partial_\theta + \eta\cos 2\theta\,\partial_\eta) + \lambda_1(\cos 2\theta\,\partial_\theta + \eta\sin 2\theta\,\partial_\eta - \partial_\theta)], \tag{3.90}$$

$$L_{20} = \xi_0[\cos\theta\,\partial_\theta + \sin\theta\,(\eta\partial_\eta + 1)]. \tag{3.91}$$

The right-hand sides of (3.86) and (3.89) represent the effects of the simple shear on the fluctuation vorticity. Asymptotic solutions to (3.86) and (3.89) at large Reynolds numbers ($Re \gg 1$, $\epsilon \ll 1$) are derived in Appendices A and B. Here, we summarize the results.

First, an asymptotic solution to (3.86) is written as

$$\omega^{(1,0)} = -\tfrac{1}{4}\nabla_\eta^2\psi^{(1,1)} = \epsilon B_0 M_0(\eta)\sin(2\theta - \phi_0), \tag{3.92}$$

where

$$M_0(\eta) = -\frac{\eta^2}{e^{\eta^2} - 1}\left(\eta^2 - f_1(\eta)\right), \tag{3.93}$$

and

$$B_0 = (\gamma_0^2 + \lambda_0^2)^{\frac{1}{2}}, \quad \phi_0 = \arctan\left(\frac{\lambda_0}{\gamma_0}\right) \tag{3.94}$$

(see Appendix A). Real function $f_1(\eta)$ is determined by differential equation (A.9). As $\eta \to 0$, $M_0(\eta)$ approaches zero as

$$M_0(\eta) \approx (a-1)\eta^2, \tag{3.95}$$

where a is a constant (see (A.13)). For large values of η, on the other hand, $M_0(\eta)$ behaves as

$$M_0(\eta) \approx -\eta^4 e^{-\eta^2}, \tag{3.96}$$

and so $|M_0(\eta)|$ decreases rapidly as $\eta \to \infty$. As shown in figure 11, $M_0(\eta)$ is negative and has a single peak at $\eta = O(1)$.

Next, an asymptotic solution to (3.89) is written as

$$\omega^{(1,1)} = \epsilon M_1(\eta) + \epsilon\,\mathrm{Real}\,[M_2(\eta)e^{-i2\theta}], \tag{3.97}$$

where

$$M_1(\eta) = 2\gamma_0\lambda_0 + \frac{8\xi_0 \cos\beta\eta^2}{Re} - \xi_0 D_0 \frac{8\eta^2}{Re}\left[\sin\left(\frac{Re}{4\eta^2}+\varphi_0\right) - \frac{Re}{8\eta^2}\cos\left(\frac{Re}{4\eta^2}+\varphi_0\right)\right]\exp\left(-\frac{Re^2}{48\eta^6}\right) \tag{3.98}$$

and

$$M_2(\eta) = \begin{cases} \mathrm{i}e^{-\mathrm{i}\phi_1} B_1 M_0(\eta) & \text{for } \eta = O(1), \\ -\mathrm{i}\xi_0 D_0 e^{\mathrm{i}\varphi_0}\dfrac{4\eta^2}{Re} \times \left[\left(1+\dfrac{\mathrm{i}Re}{4\eta^2}\right)\exp\left(\dfrac{\mathrm{i}Re}{4\eta^2}-\dfrac{Re^2}{48\eta^6}\right) - \exp\left(\dfrac{\mathrm{i}Re}{2\eta^2}-\dfrac{Re^2}{12\eta^6}\right)\right] & \text{for } \eta \gg 1 \end{cases} \tag{3.99}$$

with

$$B_1 = (\gamma_1^2+\lambda_1^2)^{\frac{1}{2}}, \quad \phi_1 = \arctan\left(\frac{\lambda_1}{\gamma_1}\right) \tag{3.100}$$

(see Appendix B). Note that for $\eta = O(1)$, $M_2(\eta)$ is expressed in terms of $M_0(\eta)$. For $\eta \ll Re^{\frac{1}{3}}$, $M_1(\eta)$ behaves as

$$M_1 \approx 2\gamma_0\lambda_0 + \frac{8\xi_0\cos\beta\eta^2}{Re}, \tag{3.101}$$

while $M_2(\eta)$ is exponentially small. For $\eta \gg Re^{\frac{1}{2}}$, on the other hand, both of them approach zero algebraically as

$$M_1 \approx -\frac{\xi_0 Re^2 \cos\alpha_0 \sin\beta}{96\eta^4}, \tag{3.102}$$

$$M_2 \approx -\frac{\mathrm{i}\xi_0 Re D_0 e^{\mathrm{i}\varphi_0}}{8\eta^2}. \tag{3.103}$$

In figures 12 and 13, we show asymptotic solutions (3.98) and (3.99) at $Re = 1\,000$ respectively for the cyclonic ($\alpha_0 = \arctan\sqrt{2}$, $\beta = -\frac{1}{4}\pi$), neutral ($\alpha_0 = \frac{1}{4}\pi$, $\beta = 0$), and anti-cyclonic ($\alpha_0 = \arctan\sqrt{2}$, $\beta = \frac{1}{4}\pi$) cases. Function $M_1(\eta)$, which represents the θ-averaged structure of the higher-order axial vorticity, takes a significant negative peak at a relatively large value of

η. As η decreases, it oscillates and then approaches a constant $2\gamma_0\lambda_0$, which is positive, zero or negative according to a cyclonic, neutral or anti-cyclonic case. Phases in the oscillation of $M_1(\eta)$ and $M_2(\eta)$ depend on the values of φ_0. Peak positions of $M_1(\eta)$ and $M_2(\eta)$ in a cyclonic case ($\varphi_0 > \frac{1}{2}\pi$) are located farther away from the vortex tube as compared with those in a neutral case ($\varphi_0 = \frac{1}{2}\pi$) while those in an anti-cyclonic case ($\varphi_0 < \frac{1}{2}\pi$) are located nearer.

At this level of approximation, (3.77), (3.92) and (3.97) provide $\omega^{(1)}$ up to the order of T. Remembering (2.40) and using an expansion for dimensionless form of (2.32)

$$A(t) = 1 + \gamma_0 T + \cdots, \tag{3.104}$$

we have the higher-order axial vorticity

$$A(t)\omega^{(1)} = \omega^{(1,0)} + (\gamma_0\omega^{(1,0)} + \omega^{(1,1)})T + O(T^2). \tag{3.105}$$

For $\eta \lesssim Re^{\frac{1}{4}}$, it follows from (3.92) and (3.97) that

$$A(t)\omega^{(1)} \approx \epsilon M_0(\eta)\left[B_0\sin(2\theta - \phi_0) + T\mathrm{d}_T\left(B(t)\sin(2\theta - \phi(t))\right)|_{T=0}\right] + \epsilon T 2\gamma_0\lambda_0, \tag{3.106}$$

where we have used relation

$$B_1\sin(2\theta - \phi_1) = \mathrm{d}_T\left[B(t)\sin(2\theta - \phi(t))\right]|_{T=0} - \gamma_0 B_0\sin(2\theta - \phi_0) \tag{3.107}$$

with

$$B(t) = \left(\gamma(t)^2 + \lambda(t)^2\right)^{\frac{1}{2}} = |\sin\alpha|(\cos^2\alpha\cos^2\beta + \sin^2\beta)^{\frac{1}{2}} \tag{3.108}$$

and

$$\phi(t) = \arctan\left(\frac{\lambda(t)}{\gamma(t)}\right) = \arctan\left(\frac{-\sin\beta}{\cos\alpha\cos\beta}\right) \quad (-\pi \le \phi(t) \le \pi), \tag{3.109}$$

which represents an angle from the x_2-axis to a projection of the X_2-axis on the normal (x_2, x_3)-plane (see (2.2) and (2.3)). Solution (3.106) represents the leading and first orders of a Taylor

expansion of

$$A(t)\omega^{(1)} = \epsilon M_0(\eta)B(t)\sin(2\theta - \phi(t)) + \epsilon(A(t)\lambda_0 - \lambda(t)). \tag{3.110}$$

In the near region of $\eta \lesssim Re^{\frac{1}{4}}$, we can drop the second term on the right-hand side of (3.15), which is exponentially small as $Re \to \infty$ (see §3.4). Then, by expanding $\omega^{(1)}$ in a power series of ϵ, we may obtain (3.110) without the assumption that $T \ll 1$.

The first term on the right-hand side of (3.110) represents a quadrupole-type distribution, which means a deformation of the vortex core into an elliptical shape by the effect of the simple shear (Moffatt, Kida & Ohkitani 1994). The major and minor axes of the resulting elliptical core are aligned at an angle of $\theta = \frac{1}{2}\phi(t) + \frac{1}{2}\pi \pm \frac{1}{4}\pi$, respectively. If the normal velocity components, $(\overline{u}_2, \overline{u}_3)$, of the simple shear flow relative to the structural coordinate system are decomposed into symmetric and anti-symmetric tensors, we find that the symmetric one, which represents straining flow, has a principal direction with a positive rate of strain at an angle of $\theta = \frac{1}{2}\phi(t) + \frac{1}{2}\pi$ (the values of rates of strain which are normalized by the uniform shear rate S are $\frac{1}{2}(-\gamma(t) \pm B(t))$). Therefore, the major and minor axes of the ellipse are inclined from the direction of strain by $\pm\frac{1}{4}\pi$, respectively (Moffatt, Kida & Ohkitani 1994). This quadrupole distribution of vorticity, which does not include the stretch factor $A(t)$, is not affected by the axial component of the simple shear stress. In the case of $\alpha = 0$, which was considered by Moore (1985), the vortex tube is aligned with the simple shear flow and therefore the vortex core is not deformed ($B(t) \equiv 0$).

The second term on the right-hand side of (3.110) represents the stretching of the axial vorticity component of the simple shear by the axial stress (see §4.2).

4. Physical interpretation

A physical interpretation of the asymptotic solutions derived in §3 will be given in this section to understand the structure of vorticity field and the physical process. We restore here dimensional variables, following Table 2, as

$$T = T^*/S, \quad R = (\nu/S)^{\frac{1}{2}} R^*, \quad \omega_1' = \epsilon^{-1} S \omega_1'^* \quad u_1' = (\nu S)^{\frac{1}{2}} u_1'^*. \tag{4.1}$$

A similarity variable η is then $\eta = R^*/(2T^{*\frac{1}{2}}) = R/(2(\nu T)^{\frac{1}{2}})$. Recall that the asterisks, which are attached to dimensionless variables, have been dropped in §3.

4.1. Structure of vorticity field

We first express vorticity field in physical space (R, θ, T) and discuss its structure. The axial component of vorticity fluctuation in the near region of $R \lesssim Re^{\frac{1}{4}}(\nu T)^{\frac{1}{2}}$ is written, using (3.22) and (3.110), as

$$\omega_1' \approx \frac{\Gamma A(t)}{4\pi\nu T} \exp\left(-\frac{R^2}{4\nu T}\right) + SM_0 \left(\frac{R}{2(\nu T)^{\frac{1}{2}}}\right) B(t) \sin(2\theta - \phi(t)) + S(A(t)\lambda_0 - \lambda(t)). \tag{4.2}$$

This equation tells us that the vortex tube is diffused, stretched and deformed by effects of viscosity and the simple shear. In a stationary coordinate system the vortex tube also rotates toward the streamwise (X_1) direction with an angular velocity given by (2.19). The normal components of fluctuation vorticity, $\omega_2' \approx \partial_3 u_{1p}'$ and $\omega_3' \approx -\partial_2 u_{1p}'$, on the other hand, cancel out with those of the simple shear vorticity so that the normal component of the total vorticity disappears and vorticity vectors are aligned with the axial direction. This alignment of a vortex tube and vorticity vectors has been observed in homogeneous isotropic turbulence as well as in homogeneously sheared turbulence and near-wall turbulence (see She, Jackson & Orszag

(1990); Kida & Tanaka 1994; Bernard, Thomas & Handler 1993). Disappearance of the normal vorticity leads to stretching of the axial component of the simple shear vorticity, which is represented by $S(A(t)\lambda_0 - \lambda(t))$ (see §4.2 for the mechanism). Note that this effect disappears when the vortex tube is not inclined vertically ($\alpha = 0$ or $\beta = \pm\frac{1}{2}\pi$), or when it is not inclined to the spanwise (X_3) direction ($\alpha = 0$ or $\beta = 0$).

In the far region of $R \gg Re^{\frac{1}{4}}(\nu T)^{\frac{1}{2}}$, the axial vorticity of the vortex tube itself is exponentially small, and therefore it follows from (3.105), (3.97)—(3.99) that

$$\begin{aligned}\omega_1' \approx\ & 2S^2T\gamma_0\lambda_0 + S^2\xi_0\frac{4\pi R^2}{\Gamma}\cos\beta \\ & + S^2\xi_0 D_0\left[2T\cos\left(\frac{\Gamma T}{2\pi R^2}+\varphi_0-\theta\right)\cos\theta - \frac{4\pi R^2}{\Gamma}\sin\left(\frac{\Gamma T}{2\pi R^2}+\varphi_0\right)\right. \\ & \left. + \frac{2\pi R^2}{\Gamma}\sin\left(\frac{\Gamma T}{2\pi R^2}+\varphi_0-2\theta\right)\right]\exp\left[-\frac{8\pi\nu}{3\Gamma}\left(\frac{\Gamma T}{2\pi R^2}\right)^3\right] \\ & - S^2\xi_0 D_0\frac{2\pi R^2}{\Gamma}\sin\left(\frac{\Gamma T}{\pi R^2}+\varphi_0-2\theta\right)\exp\left[-\frac{32\pi\nu}{3\Gamma}\left(\frac{\Gamma T}{2\pi R^2}\right)^3\right]. \end{aligned} \tag{4.3}$$

The normal components of the vorticity fluctuation, on the other hand, are expressed, using (3.67) and (3.68), as

$$\begin{aligned}\omega_2' \approx\ & S\cos\alpha_0\sin\beta \\ & - SD_0\left[\cos\left(\frac{\Gamma T}{2\pi R^2}+\varphi_0\right) + \frac{\Gamma T}{\pi R^2}\cos\left(\frac{\Gamma T}{2\pi R^2}+\varphi_0-\theta\right)\sin\theta\right]\exp\left[-\frac{8\pi\nu}{3\Gamma}\left(\frac{\Gamma T}{2\pi R^2}\right)^3\right] \end{aligned} \tag{4.4}$$

and

$$\begin{aligned}\omega_3' \approx\ & S\cos\beta \\ & - SD_0\left[\sin\left(\frac{\Gamma T}{2\pi R^2}+\varphi_0\right) - \frac{\Gamma T}{\pi R^2}\cos\left(\frac{\Gamma T}{2\pi R^2}+\varphi_0-\theta\right)\cos\theta\right]\exp\left[-\frac{8\pi\nu}{3\Gamma}\left(\frac{\Gamma T}{2\pi R^2}\right)^3\right]. \end{aligned} \tag{4.5}$$

The spatial distributions on the normal plane of fluctuation axial vorticity (4.3) are drawn in figure 14 for (a) cyclonic ($\alpha_0 = \arctan\sqrt{2}$, $\beta = -\frac{1}{4}\pi$), (b) neutral ($\alpha_0 = \frac{1}{4}\pi$, $\beta = 0$) and (c)

anti-cyclonic ($\alpha_0 = \arctan\sqrt{2}$, $\beta = \frac{1}{4}\pi$) cases at $Re = 1\,000$ together with projected vorticity lines. Vorticity of the vortex tube itself is not shown in these figures. Along vorticity lines at the outermost double spirals of high normal vorticity there are two crescent-shaped regions of strong negative axial vorticity, which is opposite to the vorticity of the vortex tube (cf. figure 9). Also commonly observed is relatively weak positive vorticity inside of the crescent-shaped regions of negative vorticity. Further inside, i.e. in a circular domain in the vicinity of a cyclonic (or anti-cyclonic) vortex tube the axial vorticity takes positive (or negative) values. Appearance of negative vorticity in far region as well as different signs of vorticity in the central region between cyclonic and anti-cyclonic vortex tubes were also observed in the θ-averaged structure (see figure 12).

4.2. Expulsion of normal vorticity and stretch of axial vorticity

Here, we discuss briefly a close relation between expulsion of normal vorticity around a vortex tube and stretch-and-intensification of axial vorticity. In a stationary frame the vorticity equation is written as

$$\frac{\mathrm{D}\boldsymbol{\omega}}{\mathrm{D}t} \equiv [\partial_t + (\boldsymbol{u}\cdot\nabla)]\,\boldsymbol{\omega} = (\boldsymbol{\omega}\cdot\nabla)\boldsymbol{u} + \nu\nabla^2\boldsymbol{\omega}. \tag{4.6}$$

Only the tilting-and-stretching term, the first term on the right-hand side of this equation, is responsible to the vorticity intensification. For a simple shear flow ($\boldsymbol{U} = SX_2\widehat{\boldsymbol{X}}_1$ and $\nabla\times\boldsymbol{U} = -S\widehat{\boldsymbol{X}}_3$), it vanishes identically, which means no vortex stretching. As was shown in §3.4, in the near field ($r \lesssim (\Gamma/\nu)^{\frac{1}{4}}(\nu t)^{\frac{1}{2}}$) of a straight vortex tube the normal component of the simple shear vorticity is expelled by viscous cancellation of tightly wrapped vorticity lines of opposite directions and only the axial component $(\nabla\times\boldsymbol{U})\cdot\widehat{\boldsymbol{x}}_1 = -S(\widehat{\boldsymbol{X}}_3\cdot\widehat{\boldsymbol{x}}_1)$ survives there.

The axial component of the tilting-and-stretching term is then estimated as

$$(\nabla \times \boldsymbol{U}) \cdot \hat{\boldsymbol{x}}_1 \partial_1 U_1 = -S^2 (\widehat{\boldsymbol{X}}_3 \cdot \hat{\boldsymbol{x}}_1)(\widehat{\boldsymbol{X}}_2 \cdot \hat{\boldsymbol{x}}_1)(\widehat{\boldsymbol{X}}_1 \cdot \hat{\boldsymbol{x}}_1), \tag{4.7}$$

which is proportional to the product of the three direction cosines of the axial vector $\hat{\boldsymbol{x}}_1$. It takes a maximum (or minimum) value $(\pm S^2/3^{\frac{3}{2}})$ for

$$\hat{\boldsymbol{x}}_1 = \frac{1}{\sqrt{3}}(\widehat{\boldsymbol{X}}_1 + \widehat{\boldsymbol{X}}_2 \mp \widehat{\boldsymbol{X}}_3). \tag{4.8}$$

The upper (or lower) sign represents a cyclonic (or anti-cyclonic) vortex tube whose spanwise component of vorticity has the same (or opposite) sign as the simple shear vorticity. As a consequence, a cyclonic vortex tube is intensified while an anti-cyclonic one is weakened (see the near regions of cyclonic and anti-cyclonic vortex tubes in figure 14). In near-wall turbulence, streamwise vortex tubes often take a cyclonic inclination with respect to the mean shear vorticity (see Miyake & Tsujimoto 1996), which may be connected with the above mechanism of selective intensification of a cyclonic vortex.

4.3. Wrap and tilt of vorticity lines and generation of axial vorticity

We discuss here the generation process of the axial vorticity through wrapping and tilting of vorticity lines in the far region of $R \gg Re^{\frac{1}{4}}(\nu T)^{\frac{1}{2}}$. Recall that the dominant contributor to the production of the axial vorticity is the tilting of the x_3-component of the simple shear vorticity by the velocity fluctuation (which is the second term in the right-hand side of (2.23)). Vorticity lines are wrapped around a vortex tube by a swirling motion to form spiral layers of high normal vorticity, which in turn induce axial shear flows which tilt the simple shear vorticity toward the axial direction. If the velocity gradient $\partial_3 u_1'$ $(= \omega_2')$ in the spirals is positive (or negative),

the x_3-component of the simple shear vorticity, the sign of which is negative, is tilted to the positive (or negative) axial direction to generate the negative (or positive) axial vorticity (see figure 15). As was mentioned in relation with figure 9, ω_2' is positive in the outermost spirals of intense normal vorticity, which leads to the generation of the crescent-shaped regions of strong negative axial vorticity in figure 14.

The spatial distributions of the axial and normal components of fluctuation vorticity ω_1' and $-\omega_2'$ (n.b. the minus sign) are compared in figures 16 for the neutral case ($\alpha_0 = \frac{1}{4}\pi$, $\beta = 0$). Here, two regions of (a, b) $R = O\left(Re^{\frac{1}{2}}(\nu T)^{\frac{1}{2}}\right)$ and (c, d) $R = O\left(Re^{\frac{1}{3}}(\nu T)^{\frac{1}{2}}\right)$ are shown at $Re = 1\,000$. We can see that the two components vary almost in phase in the far region (c.f. (a) and (b)), whereas the phase of the axial component is nearly $\frac{1}{2}\pi$ in advance clockwise compared with that of the normal one in the near region (c.f. (c) and (d)). This phase difference is due to the advection by the swirling flow induced by a vortex tube (see below).

In the far region $R \gg Re^{\frac{1}{2}}(\nu T)^{\frac{1}{2}}$ (or $\Gamma T/R^2 \ll 1$) the three components of fluctuation vorticity (4.3)—(4.5) are written as

$$\omega_1' \approx S^2 \xi_0 D_0 \frac{\Gamma T^2}{4\pi R^2} \sin(\varphi_0 - 2\theta), \tag{4.9}$$

$$\omega_2' \approx S D_0 \frac{\Gamma T}{2\pi R^2} \sin(\varphi_0 - 2\theta), \tag{4.10}$$

$$\omega_3' \approx S D_0 \frac{\Gamma T}{2\pi R^2} \cos(\varphi_0 - 2\theta). \tag{4.11}$$

Equations (4.9) and (4.10) show that the phases of ω_1' and $-\omega_2'$ coincide with each other since $\xi_0 \leq 0$. This is because in this region, the effect of advection by the swirling flow is negligibly small and thus the time-derivative term of ω_1' should be balanced with the production term $S\xi\omega_2'$ (see (4.26) below). For $Re^{\frac{1}{2}}(\nu T)^{\frac{1}{2}} \gg R \gg Re^{\frac{1}{4}}(\nu T)^{\frac{1}{2}}$ (or $\Gamma T/R^2 \gg 1$), on the other

hand, we have

$$\omega_1' \approx 2S^2T\gamma_0\lambda_0$$
$$+2S^2T\xi_0 D_0 \cos\left(\frac{\Gamma T}{2\pi R^2}+\varphi_0-\theta\right)\cos\theta\exp\left[-\frac{8\pi\nu}{3\Gamma}\left(\frac{\Gamma T}{2\pi R^2}\right)^3\right], \tag{4.12}$$

$$\omega_2' \approx -SD_0\frac{\Gamma T}{\pi R^2}\cos\left(\frac{\Gamma T}{2\pi R^2}+\varphi_0-\theta\right)\sin\theta\exp\left[-\frac{8\pi\nu}{3\Gamma}\left(\frac{\Gamma T}{2\pi R^2}\right)^3\right], \tag{4.13}$$

$$\omega_3' \approx +SD_0\frac{\Gamma T}{\pi R^2}\cos\left(\frac{\Gamma T}{2\pi R^2}+\varphi_0-\theta\right)\cos\theta\exp\left[-\frac{8\pi\nu}{3\Gamma}\left(\frac{\Gamma T}{2\pi R^2}\right)^3\right]. \tag{4.14}$$

By comparing (4.12) and (4.13), we can see that along a spiral of $(\Gamma T/2\pi R^2)+\varphi_0-\theta=$ const. there is the phase advance of an angle of $\frac{1}{2}\pi$ in ω_1' relative to $-\omega_2'$ (or $S\xi\omega_2'$, i.e. the production term). This phase difference is a result of the advection by the axi-symmetric swirling motion $(\Gamma/2\pi R^2)\partial_\theta\omega_1'$ which is effective at $R \lesssim Re^{\frac{1}{2}}(\nu T)^{\frac{1}{2}}$ (see (4.26) below).

The generation of $\omega_2' > 0$ and $\omega_1' < 0$ in the crescent-shaped regions of strong vorticity implies that in the stationary coordinate system $OX_1X_2X_3$ the streamwise component of vorticity, which is equal to $(\omega_1'\cos\alpha - \omega_2'\sin\alpha)$ and is opposite to that of the vortex tube, is generated along the outermost spiral vortex layers. Recently, Sendstad & Moin (1992) and Miyake & Tsujimoto (1996) observed that streamwise vorticity of opposite sign appears around the near-wall streamwise vortex tube and it develops into a new streamwise vortex. The present wrapping and tilting mechanism of vorticity lines by a vortex tube is expected to express the regeneration process of streamwise vortices in near-wall turbulence.

The three-dimensional structure of wrapped vorticity lines around a vortex tube in a simple shear is drawn in figures 17 for (a) cyclonic ($\alpha_0 = \arctan\sqrt{2}$, $\beta = -\frac{1}{4}\pi$), (b) neutral ($\alpha_0 = \frac{1}{4}\pi$, $\beta = 0$) and (c) anti-cyclonic ($\alpha_0 = \arctan\sqrt{2}$, $\beta = \frac{1}{4}\pi$) cases at $ST = 1$ and $Re = 1\,000$. They are obtained by numerical integration of the total vorticity given by adding the corresponding

components of the simple shear vorticity to (4.3)—(4.5). The vortex tubes are represented by isosurfaces of $R = (\nu T)^{\frac{1}{2}}$, and vorticity lines which starts at different points are labeled with letters A—E. Contour lines of $(\omega_2^2 + \omega_3^2)^{\frac{1}{2}} = 2S$, which represent the double spirals of high normal vorticity, are also drawn in the normal (x_2, x_3)-plane.

In the far region the vortex tube wraps and stretches vorticity lines to intensify the normal component of vorticity so that wrapped vorticity lines tend to be perpendicular to the vortex tube. As vorticity lines are further and further wrapped, the negative axial vorticity is generated and thus vorticity lines are tilted toward the axial direction. In the near region, on the other hand, the normal vorticity component is rapidly dissipated owing to the viscous cancellation of tightly wrapped vorticity of alternate sign, and eventually only the axial component of the simple shear is left and stretched. Therefore, vorticity lines near a cyclonic (or anti-cyclonic) vortex turn to the axial direction and tend to become parallel (or anti-parallel) to the vortex tube.

In the stationary coordinate system $OX_1X_2X_3$, vorticity vectors at the outermost spirals of strong vorticity region line up in the direction of $X_1 < 0$ and $X_3 < 0$ both in the upper and lower (the upstream and downstream) sides of a cyclonic vortex (figure 18). This is because, as mentioned above, vorticity lines tend to be perpendicular to the vortex tube and tilted toward the axial direction due to the generation of negative axial vorticity. Therefore, the vorticity vector of the cyclonic vortex tube, which has positive streamwise (X_1) and negative spanwise (X_3) components, and the resulting vorticity vectors on the upstream and downstream sides of it take a zig-zag arrangement in the streamwise direction. Recently, Miyake & Tsujimoto (1996) observed that the near-wall cyclonic streamwise vortices actually take this type of arrangement

in their regeneration process.

4.4. Spiral vortex layers

The asymptotic analysis at $St \ll 1$ described in §3 is exact but not so simple to understand the physical process involved. In this subsection, we focus only the region of $(\Gamma/\nu)^{\frac{1}{4}}(\nu t)^{\frac{1}{2}} \ll r \ll (\Gamma/S)^{\frac{1}{2}}$ to discuss intuitively the generation of spiral vortex layers without the short-time assumption that $St \ll 1$.

The flow structure in the far region of $r \gg (\Gamma/\nu)^{\frac{1}{4}}(\nu t)^{\frac{1}{2}}$ may be analysed more simply by replacing the vortex tube with a filament. Separating the contribution from the vortex filament in the streamfunction as

$$\psi = -\frac{\Gamma}{2\pi}\ln r + \psi', \tag{4.15}$$

and substituting it into (2.23) and (2.24), we obtain

$$\partial_t\omega_1' - \frac{\partial(\psi',\omega_1')}{\partial(x_2,x_3)} + \frac{\Gamma}{2\pi r^2}\partial_\theta\omega_1' - S\sin\alpha(\cos\alpha\cos\beta\, x_2 - \sin\beta\, x_3)\partial_2\omega_1'$$
$$= S\gamma(t)\omega_1' + S\xi(t)\partial_3 u_1' + \nu\nabla_\perp^2\omega_1' \tag{4.16}$$

and

$$\partial_t u_1' - \frac{\partial(\psi',u_1')}{\partial(x_2,x_3)} + \frac{\Gamma}{2\pi r^2}\partial_\theta u_1' - S\sin\alpha(\cos\alpha\cos\beta\, x_2 - \sin\beta\, x_3)\partial_2 u_1'$$
$$= -S\gamma(t)u_1' + \frac{\Gamma S}{2\pi r^2}(\cos\alpha\sin\beta\, x_2 + \cos\beta\, x_3) - S(\cos\alpha\sin\beta\,\partial_2 + \cos\beta\,\partial_3)\psi' + \nu\nabla_\perp^2 u_1'. \tag{4.17}$$

These equations are supplemented by initial conditions, $\omega_1' = 0$ and $u_1' = 0$.

We first consider a behaviour of the velocity field deformed by a strong vortex filament, and suppose that

$$\frac{\Gamma}{\nu} \gg 1. \tag{4.18}$$

Within $r \ll (\Gamma/S)^{\frac{1}{2}}$, the velocity induced by the filament dominates the simple shear velocity. It is the first and third terms on the left-hand side and the second term on the right-hand side that are dominant in (4.17) except for the viscous term which will be taken into account below. Then we have

$$\partial_t u_1' + \frac{\Gamma}{2\pi r^2}\partial_\theta u_1' = \frac{\Gamma S}{2\pi r^2}(\cos\alpha \sin\beta\, x_2 + \cos\beta\, x_3). \tag{4.19}$$

This has a solution

$$u_1' = SD_0 r \sin\left(\frac{\Gamma t}{2\pi r^2} + \varphi_0 - \theta\right) - SD(t) r \sin(\varphi(t) - \theta), \tag{4.20}$$

which represents spiral vortex layers, where D_0 and φ_0, and $D(t)$ and $\varphi(t)$ are given by (3.4) and (2.38), respectively.

In order to take account of the effect of viscous diffusion, we introduce unknown functions $s_1(r,t)$ and $s_2(r,t)$ as

$$u_1' = s_1(r,t)\cos\left(\theta - \frac{\Gamma t}{2\pi r^2}\right) + s_2(r,t)\sin\left(\theta - \frac{\Gamma t}{2\pi r^2}\right) - SD(t) r \sin(\varphi(t) - \theta). \tag{4.21}$$

In the region of $r \gg (\Gamma/\nu)^{\frac{1}{4}}(\nu t)^{\frac{1}{2}}$ (which can exist if $S\,t \ll (\Gamma/\nu)^{\frac{1}{2}}$) the viscous term may be approximated by

$$\nu\nabla_\perp^2 u_1' \approx -4\nu\left(\frac{\Gamma t}{2\pi r^3}\right)^2 \left[s_1 \cos\left(\theta - \frac{\Gamma t}{2\pi r^2}\right) + s_2 \sin\left(\theta - \frac{\Gamma t}{2\pi r^2}\right)\right]. \tag{4.22}$$

Substituion of (4.21) and (4.22) into (4.19) added the viscous term gives a set of differential equations for s_1 and s_2, which are solved easily under initial condition $u_1' = 0$, i.e. $s_1|_{t=0} = Sr\cos\beta$, $s_2|_{t=0} = -Sr\cos\alpha_0 \sin\beta$ to yield

$$u_1' = SD_0 r \sin\left(\frac{\Gamma t}{2\pi r^2} + \varphi_0 - \theta\right) \exp\left[-\frac{8\pi\nu}{3\Gamma}\left(\frac{\Gamma t}{2\pi r^2}\right)^3\right] - SD(t) r \sin(\varphi(t) - \theta). \tag{4.23}$$

This is a viscous version of (4.20).

The x_2- and x_3-components of the fluctuation vorticity are then calculated to be

$$\omega_2' = \partial_3 u_1' = S\cos\alpha\sin\beta$$
$$-SD_0\left[\cos\left(\frac{\Gamma t}{2\pi r^2}+\varphi_0\right)+\frac{\Gamma t}{\pi r^2}\cos\left(\frac{\Gamma t}{2\pi r^2}+\varphi_0-\theta\right)\sin\theta\right]\exp\left[-\frac{8\pi\nu}{3\Gamma}\left(\frac{\Gamma t}{2\pi r^2}\right)^3\right] \qquad (4.24)$$

and

$$\omega_3' = -\partial_2 u_1' = S\cos\beta$$
$$-SD_0\left[\sin\left(\frac{\Gamma t}{2\pi r^2}+\varphi_0\right)-\frac{\Gamma t}{\pi r^2}\cos\left(\frac{\Gamma t}{2\pi r^2}+\varphi_0-\theta\right)\cos\theta\right]\exp\left[-\frac{8\pi\nu}{3\Gamma}\left(\frac{\Gamma t}{2\pi r^2}\right)^3\right], \qquad (4.25)$$

which agrees with (4.4) and (4.5) for $St \ll 1$. The x_2-component of the fluctuation vorticity (4.24) appears in axial-vorticity equation (4.16) as a source term.

In the near-field of $r \ll (\Gamma/S)^{\frac{1}{2}}$ and during $St \ll (\Gamma/\nu)^{\frac{1}{2}}$ the dominant terms in (4.16) are the first and third terms on the left-hand side and the second and third terms on the right-hand side. Then we have

$$\partial_t\omega_1' + \frac{\Gamma}{2\pi r^2}\partial_\theta\omega_1' = S\xi(t)\partial_3 u_1' + \nu\nabla_\perp^2\omega_1'. \qquad (4.26)$$

A solution to this equation under initial condition $\omega_1'|_{t=0} = 0$ is

$$\omega_1' = S(A(t)\lambda_0 - \lambda(t)) + \left[1+O\left(\frac{\nu}{\Gamma}\right)\right]S^2\xi(t)\frac{4\pi r^2}{\Gamma}\cos\beta$$
$$+S^2\xi(t)D_0\left[2t\cos\left(\frac{\Gamma t}{2\pi r^2}+\varphi_0-\theta\right)\cos\theta-\frac{4\pi r^2}{\Gamma}\sin\left(\frac{\Gamma t}{2\pi r^2}+\varphi_0\right)\right.$$
$$\left.+\frac{2\pi r^2}{\Gamma}\sin\left(\frac{\Gamma t}{2\pi r^2}+\varphi_0-2\theta\right)\right]\exp\left[-\frac{8\pi\nu}{3\Gamma}\left(\frac{\Gamma t}{2\pi r^2}\right)^3\right]$$
$$-S^2\xi(t)D_0\frac{2\pi r^2}{\Gamma}\sin\left(\frac{\Gamma t}{\pi r^2}+\varphi_0-2\theta\right)\exp\left[-\frac{32\pi\nu}{3\Gamma}\left(\frac{\Gamma t}{2\pi r^2}\right)^3\right] \qquad (4.27)$$

which agrees with (4.3) for $St \ll 1$. If we restrict ourselves in a period of $1 \lesssim St \ll (\Gamma/\nu)^{\frac{1}{2}}$ (and so the region of $(\Gamma/\nu)^{\frac{1}{4}}(\nu t)^{\frac{1}{2}} \ll r \ll (\Gamma/\nu)^{\frac{1}{2}}(\nu t)^{\frac{1}{2}}$), four terms containing $O(S^2r^2/\Gamma)$ may be neglected in (4.27).

It should be emphasized that solutions (4.24), (4.25) and (4.27) have been obtained for $(\Gamma/\nu)^{\frac{1}{4}}(\nu t)^{\frac{1}{2}} \ll r \ll (\Gamma/S)^{\frac{1}{2}}$ without the short-time assumption that $St \ll 1$. A similarity in the functional forms between asymptotic solutions (4.3)—(4.5) and (4.24), (4.25) and (4.27) suggests that the former may be approximated well even for $St \approx 1$.

The position of the maximum normal vorticity and spacing of the spirals are intuitively estimated as follows. The spirals of high normal vorticity is primarily generated by a strong swirling potential velocity induced by the vortex tube in the form (see the first term of (4.20))

$$\theta - \frac{\Gamma t}{2\pi r^2} = \text{const.} \tag{4.28}$$

The spacing Δr of the spiral is given by the change of r when angle θ changes by 2π, so that it follows from (4.28) that

$$\frac{\Gamma t}{r^3}\Delta r \approx 1. \tag{4.29}$$

The region in which viscous effects play a role is estimated by equating the viscous and the time-derivative terms

$$\frac{1}{t} \approx \nu \left(\frac{\Gamma t}{r^3}\right)^2, \tag{4.30}$$

or

$$r \approx \left(\frac{\Gamma}{\nu}\right)^{\frac{1}{3}} (\nu t)^{\frac{1}{2}}. \tag{4.31}$$

Combination of (4.29) and (4.31) yields

$$\Delta r = (\nu t)^{\frac{1}{2}}. \tag{4.32}$$

Finally, we discuss intuitively the order of magnitude of the axial vorticity generated through the tilting of the x_3-component of the simple shear vorticity by the spiral vortex layers. The

gradient of axial velocity across the spirals may be estimated, by using (4.29), as

$$\frac{u_1'}{\Delta r} \approx S\frac{\Gamma t}{r^2}, \tag{4.33}$$

which works to tilt the simple shear vorticity toward the axial direction. In the region of $(\Gamma/\nu)^{\frac{1}{2}}(\nu t)^{\frac{1}{2}} \gg r \gg (\Gamma/\nu)^{\frac{1}{4}}(\nu t)^{\frac{1}{2}}$ the time-scale of the time-derivative term is much smaller than that of the advection term by the swirling flow,

$$\frac{1}{t} \ll \frac{\Gamma}{r^2}, \tag{4.34}$$

so that the former may dominate the latter and balance with the production term in (4.26). Thus we have

$$\frac{\Gamma}{r^2}\omega_1' \approx S^2\frac{\Gamma t}{r^2}, \tag{4.35}$$

that is, the axial vorticity increases in time as

$$\omega_1' \approx S^2 t. \tag{4.36}$$

In the region of $r \approx (\Gamma/\nu)^{\frac{1}{2}}(\nu t)^{\frac{1}{2}}$ (which can exist if $S\,t \ll 1$), on the other hand, the two time-scales are comparable,

$$\frac{1}{t} \approx \frac{\Gamma}{r^2}, \tag{4.37}$$

and we have

$$\omega_1' \approx S^2 t \approx S^2\frac{\Gamma t^2}{r^2} \approx S^2\frac{r^2}{\Gamma}, \tag{4.38}$$

which increases with radial distance. Therefore, the magnitude of ω_1' can be strongest near the outermost spirals at least during the initial time $S\,t \ll 1$ of evolution because there is no spiral and so ω_1' decays at $r \gtrsim (\Gamma/\nu)^{\frac{1}{2}}(\nu t)^{\frac{1}{2}}$.

5. Concluding remarks

Asymptotic solutions describing the mutual interactions between a straight vortex tube of circulation Γ and a simple shear flow of shear rate S have been obtained at a large Reynolds number $\Gamma/\nu \gg 1$ and at an early time $St \ll 1$ of evolution. These solutions are expected to be useful for understanding of interactions of tube-like structures with background vorticity in real turbulent flows.

Let us now summarize the global structure of the present vorticity field in terms of the original physical coordinate r and time t. A thin strong straight vortex tube which starts with a filament is diffused by viscosity and the core size increases in time as $(\nu t)^{\frac{1}{2}}$ (see figure 19). This vortex tube induces an axi-symmetric swirling flow around it, which dominates the simple shear velocity in the near region where $r \ll (\Gamma/S)^{\frac{1}{2}}$. The simple shear vorticity (denoted by double arrows) is stretched and wrapped by this swirling flow to make double spirals around the vortex tube. The stretching (in planes normal to the vortex tube) of the vorticity lines is more effective and intensity of vorticity is enhanced more near the vortex tube because the swirling motion is more rapid there. Therefore the magnitude of the normal components of vorticity increases as it approaches the vortex tube. The rapid swirling motion around the vortex tube also makes the spirals to wind so tightly that viscous effects may become important there. Because the normal vorticity changes the direction alternately on the neighouring layers of spirals, viscous diffusion smooths out the vorticity in the region where $r \lesssim (\Gamma/\nu)^{\frac{1}{4}}(\nu t)^{\frac{1}{2}}$. This expulsion of normal vorticity around the vortex tube leads to a stretch-and-intensification of the axial-component of vorticity. This partial cancellation of vorticity by viscous diffusion has a counter effect against enhancement of normal vorticity due to stretching by the swirling

motion mentioned above. As a result, the magnitude of the normal vorticity has a peak at $r = O\left((\Gamma/\nu)^{\frac{1}{3}}(\nu t)^{\frac{1}{2}}\right)$, where the distance between neighbouring layers of spirals is of $O\left((\nu t)^{\frac{1}{2}}\right)$ (see (4.32)). The spirals of normal vorticity induce the axial shear velocity which changes the directions alternately at each successive spiral layer. This axial shear velocity works to tilt (the x_3-component of) the simple shear vorticity toward the axial direction. It is remarkable that the axial vorticity opposed to that of the vortex tube is being induced in the outermost layers of the spirals where the axial vorticity is strongest.

Applications of this analysis to real flows should be restricted by the assumption of uniformity of the fluctuation flow field along a vortex tube and by the initial condition (3.1). However, tube-like structures of concentrated intense vorticity in many turbulent flows are likely elongated rather straight so that the essential process of their vorticity interactions may be approximately described in terms of the present asymptotic solutions at $r \gg (\nu t)^{\frac{1}{2}}$. In the following we discuss a few of relevant aspects in the flow structure of the present asymptotic solutions and real turbulent flows.

First, it has been often observed that vorticity vectors align quite well with tube-like structures in the core region in spite of the presence of background vorticity in isotropic turbulence, homogeneous shear turbulence and near-wall turbulence (see She, Jackson & Orszag 1990; Kida & Tanaka 1994; Bernard, Thomas & Handler 1993). The expulsion of vorticity normal to a vortex tube (see §3.4) may explain this alignment of tube-like structures and vorticity vectors therein. Secondly, helically winding vorticity lines similar to those in figures 17 were observed in She, Jackson & Orszag (1990). In their numerical analysis of homogeneous isotropic turbulence, they showed that vorticity lines are wrapped around the vortex tube forming a spiral. The helically wrapping of vorticity lines was also observed around streamwise vortex tubes in

near-wall turbulence by Jiménez & Moin (1991). Thirdly, cyclonic vortex tubes, which are tilted toward the direction of the mean shear vorticity, have often been observed in near-wall turbulence (see Miyake & Tsujimoto 1996). The selective intensification of a cyclonic vortex tube (see §4.2) is conjectured to explain the dominance of this type of vortical structures in real shear flows. Fourthly, it has been also observed in near-wall turbulence that streamwise vorticity of the opposite sign is generated around a streamwise vortex tube to develop into a new streamwise vortex (Sendstad & Moin 1992; Miyake & Tsujimoto 1996) and that the streamwise vortices take a zig-zag arrangement in the streamwise direction in their regeneration process (Miyake & Tsujimoto 1996). In our analytical solution, as shown in figure 18, the streamwise component of vorticity vector in the most-intensified part has an opposite sign to that of the vortex tube, that is, they are oriented as in the same manner as the above zig-zag arrangement. All of these similarities between our analytical solution and the observations suggest that the wrapping, tilting and stretching mechanisms of vorticity lines associated with an oblique vortex tube may play a key role in the dynamics of vortex tubes in various kinds of turbulence.

Finally, we would like to stress that a vortex tube in a simple shear flow should be inclined from the streamwise direction both vertically and horizontally in order that all the three fundamental processes, i.e. wrapping, tilting and stretching, may take part in the vortex dynamics. In figure 20 illustrated are typical vorticity lines around (a) a spanwise, (b) a streamwise and (c) an oblique vortex tube in a simple shear flow. If a vortex tube is aligned with the spanwise direction ($\alpha = \frac{1}{2}\pi$, $\beta = \pm\frac{1}{2}\pi$), it is parallel to the background vorticity lines and thus they are neither wrapped, tilted nor stretched. If a vortex tube is aligned with the streamwise direction ($\alpha = 0$), it is stationary and perpendicular to background vorticity lines, so that vorticity lines are wrapped on planes normal to the tube but they are neither tilted nor stretched to the axial

direction. Only in the case of an oblique vortex tube inclined from the streamwise direction both vertically and horizontally, vorticity lines are wrapped around the vortex tube, and tilted and stretched to the axial direction so that the simple shear vorticity may be converted to the axial direction as well as the streamwise direction (see §§4.2 and 4.3). When a vortex tube is inclined only horizontally ($\alpha \neq \frac{1}{2}\pi$, $\beta = \pm\frac{1}{2}\pi$), the simple shear vorticity can be converted to the streamwise direction via the wrapping on the normal plane but not to the axial direction (see (2.23)). When a tube is not inclined to the spanwise direction ($\alpha \neq 0$, $\beta = 0$), the stretch-and-intensification of the axial component of the simple shear vorticity (see §4.2) is not observed.

G. K. appreciates helpful discussions with Professor K. Ayukawa, Ehime University, in the development of this study. This work was partially supported by a Grant-in-Aid for Scientific Research from the Ministry of Education, Science and Culture.

Appendix A. Solution to (3.86)

Since the leading-order solutions, $\omega^{(0,0)}$ and $\psi^{(0)}$, are independent of θ, (3.86) can be rewritten, using (3.78), as

$$\frac{1}{4\eta}\partial_\theta\left[\tfrac{1}{4}(\partial_\eta\psi^{(0)})\nabla_\eta^2\psi^{(1,1)}+(\partial_\eta\omega^{(0,0)})\psi^{(1,1)}\right]$$
$$=-\epsilon\tfrac{1}{8}\eta\partial_\eta\nabla_\eta^2\psi^{(1,1)}-\epsilon\tfrac{1}{16}\nabla_\eta^4\psi^{(1,1)}+\epsilon\tfrac{1}{2}B_0\eta(\partial_\eta\omega^{(0,0)})\,\mathrm{Real}\,[\mathrm{e}^{\mathrm{i}(2\theta-\phi_0)}], \tag{A.1}$$

where B_0 and ϕ_0 are given by (3.94). We then seek a solution to (A.1) in the form

$$\psi^{(1,1)}=\mathrm{Real}\,[F_1(\eta)\mathrm{e}^{\mathrm{i}(2\theta-\phi_0)}]. \tag{A.2}$$

Substituting (A.2) into (A.1), and using (3.24) and (3.88), we obtain

$$\epsilon\left[F_1^{\mathrm{iv}}+2\left(\eta+\frac{1}{\eta}\right)F_1'''+\left(2-\frac{9}{\eta^2}\right)F_1''-\frac{1}{\eta}\left(10-\frac{9}{\eta^2}\right)F_1'+\frac{16}{\eta^2}F_1\right]$$
$$-\frac{\mathrm{i}}{\pi}\left[\frac{1-\mathrm{e}^{-\eta^2}}{\eta^2}\left(F_1''+\frac{1}{\eta}F_1'-\frac{4}{\eta^2}F_1\right)+4\mathrm{e}^{-\eta^2}F_1\right]=-\epsilon\frac{4}{\pi}B_0\eta^2\mathrm{e}^{-\eta^2}, \tag{A.3}$$

where the right-hand side originates from the deformation of the spatial distribution of the axial vorticity in the (x_2,x_3)-plane by the simple shear (the first term in (3.7)). Boundary conditions to be imposed are that $TF_1(\eta)$ is regular at $\eta=0$ and $TF_1(\eta)\to 0$ as $\eta\to\infty$ (see (3.18)). For $\epsilon\ll 1$, we expand a solution to (A.3) in a power series of ϵ as

$$F_1=F_{10}+\epsilon F_{11}+\cdots. \tag{A.4}$$

Substituting (A.4) into (A.3), and equating ϵ^0-order terms, we find

$$F_{10}''+\frac{1}{\eta}F_{10}'-\frac{4}{\eta^2}F_{10}+\frac{4\eta^2}{\mathrm{e}^{\eta^2}-1}F_{10}=0. \tag{A.5}$$

This has a solution regular at $\eta=0$ as

$$F_{10}\approx a_2\eta^2\quad\text{as}\quad\eta\to 0, \tag{A.6}$$

where a_2 is a constant. However, the asymptotic behaviour at large η of this solution can be numerically shown to be

$$F_{10} \approx b_2 \eta^2 \quad \text{as } \eta \to \infty, \tag{A.7}$$

where b_2 is a zero or non-zero constant according as a_2 is zero or non-zero. Equation (A.7) implies that $TF_{10} \approx b_2 R^2/4$ as $\eta \to \infty$, which is inconsistent with the boundary condition unless $b_2 = 0$. Hence, we conclude that

$$F_{10}(\eta) \equiv 0. \tag{A.8}$$

At ϵ order, (A.3) is written as

$$f_1'' + \frac{1}{\eta} f_1' - \frac{4}{\eta^2} f_1 = \frac{4\eta^2}{\mathrm{e}^{\eta^2} - 1}(\eta^2 - f_1) \ (\equiv -4M_0(\eta), \ \text{say}), \tag{A.9}$$

where

$$\mathrm{Real}\,[F_{11}(\eta)] \equiv 0, \quad \mathrm{Imag}\,[F_{11}(\eta)] = -B_0 f_1(\eta) \tag{A.10}$$

and (A.8) has been used. Recall that (A.9) is identical with the first-order equation obtained by Moffatt, Kida & Ohkitani (1994) in their analysis of a large-Reynolds-number asymptotic solution for a non-axisymmetric Burgers vortex tube. For small η a solution regular at $\eta = 0$ is expanded as

$$f_1(\eta) = a\eta^2 + \tfrac{1}{3}(1-a)\left(\eta^4 - \tfrac{5}{16}\eta^6 + \cdots\right), \tag{A.11}$$

where a is a constant. For $\eta \gg 1$, it decays as

$$f_1(\eta) = \frac{b}{\eta^2} + O(\mathrm{e}^{-\eta^2}). \tag{A.12}$$

Constants a and b were numerically determined to be

$$a = -1.5259\cdots, \quad b = -4.3680\cdots \tag{A.13}$$

by Moffatt, Kida & Ohkitani (1994). By using (3.78), (A.2) and (A.9), we obtain (3.92) in §3.5 up to order ϵ.

Appendix B. Solution to (3.89)

Substitution of (3.25) and (3.78) into (3.89) gives

$$\frac{1}{4\eta}\partial_\theta\left[\tfrac{1}{4}(\partial_\eta\psi^{(0)})\nabla_\eta^2\psi^{(1,2)}+(\partial_\eta\omega^{(0,0)})\psi^{(1,2)}\right]$$
$$=\epsilon\tfrac{1}{4}(1-\tfrac{1}{2}\eta\partial_\eta)\nabla_\eta^2\psi^{(1,2)}-\epsilon\tfrac{1}{16}\nabla_\eta^4\psi^{(1,2)}+\epsilon\tfrac{1}{2}B_1\eta(\partial_\eta\omega^{(0,0)})\,\mathrm{Real}\,[\mathrm{e}^{-\mathrm{i}(2\theta-\phi_1)}]$$
$$-\epsilon^2\tfrac{1}{2}\xi_0\eta\,\mathrm{Real}\,[f'\mathrm{e}^{-\mathrm{i}2\theta}]+\epsilon^2\tfrac{1}{2}\xi_0\,\mathrm{Real}\,[2f+\eta f']+\epsilon^2 2\gamma_0\lambda_0, \tag{B.1}$$

where B_1 and ϕ_1 are given by (3.100). Suggested by the source terms in (B.1), we seek for a solution in the form

$$\psi^{(1,2)}=G_2(\eta)+\mathrm{Real}\,[F_2(\eta)\mathrm{e}^{-\mathrm{i}2\theta}]. \tag{B.2}$$

Substituting (B.2) into (B.1), and using (3.24) and (3.88), we obtain, for the θ-independent part,

$$M_1''+\left(2\eta+\frac{1}{\eta}\right)M_1'-4M_1=-2\xi_0\,\mathrm{Real}\,[2f+\eta f']-8\gamma_0\lambda_0, \tag{B.3}$$

where

$$\epsilon M_1(\eta)=-\tfrac{1}{4}\nabla_\eta^2 G_2=-\tfrac{1}{4}\left(G_2''+\frac{1}{\eta}G_2'\right) \tag{B.4}$$

is the θ-independent part of the vorticity associated with streamfunction G_2. The right-hand side of (B.3) originates from the production of the axial vorticity through the tilting of the x_2-component of the fluctuation vorticity by the simple shear, the tilting of the x_3-component of the simple shear vorticity via the velocity fluctuation, and the effect of frame rotation. On

the other hand, for the θ-dependent part, we obtain

$$\epsilon\left[F_2^{\mathrm{iv}}+2\left(\eta+\frac{1}{\eta}\right)F_2'''-\left(2+\frac{9}{\eta^2}\right)F_2''-\frac{1}{\eta}\left(14-\frac{9}{\eta^2}\right)F_2'+\frac{32}{\eta^2}F_2\right]$$
$$+\frac{\mathrm{i}}{\pi}\left[\frac{1-\mathrm{e}^{-\eta^2}}{\eta^2}\left(F_2''+\frac{1}{\eta}F_2'-\frac{4}{\eta^2}F_2\right)+4\mathrm{e}^{-\eta^2}F_2\right]=-\epsilon\frac{4}{\pi}B_1\mathrm{e}^{-\mathrm{i}\phi_1}\eta^2\mathrm{e}^{-\eta^2}-\epsilon^2 8\xi_0\eta f'. \quad \text{(B.5)}$$

There exist two different types of source terms on the right-hand side of (B.5). The first and second ones come from the deformation and the production of the axial vorticity by the simple shear, respectively.

B.1. θ-independent part

We consider here a solution to (B.3). Boundary conditions to be imposed are that $TM_1(\eta)$ is regular at $\eta=0$ and that $TM_1(\eta)\to 0$ as $\eta\to\infty$ (see (3.17)). The asymptotic expansion of the solution to (B.3) for small and large values of η may be obtained using (3.28) and (3.27). For $\eta \ll Re^{-\frac{1}{2}}$, we have

$$M_1(\eta)=2\gamma_0\lambda_0+m_0+(m_0-\xi_0\mathrm{Real}(c_0))\eta^2-\frac{Re\xi_0\mathrm{Imag}(c_0)}{16}\eta^4+\cdots \quad \text{(B.6)}$$

with some constant m_0, where c_0 is an exponentially small constant given by (3.57). For $\eta \gg Re^{\frac{1}{2}}$, using (3.4), we find

$$M_1(\eta)=-\xi_0\left(\frac{Re^2\cos\alpha_0\sin\beta}{96\eta^4}+\frac{18Re^2\cos\alpha_0\sin\beta-Re^3\cos\beta}{768\eta^6}+\cdots\right). \quad \text{(B.7)}$$

The homogeneous equation associated with (B.3) has two linearly independent solutions

$$M_{1a}=1+\eta^2, \quad M_{1b}=(1+\eta^2)\int_\eta^\infty \frac{\mathrm{e}^{-s^2}}{s(1+s^2)^2}\,\mathrm{d}s. \quad \text{(B.8)}$$

It can be shown that

$$\int_\eta^\infty \frac{\mathrm{e}^{-s^2}}{s(1+s^2)^2}\,\mathrm{d}s$$

$$= -\ln\eta + \int_1^\infty \frac{\mathrm{e}^{-s^2}}{s(1+s^2)^2}\,\mathrm{d}s + \int_0^1 \left[\frac{\mathrm{e}^{-s^2}}{s(1+s^2)^2} - \frac{1}{s}\right]\mathrm{d}s + O(\eta^2) \qquad (\text{for } \eta \ll 1), \quad \text{(B.9)}$$

and that

$$\int_\eta^\infty \frac{\mathrm{e}^{-s^2}}{s(1+s^2)^2}\,\mathrm{d}s = \frac{\mathrm{e}^{-\eta^2}}{2\eta^6}\left[1 - \frac{5}{\eta^2} + O\left(\frac{1}{\eta^4}\right)\right] \qquad (\text{for } \eta \gg 1). \quad \text{(B.10)}$$

By making use of (B.8), we can write a solution to inhomogeneous equation (B.3) as

$$M_1 = 2\gamma_0\lambda_0 + (c_{1a} + \widetilde{M}_{1a})M_{1a} + (c_{1b} + \widetilde{M}_{1b})M_{1b}, \quad \text{(B.11)}$$

where

$$\widetilde{M}_{1a}(\eta) = -2\xi_0 \int_0^\eta s\,\mathrm{e}^{s^2}\,\mathrm{Real}\,[2f(s) + sf'(s)]M_{1b}(s)\,\mathrm{d}s, \quad \text{(B.12)}$$

$$\widetilde{M}_{1b}(\eta) = 2\xi_0 \int_0^\eta s\,\mathrm{e}^{s^2}\,\mathrm{Real}\,[2f(s) + sf'(s)]M_{1a}(s)\,\mathrm{d}s. \quad \text{(B.13)}$$

Constants c_{1a} and c_{1b} are determined by invoking boundary conditions at $\eta = 0$ and ∞. For $\eta \ll 1$, since $f(\eta)$ and therefore the first term on the right-hand side of (B.3) are very small, we obtain, using (B.9) and (B.11), that

$$\begin{aligned} M_1 &\approx 2\gamma_0\lambda_0 + c_{1a}M_{1a} + c_{1b}M_{1b} \\ &\approx 2\gamma_0\lambda_0 + c_{1a} + c_{1b}\left\{-\ln\eta + \int_1^\infty \frac{\mathrm{e}^{-s^2}}{s(1+s^2)^2}\,\mathrm{d}s + \int_0^1 \left[\frac{\mathrm{e}^{-s^2}}{s(1+s^2)^2} - \frac{1}{s}\right]\mathrm{d}s\right\}. \end{aligned} \quad \text{(B.14)}$$

Thus, the regularity of M_1 at $\eta = 0$ requires

$$c_{1b} = 0. \quad \text{(B.15)}$$

By comparing (B.14) with (B.6), we find

$$m_0 = c_{1a}. \quad \text{(B.16)}$$

Since f is very small up to $\eta = O(Re^{\frac{1}{4}})$ (see §3.4), $\widetilde{M}_{1a}$ and $\widetilde{M}_{1b}$ may be evaluated to be

$$\widetilde{M}_{1a}(\eta)$$

$$\approx +2\xi_0 D_0 \int_0^\eta \frac{1}{s^3}\left(1 - \frac{4}{s^2}\right)\left[\cos\left(\frac{Re}{4s^2} + \varphi_0\right) + \frac{Re}{4s^2}\sin\left(\frac{Re}{4s^2} + \varphi_0\right)\right]\exp\left(-\frac{Re^2}{48s^6}\right)\mathrm{d}s, \quad \text{(B.17)}$$

$$\widetilde{M}_{1b}(\eta)$$

$$\approx -4\xi_0 D_0 \int_0^\eta s^3 \left(1+\frac{1}{s^2}\right)\left[\cos\left(\frac{Re}{4s^2}+\varphi_0\right)+\frac{Re}{4s^2}\sin\left(\frac{Re}{4s^2}+\varphi_0\right)\right]\exp\left(s^2-\frac{Re^2}{48s^6}\right)\,\mathrm{d}s \quad \text{(B.18)}$$

by using (3.63), (3.64), (B.8) and (B.10). After elementary calculation, we arrive at

$$\widetilde{M}_{1a}(\eta)$$

$$\approx -\xi_0 D_0 \left\{\frac{8}{Re}\left[\sin\left(\frac{Re}{4\eta^2}+\varphi_0\right)-\frac{Re}{8\eta^2}\cos\left(\frac{Re}{4\eta^2}+\varphi_0\right)\right]-\frac{16}{Re^2}\left[\left(\frac{Re^2}{16\eta^4}+2\right)\cos\left(\frac{Re}{4\eta^2}+\varphi_0\right)\right.\right.$$
$$\left.\left.+\frac{Re}{4\eta^2}\left(\frac{Re^2}{16\eta^4}+2\right)\sin\left(\frac{Re}{4\eta^2}+\varphi_0\right)+\cdots\right]\right\}\exp\left(-\frac{Re^2}{48\eta^6}\right), \quad \text{(B.19)}$$

$$\widetilde{M}_{1b}(\eta)$$

$$\approx -\xi_0 D_0 \left\{\eta^2\left[2\cos\left(\frac{Re}{4\eta^2}+\varphi_0\right)+\frac{Re}{2\eta^2}\sin\left(\frac{Re}{4\eta^2}+\varphi_0\right)\right]\exp\left(-\frac{Re^2}{48\eta^6}\right)\right.$$
$$\left.+\left[\left(4-\frac{Re^2}{8\eta^4}\right)\cos\left(\frac{Re}{4\eta^2}+\varphi_0\right)+\frac{Re}{\eta^2}\sin\left(\frac{Re}{4\eta^2}+\varphi_0\right)\right]\exp\left(-\frac{Re^2}{48\eta^6}\right)+\cdots\right\}\mathrm{e}^{\eta^2}. \quad \text{(B.20)}$$

For $\eta \gg Re^{\frac{1}{2}}$, (B.19) and (B.20) are reduced to

$$\widetilde{M}_{1a}(\eta) \approx -\xi_0 D_0\left[\frac{8\sin\varphi_0}{Re}-\frac{32\cos\varphi_0}{Re^2}+\frac{\cos\varphi_0}{\eta^2}-\frac{2\cos\varphi_0}{\eta^4}+\frac{Re^2\cos\varphi_0}{96\eta^6}+\cdots\right], \quad \text{(B.21)}$$

$$\widetilde{M}_{1b}(\eta) \approx -2\xi_0 D_0 \eta^2 \mathrm{e}^{\eta^2}\left[\cos\varphi_0+\frac{2\cos\varphi_0}{\eta^2}+\frac{Re^2\cos\varphi_0}{32\eta^4}+\cdots\right]. \quad \text{(B.22)}$$

Then, $\widetilde{M}_{1a}M_{1a}$ and $\widetilde{M}_{1b}M_{1b}$ can be written, using (B.8), (B.10), (B.21) and (B.22), as

$$\widetilde{M}_{1a}M_{1a} \approx -\xi_0 D_0\left\{\frac{8\sin\varphi_0}{Re}[1+O(Re^{-1})](1+\eta^2)+\cos\varphi_0-\frac{\cos\varphi_0}{\eta^2}+\frac{Re^2\cos\varphi_0}{96\eta^4}\right\}, \quad \text{(B.23)}$$

$$\widetilde{M}_{1b}M_{1b} \approx -\xi_0 D_0\frac{\cos\varphi_0}{\eta^2}. \quad \text{(B.24)}$$

It follows from (3.4), (B.8), (B.10), (B.11), (B.15), (B.23) and (B.24) that

$$M_1 \approx \left[c_{1a}-\frac{8\xi_0\cos\beta}{Re}+O(Re^{-2})\right](1+\eta^2)-\frac{\xi_0 Re^2\cos\alpha_0\sin\beta}{96\eta^4} \qquad (\text{for } \eta \gg Re^{\frac{1}{2}}). \quad \text{(B.25)}$$

Since $M_1(\eta)$ must approach zero as $\eta \to \infty$, we find

$$m_0 = c_{1a} \approx \frac{8\xi_0\cos\beta}{Re}. \quad \text{(B.26)}$$

Then the last term in (B.25) gives leading order, which is consistent with the leading term in asymptotic expansion (B.7). Equations (B.8), (B.11), (B.17) and (B.18) provide a solution to (B.3) for given constants c_{1a} and c_{1b}.

Consider now an asymptotic form of $M_1(\eta)$ at large Reynolds numbers. For $\eta \lesssim Re^{\frac{1}{4}}$, the first term on the right-hand side of (B.3) is very small, and so using (B.15) we have

$$M_1 \approx 2\gamma_0\lambda_0 + c_{1a}M_{1a} \approx 2\gamma_0\lambda_0 + \frac{8\xi_0 \cos\beta\eta^2}{Re}. \tag{B.27}$$

For $\eta \gg Re^{\frac{1}{4}}$, on the other hand, (B.8), (B.10), (B.19) and (B.20) give asymptotic forms of $\widetilde{M}_{1a}M_{1a}$ and $\widetilde{M}_{1b}M_{1b}$ as

$$\widetilde{M}_{1a}M_{1a} \approx -\xi_0 D_0 \left[\frac{8\eta^2}{Re}\sin\left(\frac{Re}{4\eta^2}+\varphi_0\right) - \cos\left(\frac{Re}{4\eta^2}+\varphi_0\right)\right]\exp\left(-\frac{Re^2}{48\eta^6}\right), \tag{B.28}$$

$$\widetilde{M}_{1b}M_{1b} \approx -\xi_0 D_0 \left[\frac{1}{\eta^2}\cos\left(\frac{Re}{4\eta^2}+\varphi_0\right) + \frac{Re}{4\eta^4}\sin\left(\frac{Re}{4\eta^2}+\varphi_0\right)\right]\exp\left(-\frac{Re^2}{48\eta^6}\right). \tag{B.29}$$

Since $\widetilde{M}_{1a}M_{1a} \gg \widetilde{M}_{1b}M_{1b}$ for $\eta \gg Re^{\frac{1}{4}}$, we can express an asymptotic form of $M_1(\eta)$ for $\eta \gg Re^{\frac{1}{4}}$, using (B.11), (B.26) and (B.28), as (3.98) in §3.5. Equation (3.98) matches with (B.27) for $\eta \ll Re^{\frac{1}{3}}$, and thus (3.98) turns out to be available for any value of η.

B.2. θ-dependent part with zero mean

Solutions to (B.5) are considered here. Boundary conditions to be imposed are that $T^2F_2(\eta)$ is regular at $\eta = 0$ and that $T^2F_2(\eta) \to 0$ as $\eta \to \infty$ (see (3.18)). Two source terms on the right-hand side of (B.5) take peak values at extremely different locations for $Re \gg 1$. The first term takes a peak value of $O(Re^{-1})$ at $\eta = 1$ and rapidly decreases as η increases. The second is, on the other hand, exponentially small up to $\eta = O(Re^{\frac{1}{4}})$, and it takes a peak value of $O(Re^{-\frac{5}{3}})$ at $\eta = 2^{-\frac{2}{3}}Re^{\frac{1}{3}}$ (see §3.4). Hence, for $Re \gg 1$, we consider two regions of values of η separately, that is, $\eta = O(1)$ and $\eta \gg 1$.

First, in the region of $\eta = O(1)$ we take only the first term on the right-hand side of (B.5). By substituting an ϵ-expansion,

$$F_2 = F_{20} + \epsilon F_{21} + \cdots \tag{B.30}$$

into (B.5), we obtain, at ϵ^0 order,

$$F_{20}'' + \frac{1}{\eta} F_{20}' - \frac{4}{\eta^2} F_{20} + \frac{4\eta^2}{\mathrm{e}^{\eta^2} - 1} F_{20} = 0, \tag{B.31}$$

which is the same as (A.5), and therefore

$$F_{20}(\eta) \equiv 0. \tag{B.32}$$

At ϵ order of (B.5), by putting

$$F_{21}(\eta) = \mathrm{i} B_1 \mathrm{e}^{-\mathrm{i}\phi_1} f_2(\eta), \tag{B.33}$$

we obtain

$$f_2'' + \frac{1}{\eta} f_2' - \frac{4}{\eta^2} f_2 = \frac{4\eta^2}{\mathrm{e}^{\eta^2} - 1} (\eta^2 - f_2), \tag{B.34}$$

which is identical to (A.9). Hence, we can take

$$\mathrm{Real}[f_2(\eta)] \equiv f_1(\eta), \quad \mathrm{Imag}[f_2(\eta)] \equiv 0, \tag{B.35}$$

so that

$$F_{21}(\eta) = \mathrm{i} B_1 \mathrm{e}^{-\mathrm{i}\phi_1} f_1(\eta). \tag{B.36}$$

Combination of (A.9), (B.30), (B.32) and (B.36) leads to the first equation of (3.99) in §3.5.

By introducing

$$\epsilon M_2(\eta) = -\tfrac{1}{4} \left(F_2'' + \frac{1}{\eta} F_2' - \frac{4}{\eta^2} F_2 \right) \tag{B.37}$$

and using (3.78) we may express the θ-dependent part of vorticity associated with streamfunction $\mathrm{Real}\,[F_2(\eta)\mathrm{e}^{-\mathrm{i}2\theta}]$ as

$$-\tfrac{1}{4} \nabla_\eta^2 \mathrm{Real}\,[F_2(\eta)\mathrm{e}^{-\mathrm{i}2\theta}] = \epsilon \mathrm{Real}\,[M_2(\eta)\mathrm{e}^{-\mathrm{i}2\theta}]. \tag{B.38}$$

Second, we consider the region of $\eta \gg 1$ in which all the terms that include $\mathrm{e}^{-\eta^2}$ may be neglected. By dropping them and using (B.37), we can rewrite (B.5) as

$$M_2'' + \left(2\eta + \frac{1}{\eta}\right) M_2' + 2\left(\frac{\mathrm{i}Re - 2}{\eta^2} - 2\right) M_2 = 2\xi_0 \eta f'. \tag{B.39}$$

Boundary conditions to be imposed are that $TM_2(\eta)$ is regular at $\eta = 0$ and that $TM_2(\eta) \to 0$ as $\eta \to \infty$ (see (3.17)). Using (3.28) and (3.27), we can expand a solution to (B.39) as

$$M_2(\eta)$$
$$= -\xi_0 c_0 \left[\frac{\mathrm{i}Re}{4(\mathrm{i}Re + 6)}\eta^4 - \frac{24\mathrm{i}Re + (\mathrm{i}Re + 6)(8\mathrm{i}Re - Re^2)}{48(\mathrm{i}Re + 6)(\mathrm{i}Re + 16)}\eta^6 + \cdots\right] \qquad (\text{for } \eta \ll Re^{-\frac{1}{2}}), \tag{B.40}$$

and

$$M_2(\eta) = -\xi_0 D_0 \mathrm{e}^{\mathrm{i}\varphi_0}\left[\frac{\mathrm{i}Re}{8\eta^2} - \frac{Re^2}{24\eta^4} - \frac{(11\mathrm{i}Re + 72)Re^2}{1536\eta^6} + \cdots\right] \qquad (\text{for } \eta \gg Re^{\frac{1}{2}}), \tag{B.41}$$

where c_0 is an exponentially small constant given by (3.57).

Now, following the asymptotic analysis performed for (3.26) in §3.4, we employ the WKB method in order to construct solutions to the homogeneous equation associated with (B.39). Let us introduce a new dependent variable $g_2(\eta)$ by

$$M_2(\eta) = \eta^{-\frac{1}{2}} \mathrm{e}^{-\frac{1}{2}\eta^2} g_2(\eta). \tag{B.42}$$

By substituting (B.42) into (B.39), we obtain

$$g_2'' + \left(\frac{2\mathrm{i}Re}{\eta^2} - \eta^2 - 6 - \frac{15}{4\eta^2}\right) g_2 = 2\xi_0 \eta^{\frac{3}{2}} \mathrm{e}^{\frac{1}{2}\eta^2} f'. \tag{B.43}$$

We consider the region of $\eta = O(Re^{\frac{1}{4}})$ and put $\eta = Re^{\frac{1}{4}}\chi$. Then, (B.43) becomes

$$g_2'' + Re\left[\frac{2\mathrm{i}}{\chi^2} - \chi^2 - 6Re^{-\frac{1}{2}} + O(Re^{-1})\right] g_2 = 2Re^{\frac{3}{4}} \xi_0 \chi^{\frac{3}{2}} \exp\left(\tfrac{1}{2} Re^{\frac{1}{2}} \chi^2\right) f'. \tag{B.44}$$

The homogeneous equation associated with (B.44) has two linearly independent WKB solutions

$$g_{2a} = \chi^{\frac{1}{2}}(\chi^4 - 2\mathrm{i})^{-\frac{1}{4}} \left(\chi^2 + (\chi^4 - 2\mathrm{i})^{\frac{1}{2}}\right)^{-\frac{3}{2}} \exp\left(-Re^{\frac{1}{2}}\sigma_1(\chi)\right), \tag{B.45}$$

$$g_{2b} = \chi^{\frac{1}{2}}(\chi^4 - 2\mathrm{i})^{-\frac{1}{4}} \left(\chi^2 + (\chi^4 - 2\mathrm{i})^{\frac{1}{2}}\right)^{\frac{3}{2}} \exp\left(Re^{\frac{1}{2}}\sigma_1(\chi)\right), \tag{B.46}$$

where

$$\sigma_1(\chi) = 2^{-\frac{1}{2}}\mathrm{e}^{\frac{1}{4}\pi\mathrm{i}}\left[\mathrm{e}^{-\frac{1}{4}\pi\mathrm{i}}(\tfrac{1}{2}\chi^4 - \mathrm{i})^{\frac{1}{2}} - \arctan\left(\mathrm{e}^{-\frac{1}{4}\pi\mathrm{i}}(\tfrac{1}{2}\chi^4 - \mathrm{i})^{\frac{1}{2}}\right) + \tfrac{1}{2}\pi\right]. \tag{B.47}$$

For small values of χ, function $\sigma_1(\chi)$ may be expressed asymptotically as

$$\sigma_1 = 2^{\frac{1}{2}}\mathrm{e}^{-\frac{1}{4}\pi\mathrm{i}}\ln\chi + \rho_1 + O(\chi^4), \tag{B.48}$$

where

$$\rho_1 = \tfrac{3}{2}2^{-\frac{1}{2}}\mathrm{e}^{\frac{3}{4}\pi\mathrm{i}}\ln 2 + \tfrac{1}{2}\left[\tfrac{1}{4}\pi + 1 + \mathrm{i}\left(\tfrac{1}{4}\pi - 1\right)\right]. \tag{B.49}$$

For large χ, on the other hand, it is expanded as

$$\sigma_1 = \tfrac{1}{2}\chi^2 + \frac{\mathrm{i}}{2\chi^2} - \frac{1}{12\chi^6} + \cdots. \tag{B.50}$$

Then, we use (B.48) and (B.50), and restore the original variable η to obtain, for $\eta \ll Re^{\frac{1}{4}}$ ($\chi \ll 1$),

$$g_{2a}(\eta) \approx Re^{-\frac{1}{8}}2^{-1}\eta^{\frac{1}{2}} \exp\left(-Re^{1/2}(2^{\frac{1}{2}}\mathrm{e}^{-\frac{1}{4}\pi\mathrm{i}}\ln\eta + 2^{\frac{1}{2}}\mathrm{e}^{\frac{3}{4}\pi\mathrm{i}}\ln Re^{\frac{1}{4}} + \rho_1)\right), \tag{B.51}$$

$$g_{2b}(\eta) \approx Re^{-\frac{1}{8}}2^{\frac{1}{2}}\mathrm{e}^{-\frac{1}{4}\pi\mathrm{i}}\eta^{\frac{1}{2}} \exp\left(Re^{\frac{1}{2}}(2^{\frac{1}{2}}\mathrm{e}^{-\frac{1}{4}\pi\mathrm{i}}\ln\eta + 2^{\frac{1}{2}}\mathrm{e}^{\frac{3}{4}\pi\mathrm{i}}\ln Re^{\frac{1}{4}} + \rho_1)\right), \tag{B.52}$$

and, for $\eta \gg Re^{\frac{1}{4}}$ ($\chi \gg 1$),

$$g_{2a}(\eta) \approx 2^{-\frac{3}{2}}Re^{\frac{7}{8}}\eta^{-\frac{7}{2}} \exp\left(-\tfrac{1}{2}\eta^2 - \frac{\mathrm{i}Re}{2\eta^2} + \frac{Re^2}{12\eta^6}\right), \tag{B.53}$$

$$g_{2b}(\eta) \approx 2^{\frac{3}{2}}Re^{-\frac{5}{8}}\eta^{\frac{5}{2}} \exp\left(\tfrac{1}{2}\eta^2 + \frac{\mathrm{i}Re}{2\eta^2} - \frac{Re^2}{12\eta^6}\right). \tag{B.54}$$

In order to solve the full equation of (B.44), we write a solution in terms of (B.45) and (B.46) as

$$g_2(\eta) = (c_{2a} + \tilde{g}_{2a}(\eta))g_{2a}(\eta) + (c_{2b} + \tilde{g}_{2b}(\eta))g_{2b}(\eta), \tag{B.55}$$

where

$$\tilde{g}_{2a}(\eta) = -2\xi_0 \int_0^\eta \frac{s^{\frac{3}{2}} \mathrm{e}^{\frac{1}{2}s^2} f'(s) g_{2b}(s)}{W(s)} \,\mathrm{d}s, \tag{B.56}$$

$$\tilde{g}_{2b}(\eta) = -2\xi_0 \int_\eta^\infty \frac{s^{\frac{3}{2}} \mathrm{e}^{\frac{1}{2}s^2} f'(s) g_{2a}(s)}{W(s)} \,\mathrm{d}s, \tag{B.57}$$

with

$$W(\eta) = g_{2a}(\eta) g'_{2b}(\eta) - g'_{2a}(\eta) g_{2b}(\eta). \tag{B.58}$$

It can be shown from (B.51)—(B.54) that

$$W(\eta) \approx 2Re^{\frac{1}{4}}. \tag{B.59}$$

Constants c_{2a} and c_{2b} are determined by the boundary conditions at $\eta = 0$ and ∞. For $\eta \ll Re^{\frac{1}{4}}$, since $f(\eta)$ and therefore the right-hand side of (B.44) are very small, (B.55) is written, using (B.51) and (B.52), as

$$g_2 \approx c_{2a} g_{2a} + c_{2b} g_{2b} \approx c_{2a} 2^{-1} Re^{-\frac{1}{8}} \mathrm{e}^{\frac{1}{2}\pi \mathrm{i}} q_1^{-1} \eta^{-q_2 + \frac{1}{2}} + c_{2b} 2^{\frac{1}{2}} Re^{-\frac{1}{8}} \mathrm{e}^{-\frac{1}{4}\pi \mathrm{i}} q_1 \eta^{q_2 + \frac{1}{2}}, \tag{B.60}$$

where

$$q_1 = \exp\left(Re^{\frac{1}{2}} (2^{\frac{1}{2}} \mathrm{e}^{\frac{3}{4}\pi \mathrm{i}} \ln Re^{\frac{1}{4}} + \rho_1) \right), \tag{B.61}$$

$$q_2 = Re^{\frac{1}{2}} 2^{\frac{1}{2}} \mathrm{e}^{-\frac{1}{4}\pi \mathrm{i}}. \tag{B.62}$$

Since $\mathrm{Real}(q_2) = Re^{\frac{1}{2}}$, and q_1 is exponentially small for $Re \gg 1$, we obtain, using definition (B.42) of g_2,

$$M_2 \approx c_{2a} 2^{-1} Re^{-\frac{1}{8}} q_1^{-1} \eta^{-q_2} \qquad (\text{at } \eta \ll Re^{\frac{1}{4}}). \tag{B.63}$$

Hence, in order that M_2 may be connected smoothly with a regular solution at $\eta = 0$ we must take

$$c_{2a} = 0. \tag{B.64}$$

For $\eta \gg Re^{\frac{1}{4}}$, it can be shown by using (3.64), (B.53) and (B.54) that

$$\tilde{g}_{2a} \approx -\mathrm{i}2^{\frac{1}{2}}\xi_0 D_0 \mathrm{e}^{\mathrm{i}\varphi_0} Re^{\frac{1}{8}} \int_0^{\eta} s \exp\left(s^2 + \frac{\mathrm{i}3Re}{4s^2} - \frac{5Re^2}{48s^6}\right) \mathrm{d}s, \tag{B.65}$$

$$\tilde{g}_{2b} \approx -\mathrm{i}2^{-\frac{5}{2}}\xi_0 D_0 \mathrm{e}^{\mathrm{i}\varphi_0} Re^{\frac{13}{8}} \int_{\eta}^{\infty} \frac{1}{s^5} \exp\left(-\frac{\mathrm{i}Re}{4s^2} + \frac{Re^2}{16s^6}\right) \mathrm{d}s \tag{B.66}$$

because f is very small up to $\eta = O(Re^{\frac{1}{4}})$ (see §3.4). Integrations by parts of the integrals in (B.65) and (B.66) respectively lead to

$$\tilde{g}_{2a} \approx -\mathrm{i}2^{-\frac{1}{2}}\xi_0 D_0 \mathrm{e}^{\mathrm{i}\varphi_0} Re^{\frac{1}{8}} \exp\left(\eta^2 + \frac{\mathrm{i}3Re}{4\eta^2} - \frac{5Re^2}{48\eta^6}\right), \tag{B.67}$$

$$\tilde{g}_{2b} \approx -\mathrm{i}2^{\frac{1}{2}}\xi_0 D_0 \mathrm{e}^{\mathrm{i}\varphi_0} Re^{-\frac{3}{8}} \left[\left(1 + \frac{\mathrm{i}Re}{4\eta^2}\right) \exp\left(-\frac{\mathrm{i}Re}{4\eta^2} + \frac{Re^2}{16\eta^6}\right) - 1\right]. \tag{B.68}$$

Thus, it follows from (B.42), (B.53)—(B.55), (B.64), (B.67) and (B.68) that

$$\begin{aligned} M_2(\eta) \approx\ & c_{2b}2^{\frac{3}{2}} Re^{-\frac{5}{8}} \eta^2 \exp\left(\frac{\mathrm{i}Re}{2\eta^2} - \frac{Re^2}{12\eta^6}\right) \\ & -\mathrm{i}\xi_0 D_0 \mathrm{e}^{\mathrm{i}\varphi_0} \frac{4\eta^2}{Re} \left[\left(1 + \frac{\mathrm{i}Re}{4\eta^2}\right) \exp\left(\frac{\mathrm{i}Re}{4\eta^2} - \frac{Re^2}{48\eta^6}\right) - \exp\left(\frac{\mathrm{i}Re}{2\eta^2} - \frac{Re^2}{12\eta^6}\right)\right] \\ & -\mathrm{i}\xi_0 D_0 \mathrm{e}^{\mathrm{i}\varphi_0} \frac{Re}{4\eta^4} \exp\left(\frac{\mathrm{i}Re}{4\eta^2} - \frac{Re^2}{48\eta^6}\right). \end{aligned} \tag{B.69}$$

Furthermore, for $\eta \gg Re^{\frac{1}{2}}$, we expand (B.69) in a series of inverse powers of η to obtain

$$M_2 \approx c_{2b}2^{\frac{3}{2}} Re^{-\frac{5}{8}} \eta^2 - \xi_0 D_0 \mathrm{e}^{\mathrm{i}\varphi_0} \frac{\mathrm{i}Re}{8\eta^2}. \tag{B.70}$$

Function $M_2(\eta)$ must vanish as $\eta \to \infty$. This requires that

$$c_{2b} = 0, \tag{B.71}$$

and then the last term in (B.70) gives the leading order, which is consistent with the leading term in asymptotic expansion (B.41). Given constants c_{2a} and c_{2b}, then (B.55), (B.65) and (B.66) provide a solution to (B.44), and $M_2(\eta)$ is determined by (B.42).

Let us summarize an asymptotic form of $M_2(\eta)$ at a large Reynolds number. For $1 \ll \eta \lesssim Re^{\frac{1}{4}}$, the right-hand side of (B.39) is very small, and so is $M_2(\eta)$ because $c_{2a} = c_{2b} = 0$. For $\eta \gg Re^{\frac{1}{4}}$, on the other hand, the second term on the left-hand side of (B.69) dominates the third (the first term has already vanished), and then an asymptotic form of $M_2(\eta)$ is given by the second equation of (3.99) in §3.5.

REFERENCES

BERNARD, P. S., THOMAS, J. M. & HANDLER, R. A. 1993 Vortex dynamics and the production of Reynolds stress. *J. Fluid Mech.* **253**, 385–419.

BROOKE, J. W. & HANRATTY, T. J. 1993 Origin of turbulence-producing eddies in a channel flow. *Phys. Fluids* **A 5**, 1011–1022.

CHOI, H., MOIN, P. & KIM, J. 1993 Direct numerical simulation of turbulent flow over riblets. *J. Fluid Mech.* **255**, 503–539.

DOUADY, D., COUDER, Y. & BRACHET, M. E. 1991 Direct observation of the intermittency of intense vorticity filaments in turbulence. *Phys. Rev. Lett.* **67**, 983–986.

HOSOKAWA, I. & YAMAMOTO, K. 1989 Fine structure of a directly simulated isotropic turbulence. *J. Phys. Soc. Japan* **58**, 20–23.

HUSSAIN, A. K. M. F. 1986 Coherent structures and turbulence *J. Fluid Mech.* **173**, 303–356.

JIMÉMEZ, J., MOFFATT, H. K. & VASCO, C. 1996 The structure of the vortices in freely decaying two-dimensional turbulence. *J. Fluid Mech.* **313**, 209–222.

JIMÉMEZ, J. & MOIN, P. 1991 The minimal flow unit in near-wall turbulence. *J. Fluid Mech.* **225**, 213–240.

JIMÉMEZ, J., WRAY, A. A., SAFFMAN, P. G. & ROGALLO, R. S. 1993 The structure of intense vorticity in homogeneous isotropic turbulence. *J. Fluid Mech.* **255**, 65–90.

KERR, R. M. 1985 Higher-order derivative correlation and the alignment of small scale structures in isotropic turbulence. *J. Fluid Mech.* **153**, 31–58.

KIDA, S. 1993 Tube-like structures in turbulence. *Lecture Notes in Numerical Applied Analysis* **12**, 137–159.

KIDA, S. & OHKITANI, K. 1992 Spatio-temporal intermittency and instability of a forced turbulence. *Phys. Fluids* **A 4**, 1018–1027.

KIDA, S. & TANAKA, M. 1992 Reynolds stress and vortical structure in a uniformly sheared turbulence. *J. Phys. Soc. Japan* **61**, 4400–4417.

KIDA, S. & TANAKA, M. 1994 Dynamics of vortical structures in a homogeneous shear flow. *J. Fluid Mech.* **274**, 43–68.

KRAVCHENKO, A. G., CHOI, H. & MOIN, P. 1993 On the relation of near-wall streamwise vortices to wall skin friction in turbulent boundray layers. *Phys. Fluids* **A 5**, 3307–3309.

LUNDGREN, T. S. 1982 Strained spiral vortex model for turbulent fine structure. *Phys. Fluids* **25**, 2193–2203.

MIYAKE, Y. & TSUJIMOTO, K. 1996 Regeneration and self-sustenance of quasi-streamwise vortices. Submitted to *Phys. Fluids.*

MOFFATT, H. K., KIDA, S. & OHKITANI, K. 1994 Stretched vortices – the sinews of turbulence; large-Reynolds-number asymptotics. *J. Fluid Mech.* **259**, 241–264.

MOORE, D. W. 1985 The interaction of a diffusing line vortex and aligned shear flow. *Proc.*

R. Soc. Lond. **A 399**, 367–375.

PEARSON, C. F. & ABERNATHY, F. H. 1984 Evolution of the flow field associated with a streamwise diffusing vortex. *J. Fluid Mech.* **146**, 271–283.

ROBINSON, S. K., KLINE, S. J. & SPALART, P. R. 1988 Quasi-coherent structures in the turbulent boundary layer: Part II. Verification and new information from a numerically simulated flat-plate layer. In *Near-Wall turbulence* (ed. S. J. Kline & N. H. Afgan), pp. 218–247. Hemisphere.

RUETSCH, G. R. & MAXEY, M. R. 1991 Small scale features of vorticity and passive scalar fields in homogeneous isotropic turbulence. *Phys. Fluids* **A 3**, 1587–1597.

SENDSTAD, O. & MOIN, P. 1992 The near-wall mechanics of three-dimensional boundary layers. Report No. TF-57, Thermoscience Divison, Department of Mechanical Engineering, Stanford University, Stanford, CA.

SHE, Z. -S., JACKSON, E. & ORSZAG, S. A. 1990 Intermittent vortex structures in homogeneous isotropic turbulence. *Nature* **344**, 226–228.

SIGGIA, E. D. 1981 Numerical study of small scale intermittency in three-dimensional turbulence. *J. Fluid Mech.* **107**, 375–406.

VINCENT, A. & MENEGUZZI, M. 1991 The spatial structure and statistical properties of homogeneous turbulence. *J. Fluid Mech.* **225**, 1–25.

TABLE 1. List of main symbols

$A(t)$	=	stretch factor along a vortex tube $(= \exp(S\int_0^t \gamma(s)\mathrm{d}s))$
$B(t)$	=	$(\gamma(t)^2+\lambda(t)^2)^{\frac{1}{2}}$ $(B_0 = B\|_{t=0})$
$D(t)$	=	$(\cos^2\alpha\sin^2\beta+\cos^2\beta)^{\frac{1}{2}}$ $(D_0 = D\|_{t=0})$
$f(\eta)$	=	complex amplitude for $u^{(0)}$ (see (3.25))
$M_0(\eta)$	=	amplitude for $\omega^{(1,0)}$ (see (3.92))
$M_1(\eta)$	=	θ-independent part of $\omega^{(1,1)}$ (see (3.97))
$M_2(\eta)$	=	complex amplitude for $\omega^{(1,1)}$ (see (3.97))
M_{ij}	=	transformation matrix representing a system rotaion (see (2.2))
Re	=	Reynolds number $(= \Gamma/(2\pi\nu))$
R	=	modified radial coordinate $(= A(t)^{\frac{1}{2}}r)$
r	=	radial coordinate
S	=	shear rate of a simple shear flow
T	=	modified time $(= \int_0^t A(s)\mathrm{d}s)$
t	=	time
$\boldsymbol{U}$	=	velocity of a simple shear flow $(= SX_2\widehat{\boldsymbol{X}}_1)$
$\boldsymbol{u}$	=	velocity $(= \boldsymbol{U}+\boldsymbol{u}')$
$\boldsymbol{u}'$	=	fluctuation velocity
$\overline{\boldsymbol{u}}$	=	velocity of a simple shear flow relative to the structural coordinate system
u	=	transformed axial velocity fluctuation $(= A(t)u_1''/R = u^{(0)}+u^{(1)}+\cdots)$
u_1'	=	axial component of fluctuation velocity $(= u_{1p}'+u_1'')$
u_{1p}'	=	a particular solution to axial-velocity equation (2.24) (see (2.36))
u_1''	=	homogeneous solution to axial-velocity equation (2.24)
$u^{(0)}$	=	leading-order transformed axial velocity fluctuation
X_1, X_2, X_3	=	stationary coordinates
$\widehat{\boldsymbol{X}}_1, \widehat{\boldsymbol{X}}_2, \widehat{\boldsymbol{X}}_3$	=	unit vectors in X_1-, X_2- and X_3-directions
x_1, x_2, x_3	=	structural coordinates
$\widehat{\boldsymbol{x}}_1, \widehat{\boldsymbol{x}}_2, \widehat{\boldsymbol{x}}_3$	=	unit vectors in x_1-, x_2- and x_3-directions
α	=	inclination angle of a vortex tube from X_1-axis $(\alpha_0 = \alpha\|_{t=0})$
β	=	inclination angle of (x_1, x_2)-plane from X_2-axis
Γ	=	circulation of a vortex tube
$\gamma(t)$	=	axial rate of strain of the simple shear $\partial_1 U_1/S = \cos\alpha\sin\alpha\cos\beta$ $(\gamma_0 = \gamma\|_{t=0})$
ϵ	=	ν/Γ
η	=	similarity variable $R/(2(\nu T)^{\frac{1}{2}})$
θ	=	angular coordinate
$\lambda(t)$	=	axial component of the simple shear vorticity $(\nabla\times\boldsymbol{U})\cdot\widehat{\boldsymbol{x}}_1/S = -\sin\alpha\sin\beta$ $(\lambda_0 = \lambda\|_{t=0})$
ν	=	kinematic viscosity of fluid
$\xi(t)$	=	$2\Omega_3/S = -2\sin^2\alpha\cos\beta$ $(\xi_0 = \xi\|_{t=0})$
$\phi(t)$	=	$\arctan(\lambda(t)/\gamma(t))$ $(\phi_0 = \phi\|_{t=0})$
$\varphi(t)$	=	$\arctan(\cos\beta/(\cos\alpha\sin\beta))$ $(\varphi_0 = \varphi\|_{t=0})$
ψ	=	streamfunction for fluctuation flow field $(= \psi^{(0)}+\psi^{(1)}+\cdots)$
$\psi^{(0)}$	=	leading-order streamfunction
$\psi^{(1)}$	=	first-order streamfunction $(= ST\psi^{(1,1)}+(ST)^2\psi^{(1,2)}+\cdots)$
$\boldsymbol{\Omega}$	=	angular velocity of the structural coordinate system
$\boldsymbol{\omega}$	=	vorticity $(= \nabla\times\boldsymbol{u} = \nabla\times\boldsymbol{U}+\boldsymbol{\omega}')$
$\boldsymbol{\omega}'$	=	fluctuation vorticity
ω	=	transformed axial vorticity fluctuation $(= \omega_1'/A(t) = \omega^{(0)}+\omega^{(1)}+\cdots)$
$\omega^{(0)}$	=	leading-order transformed axial vorticity fluctuation
$\omega^{(1)}$	=	first-order transformed axial vorticity fluctuation $(= \omega^{(1,0)}+ST\omega^{(1,1)}+\cdots)$
$\omega_1', \omega_2', \omega_3'$	=	x_1-, x_2- and x_3-components of fluctuation vorticity

TABLE 2. Units for variables

Variables	T	R	ω	ψ	Ru
Units	$1/S$	$(\nu/S)^{\frac{1}{2}}$	$\epsilon^{-1}S\ (=\Gamma S/\nu)$	$\epsilon^{-1}\nu\ (=\Gamma)$	$(\nu S)^{\frac{1}{2}}$

Figure captions

FIGURE 1. A straight vortex tube in a simple shear flow.

FIGURE 2. Structural coordinate system $Ox_1x_2x_3$ and the original stationary coordinate system $OX_1X_2X_3$.

FIGURE 3. Movement of a vortex tube (i.e. the x_1-axis) which is shown by a white-head arrow.

FIGURE 4. Time-variation of stretch factor $A(t)$ for $\alpha_0 = \frac{1}{4}\pi$ and for three values of β.

FIGURE 5. Time-variation of modified time $T(t)$ for $\alpha_0 = \frac{1}{4}\pi$ and for three values of β.

FIGURE 6. Real part of $-\sigma + \frac{1}{2}\chi^2$ versus χ. Dashed and dotted lines denote the asymptotic forms for small and large χ, respectively (see equations (3.48)—(3.50)).

FIGURE 7. Solution $f(\eta)$ to equation (3.26) at $Re = 1000$. Numerical solutions and asymptotic form (3.63) are represented by solid and dashed curves respectively. Thick and thin curves denote the real and imaginary parts respectively. The envelopes, $\pm\exp\left(-(Re^2/48\eta^6)\right)$ are drawn also with thin solid curves.

FIGURE 8. Reynolds number dependence of asymptotic solution (3.63). The real parts of solutions are plotted against (a) $\eta Re^{-\frac{1}{3}}$ and (b) $\eta Re^{-\frac{1}{2}}$ at $Re = 1000$ and 10000. Thick dashed and solid curves denote solutions at $Re = 1000$ and 10000, respectively. Thin dashed and solid lines represent their envelopes, $\pm\exp\left(-(Re^2/48\eta^6)\right)$.

FIGURE 9. Spatial distribution of magnitude $(\omega_2^2 + \omega_3^2)^{\frac{1}{2}}$ of vorticity normal to a vortex tube at $Re = 1000$ for (a) the cyclonic ($\alpha_0 = \arctan\sqrt{2}$, $\beta = -\frac{1}{4}\pi$), (b) neutral ($\alpha_0 = \frac{1}{4}\pi$, $\beta = 0$), and (c) anti-cyclonic ($\alpha_0 = \arctan\sqrt{2}$, $\beta = \frac{1}{4}\pi$) cases. The level of the magnitude is represented by colour: Red is the highest ($7S$) and blue is the lowest (i.e. null). Solid curves represent vorticity lines projected on the (x_2, x_3)-plane. A side-length of the domain is 40 in similarity variable η.

FIGURE 10. Amplitude $(\eta f)'$ of the circumferential component of vorticity ω_θ. Solid and dashed curves represent the real and imaginary parts respectively. Thin solid lines denote the magnitude, $\pm|(\eta f)'|$.

FIGURE 11. Amplitude $M_0(\eta)$ of the first-order axial vorticity $\omega^{(1,0)}(\eta, \theta)$.

FIGURE 12. The θ-independent part $M_1(\eta)$ of the second-order axial vorticity $\omega^{(1,1)}(\eta, \theta)$. Solid, dashed and dotted lines represent the cyclonic, neutral and anti-cyclonic cases, respectively. Thin straight lines denote the values of $2\gamma_0\lambda_0$.

FIGURE 13. Amplitude $M_2(\eta)$ of the θ-dependent part of the second-order axial vorticity $\omega^{(1,1)}(\eta, \theta)$ for (a) cyclonic, (b) neutral and (c) anti-cyclonic cases. Solid and dashed bold lines represent real and imaginary parts of $M_2(\eta)$. Thin solid lines denote the magnitude, $\pm|M_2(\eta)|$.

FIGURE 14. Same as figure 9 but for spatial distribution of the fluctuation axial vorticity ω_1'. The level of ω_1' is represented by colour: Red is the highest ($+S^2T$) and blue is the lowest ($-S^2T$).

FIGURE 15. Generation mechanism of axial vorticity along spiral layers of high normal vorticity which are represented by crescent-shaped shadow regions. Double arrows denote the direction of normal vorticity. $\odot$ and $\otimes$ denote the direction of axial velocity induced by the spiral vorticity layers by which the simple shear vorticity $\nabla \times \boldsymbol{U}$ is tilted toward the axial direction.

FIGURE 16. Spatial distributions of the fluctuation vorticity field around a neutral vortex tube. (a) $\omega_1'/(S^2T|\xi_0|D_0)$ at $R = O\left(Re^{\frac{1}{2}}(\nu T)^{\frac{1}{2}}\right)$, (b) $-\omega_2'/(2SD_0)$ at $R = O\left(Re^{\frac{1}{2}}(\nu T)^{\frac{1}{2}}\right)$, (c) $\omega_1'/(S^2T|\xi_0|D_0)$ at $R = O\left(Re^{\frac{1}{3}}(\nu T)^{\frac{1}{2}}\right)$, (d) $-\omega_2'/(2SD_0)$ at $R = O\left(Re^{\frac{1}{3}}(\nu T)^{\frac{1}{2}}\right)$. The levels of contour lines are (a, b) $\pm\frac{1}{16}$, $\pm\frac{1}{8}$, $\pm\frac{1}{4}$, $\pm\frac{1}{2}$ and (c, d) $\pm\frac{1}{2}$, ± 2. Dashed lines represent negative values.

FIGURE 17. Vorticity lines in the structural coordinate system $Ox_1x_2x_3$ for (a) the cyclonic, (b) the neutral and (c) the anti-cyclonic cases. A rectangular domain of 140 × 60 × 60 (in similarity varible η) is viewed from the negative x_1- and the positive x_2-directions in the upper and lower panels, respectively. Thin curves in upper panels represent contour lines of $(\omega_2^2 + \omega_3^2)^{\frac{1}{2}} = 2S$.

FIGURE 18. Vorticity lines distorted by a cyclonic vortex tube in the stationary coordinate system $OX_1X_2X_3$. Lines attached with letters A and E are the same as the corresponding ones in figures 17. Note that the streamwise (X_1) component of vorticity of distorted vorticity lines (which is negative) is opposite to that of the vortex tube (which is positive).

FIGURE 19. An illustration of the structure of vorticity field around a straight vortex tube in a simple shear. Double arrows on the double helical layers denote the direction

of vorticity

FIGURE 20. Wrap, tilt and stretch of vorticity lines around a straight vortex tube in a simple shear flow. (a) Vorticity lines are neither wrapped, tilted nor stretched around a *spanwise* vortex tube. (b) They are wrapped on normal planes but are neither tilted nor stretched toward the axial direction around a *streamwise* one. (c) They are wrapped, tilted and stretched around an *oblique* one.

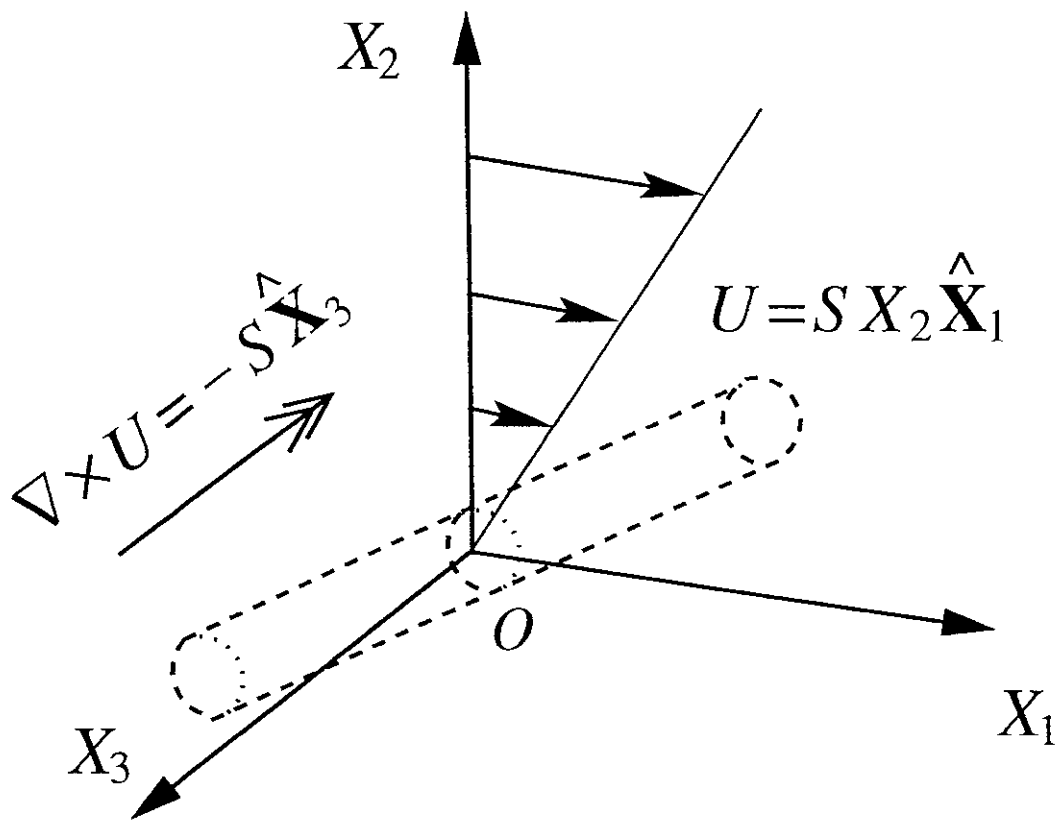

Figure 1

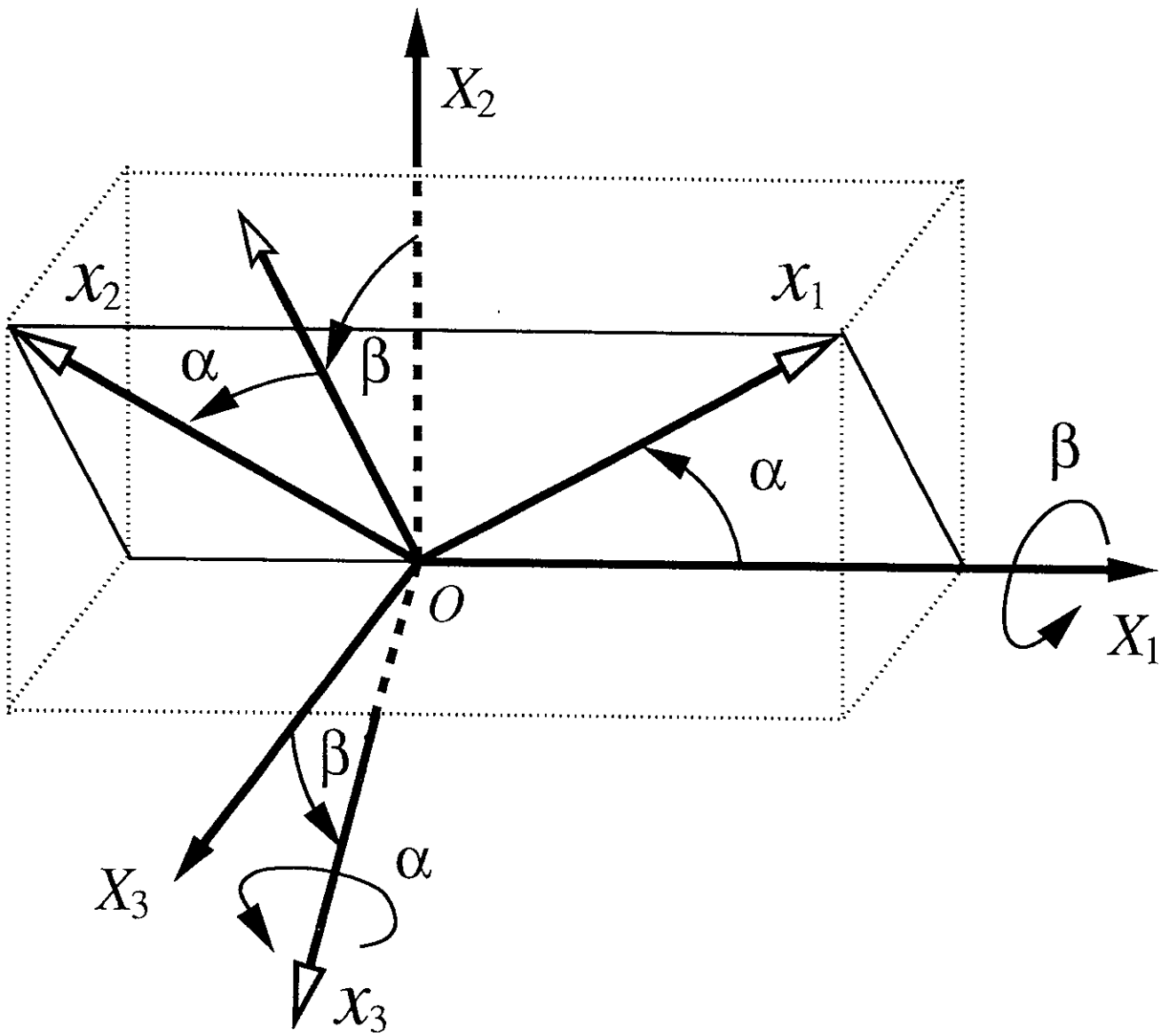

Figure 2

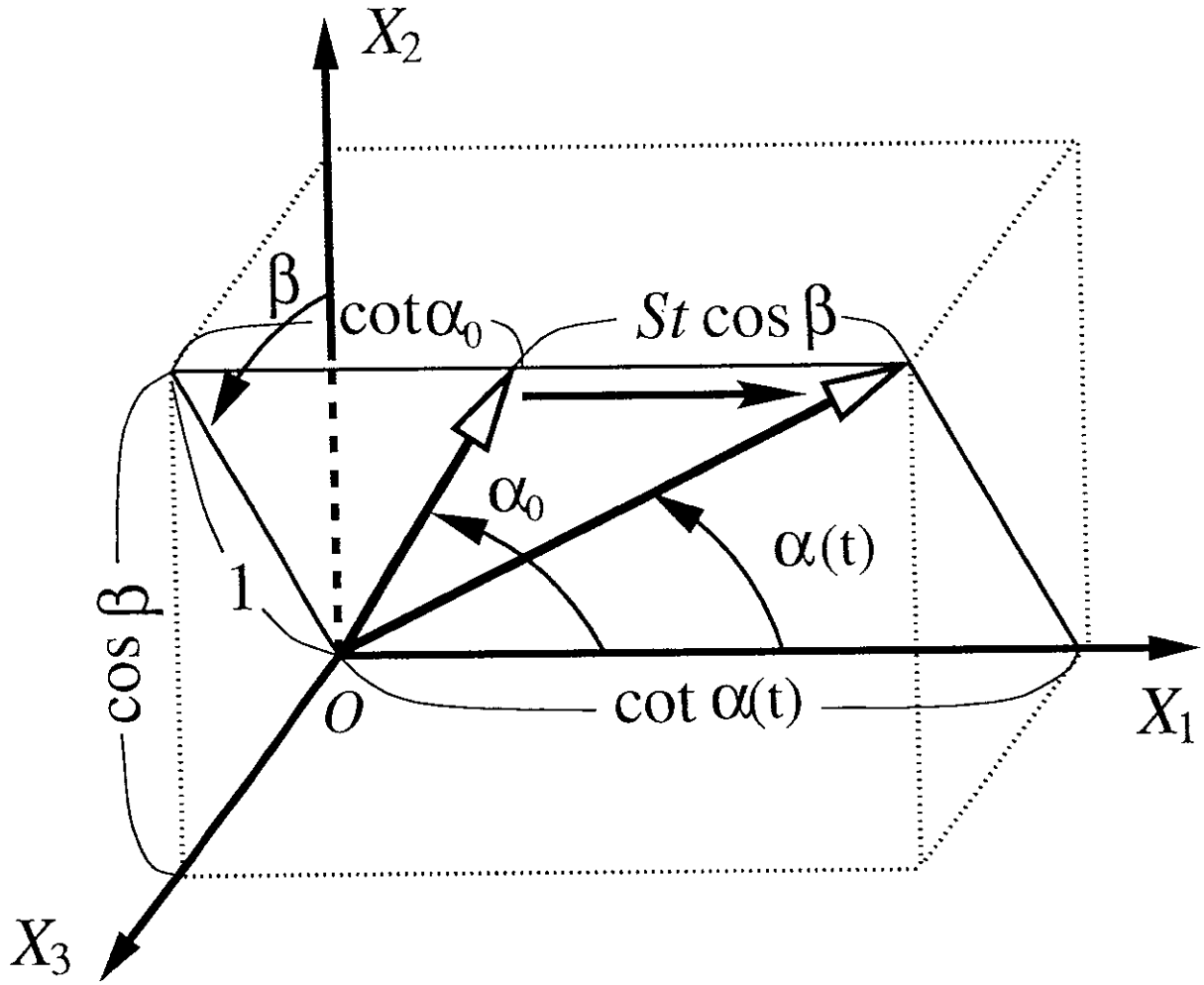

Figure 3

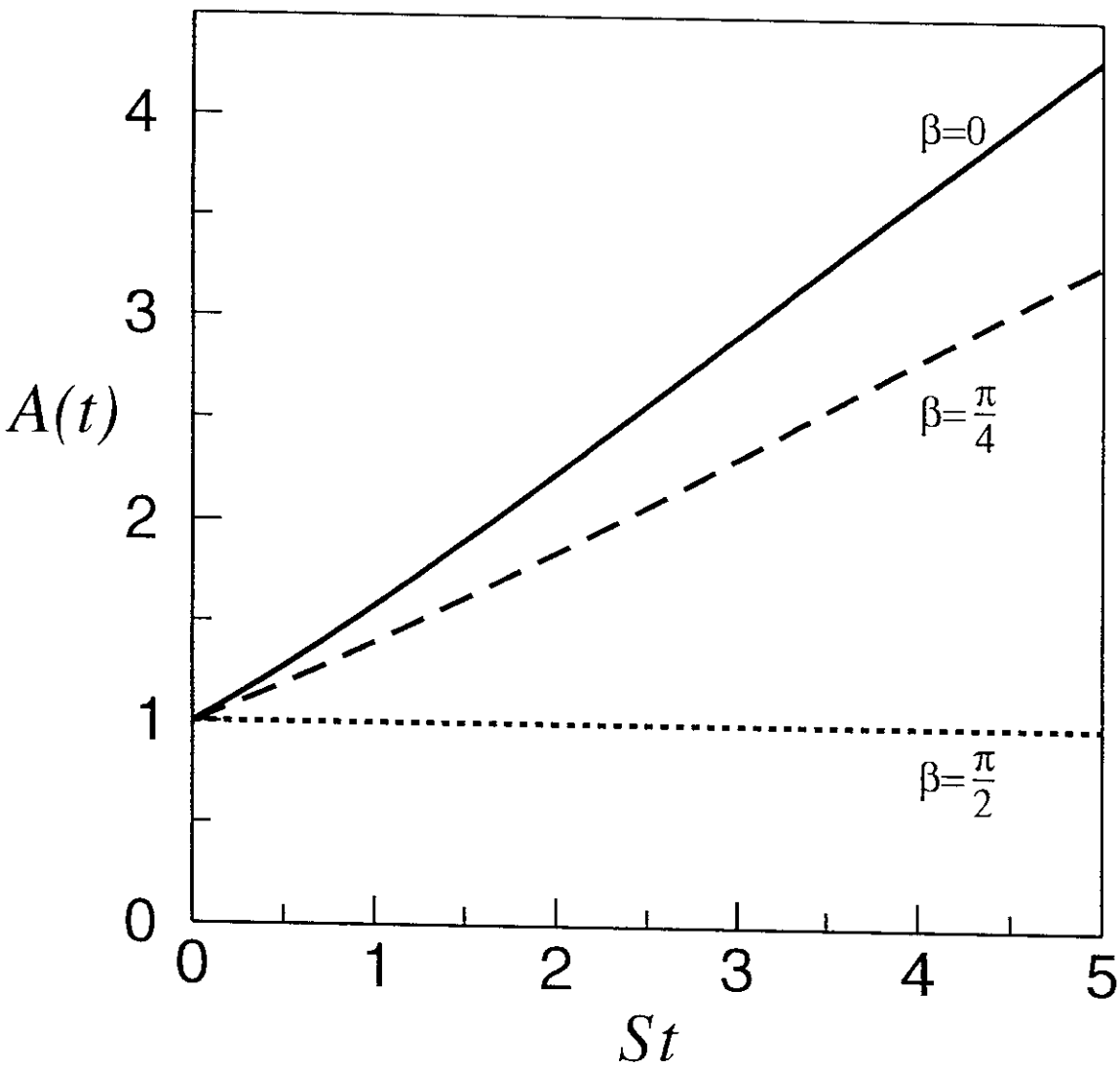

Figure 4

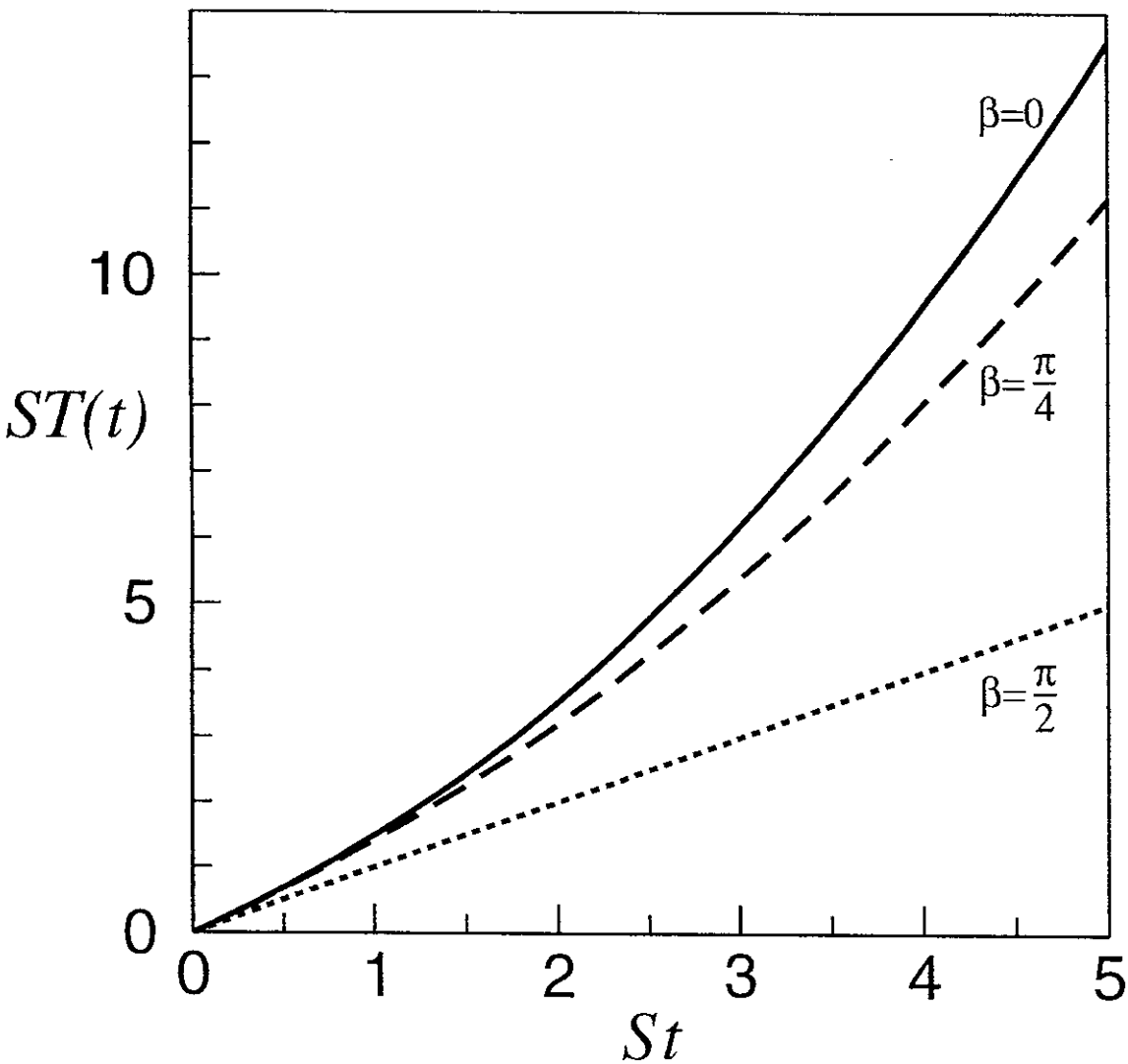

Figure 5

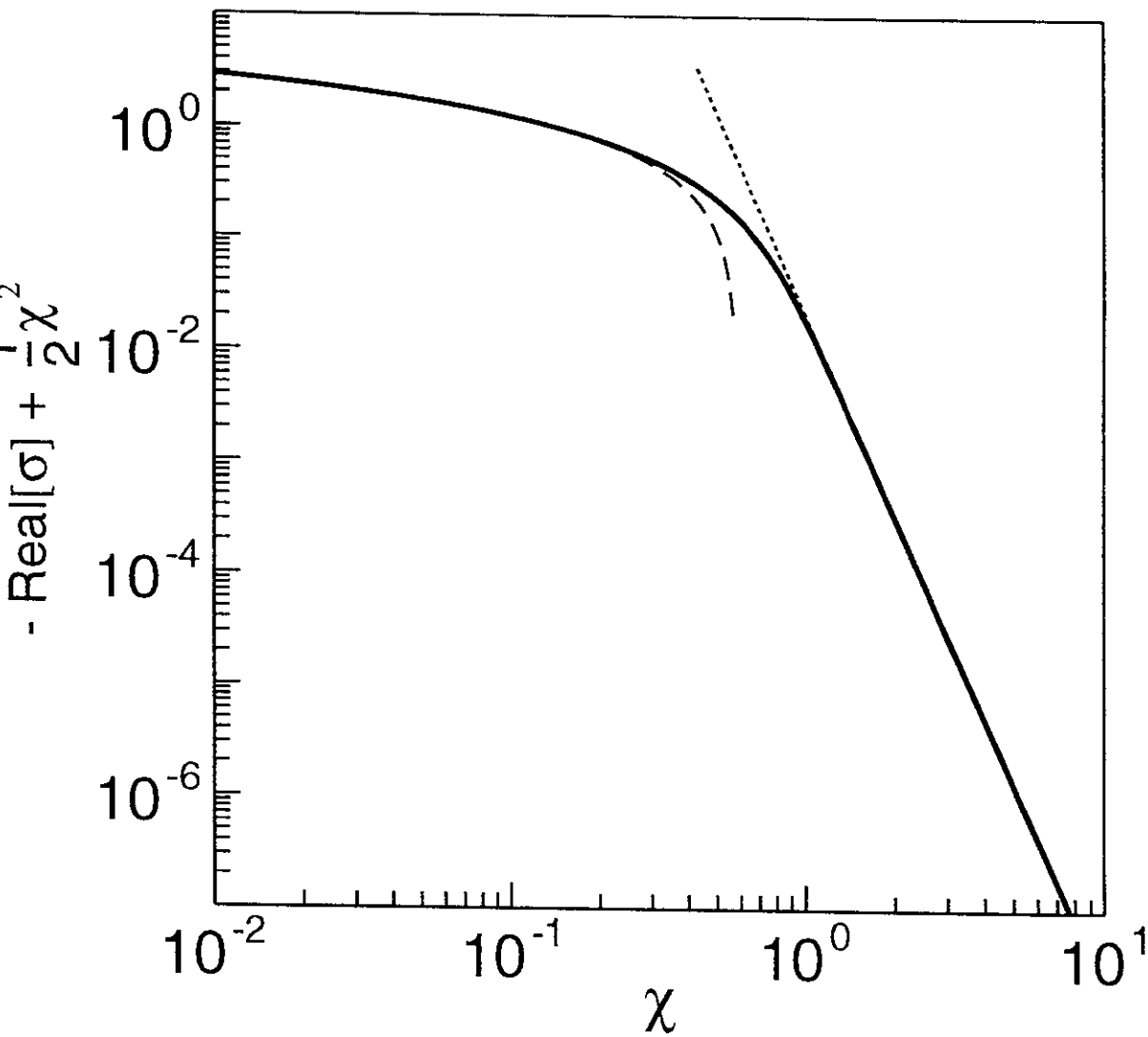

Figure 6

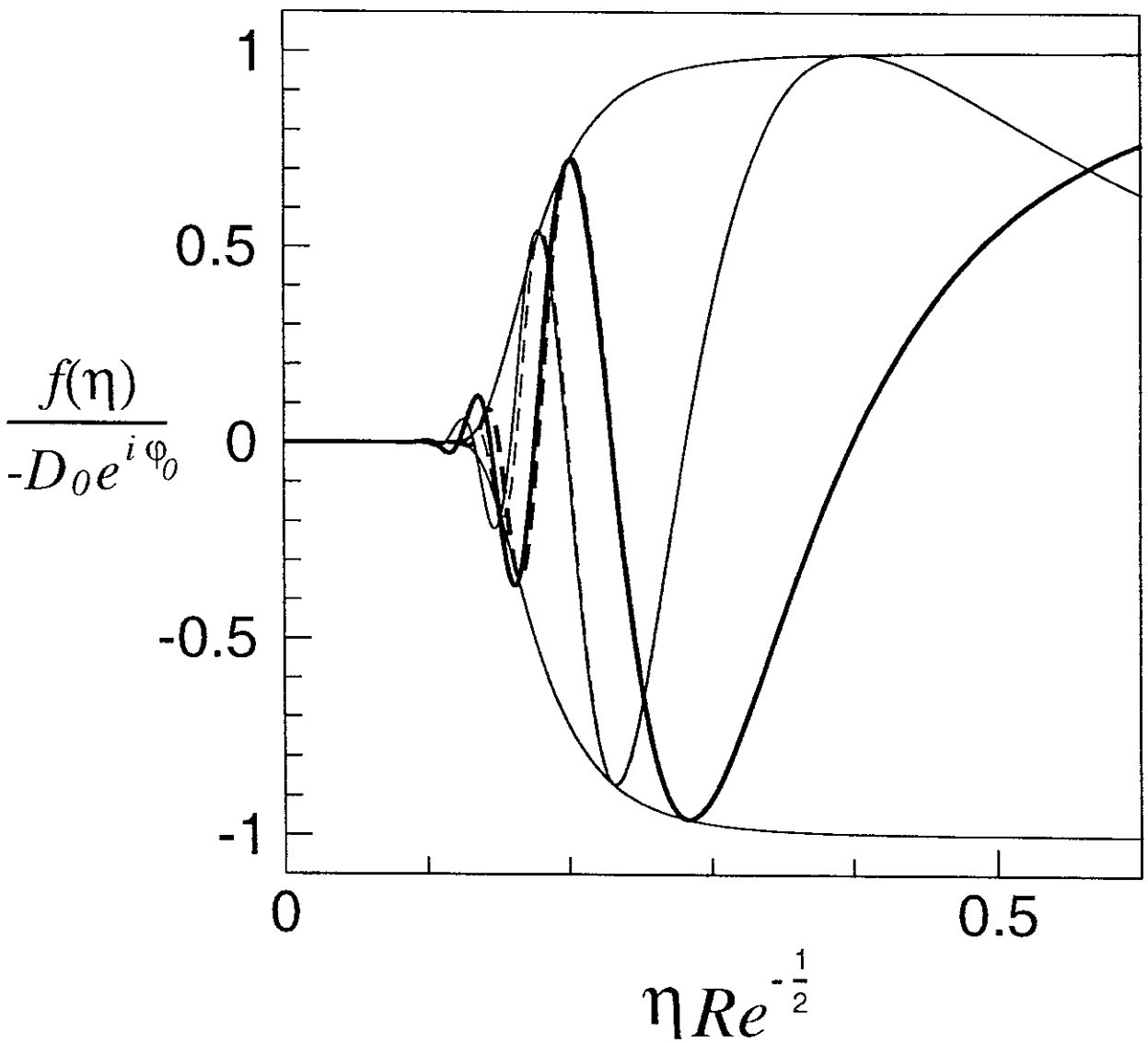

Figure 7

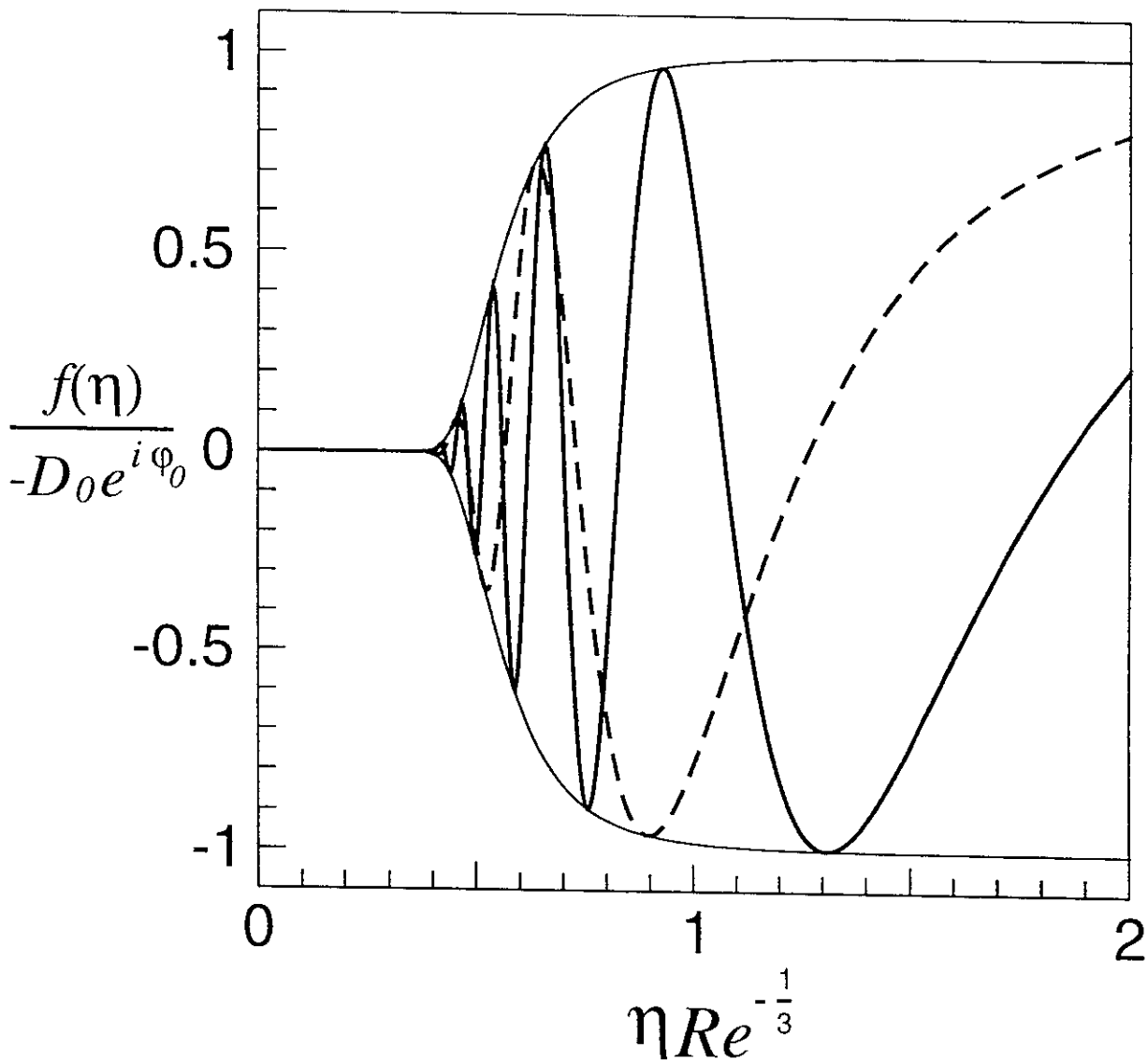

Figure 8(a)

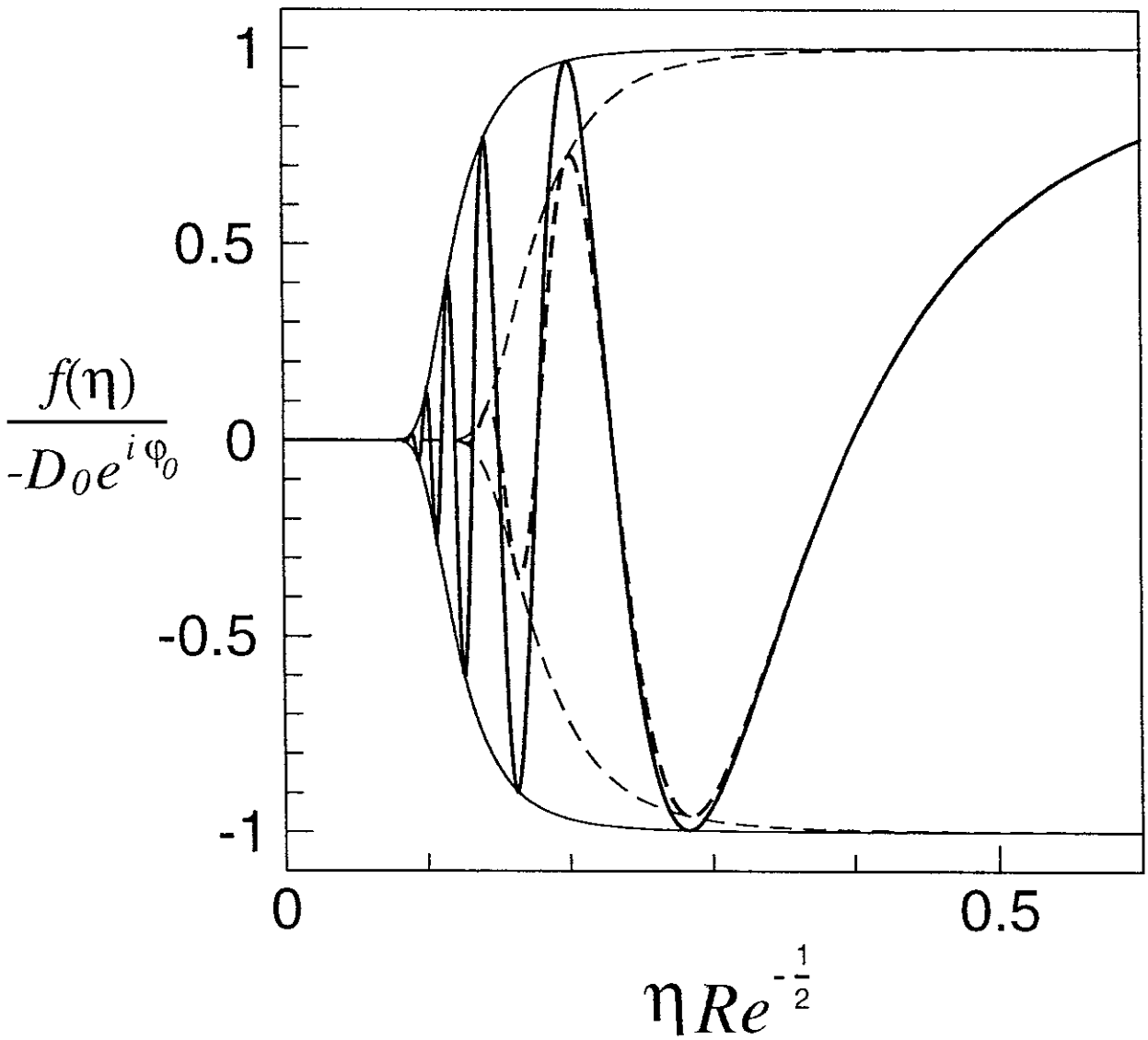

Figure 8(b)

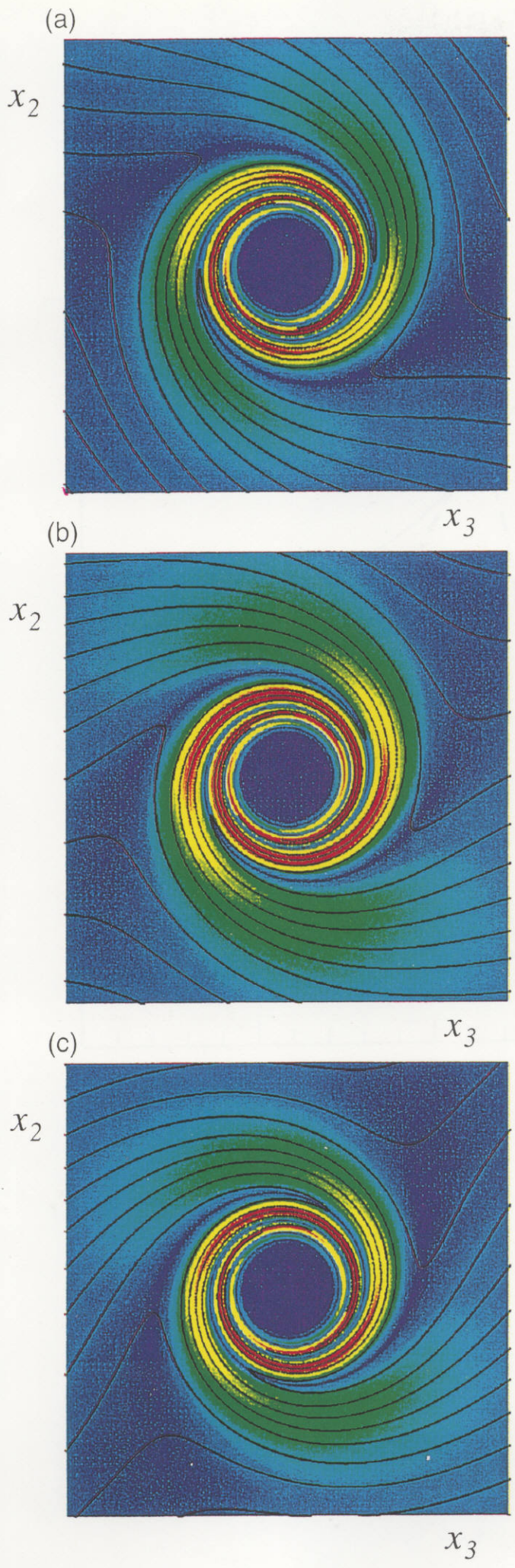

Figure 9

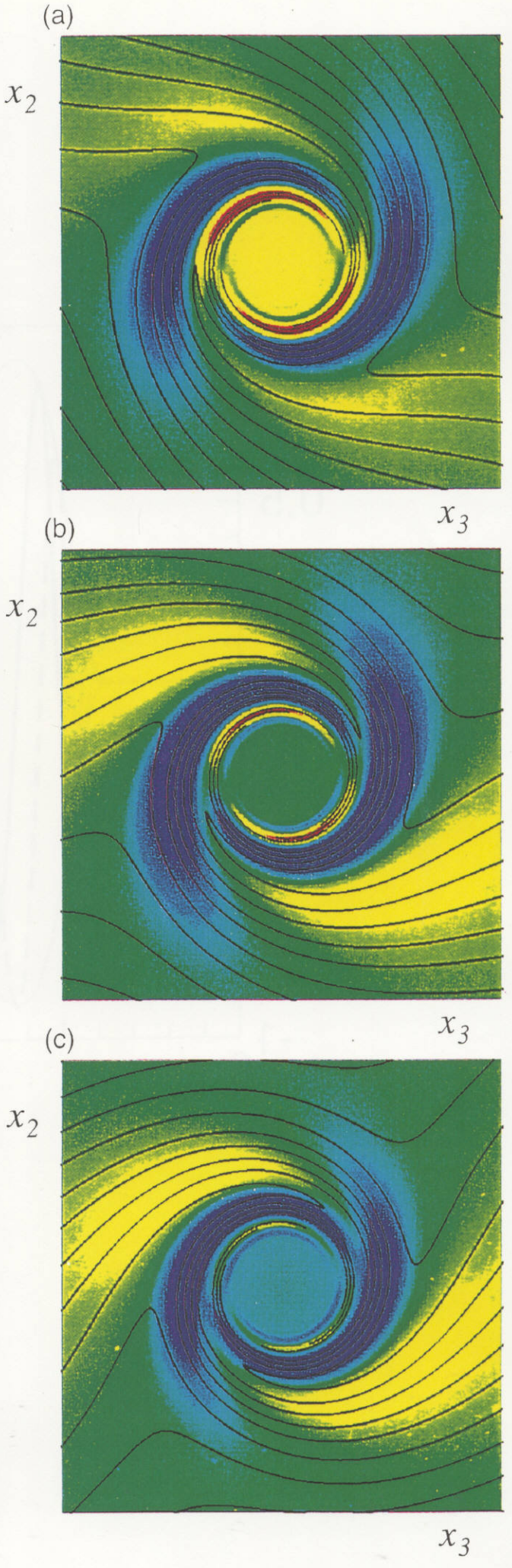

Figure 14

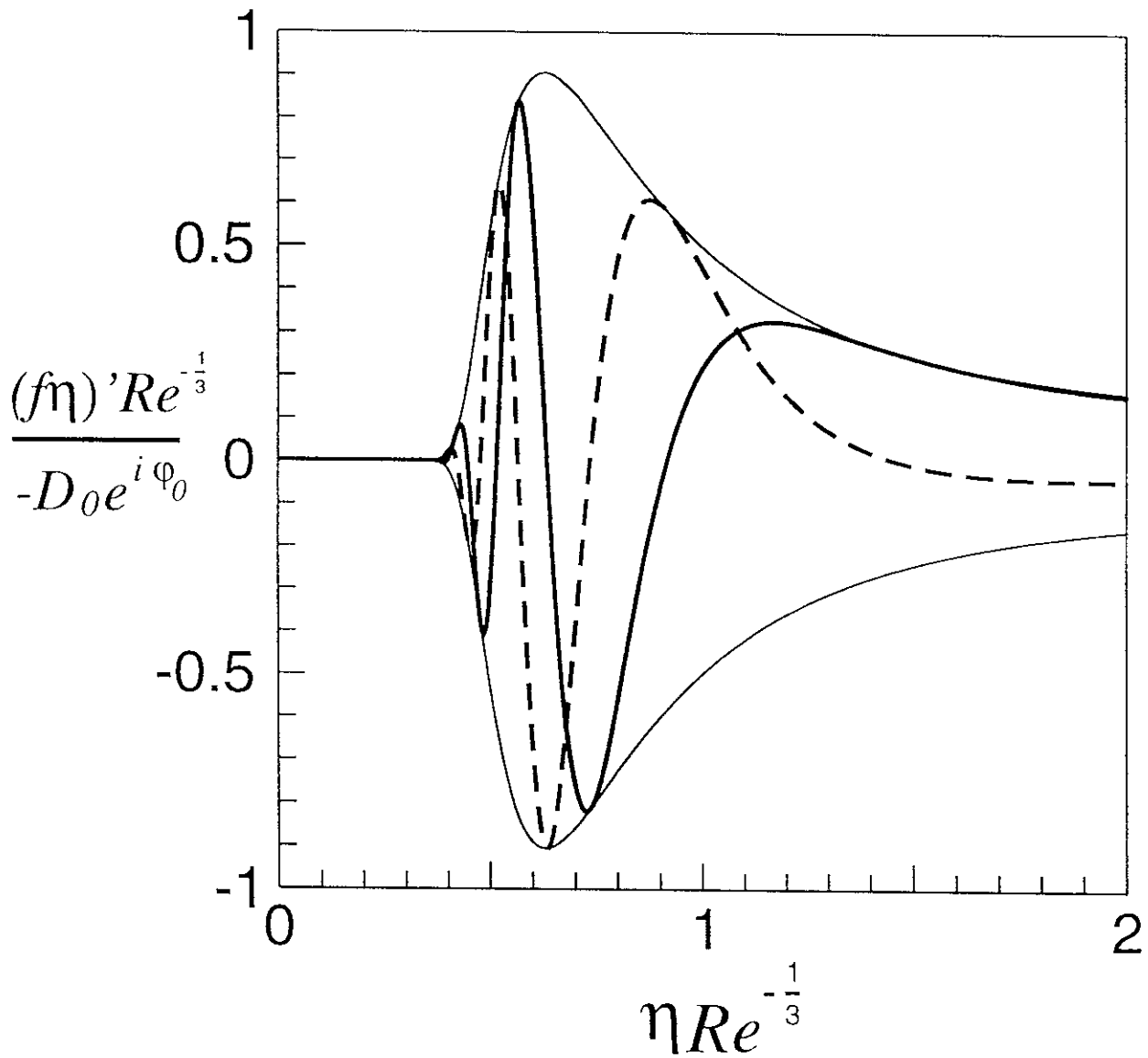

Figure 10

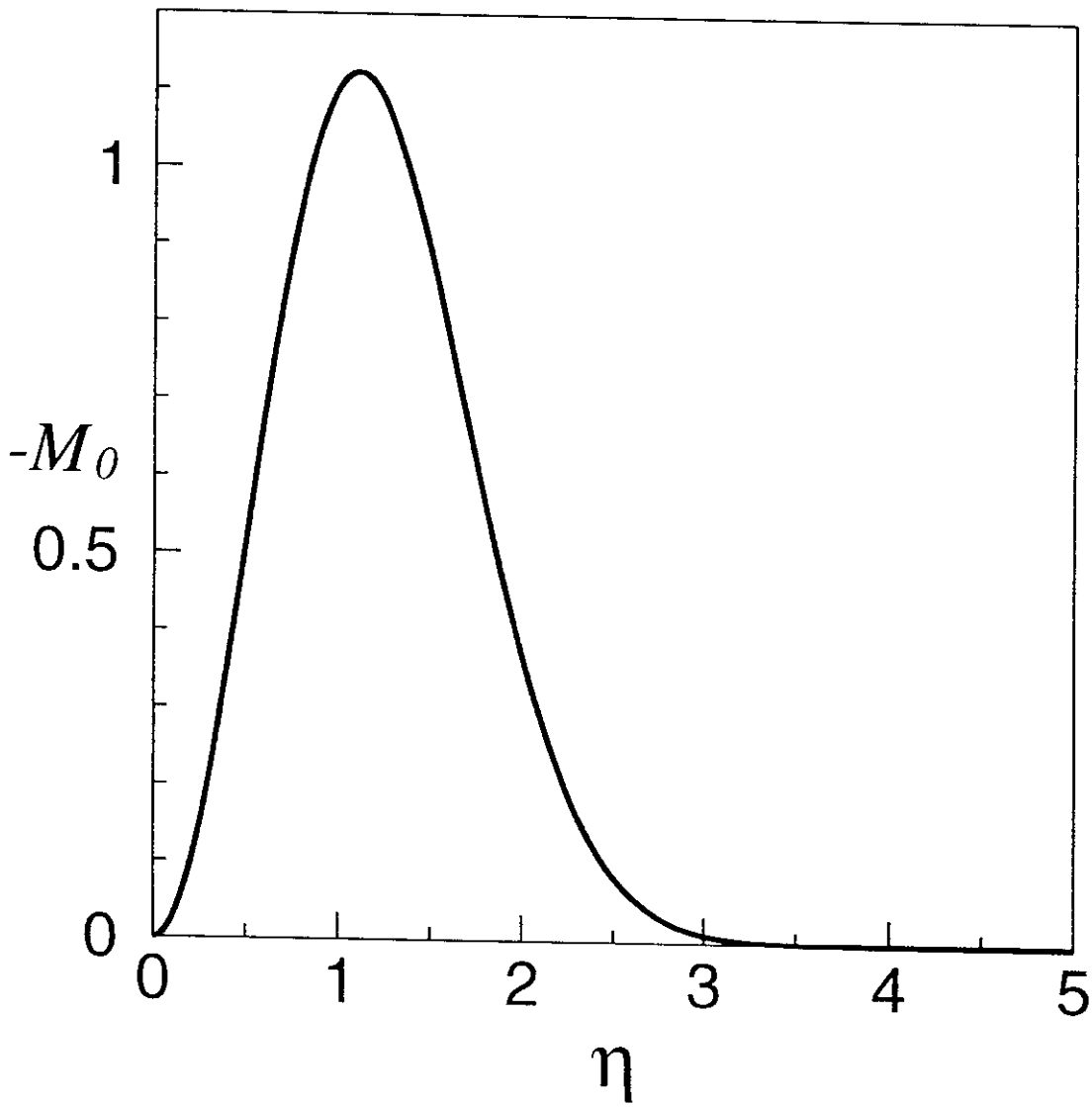

Figure 11

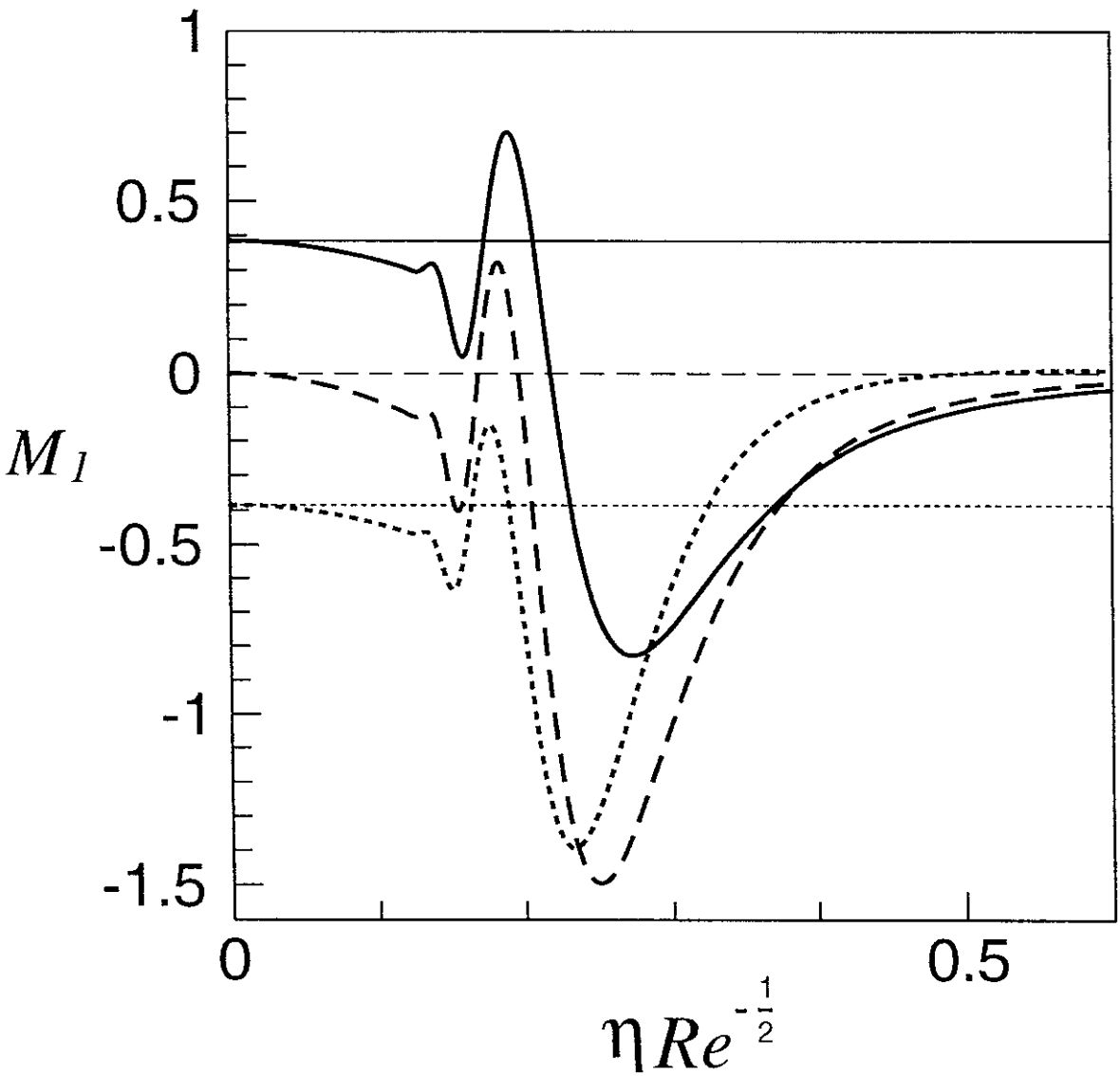

Figure 12

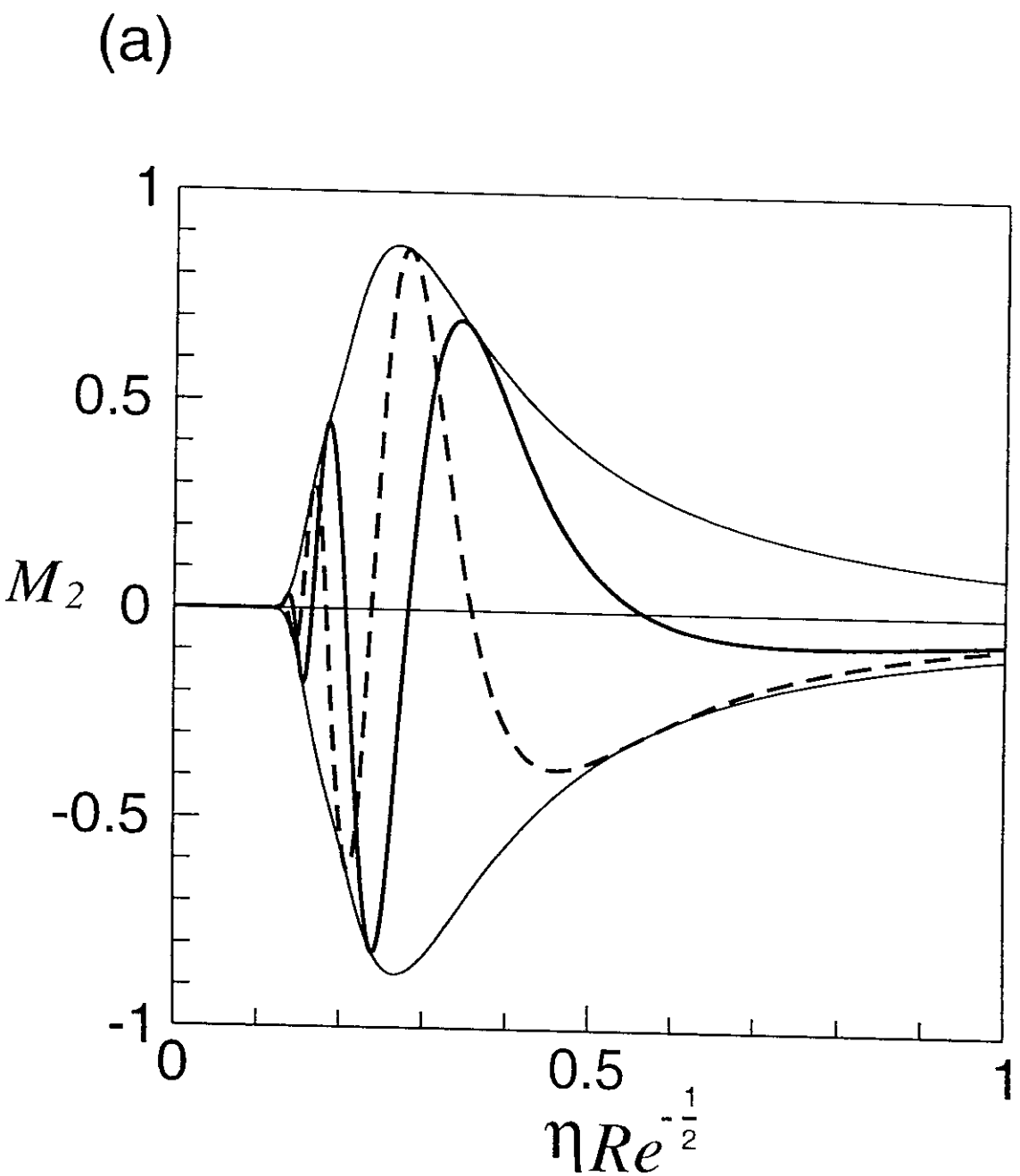

Figure 13(a)

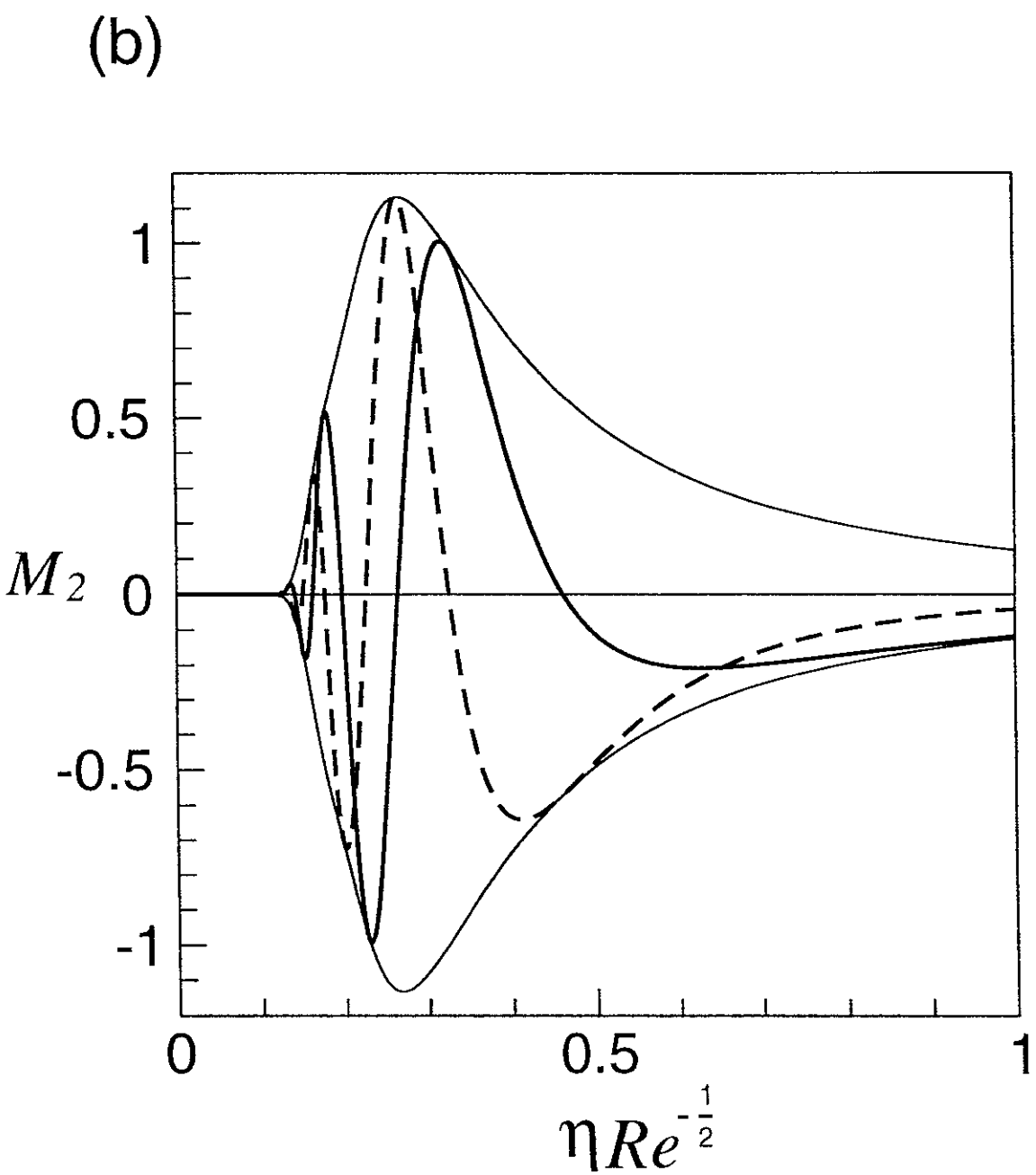

Figure 13(b)

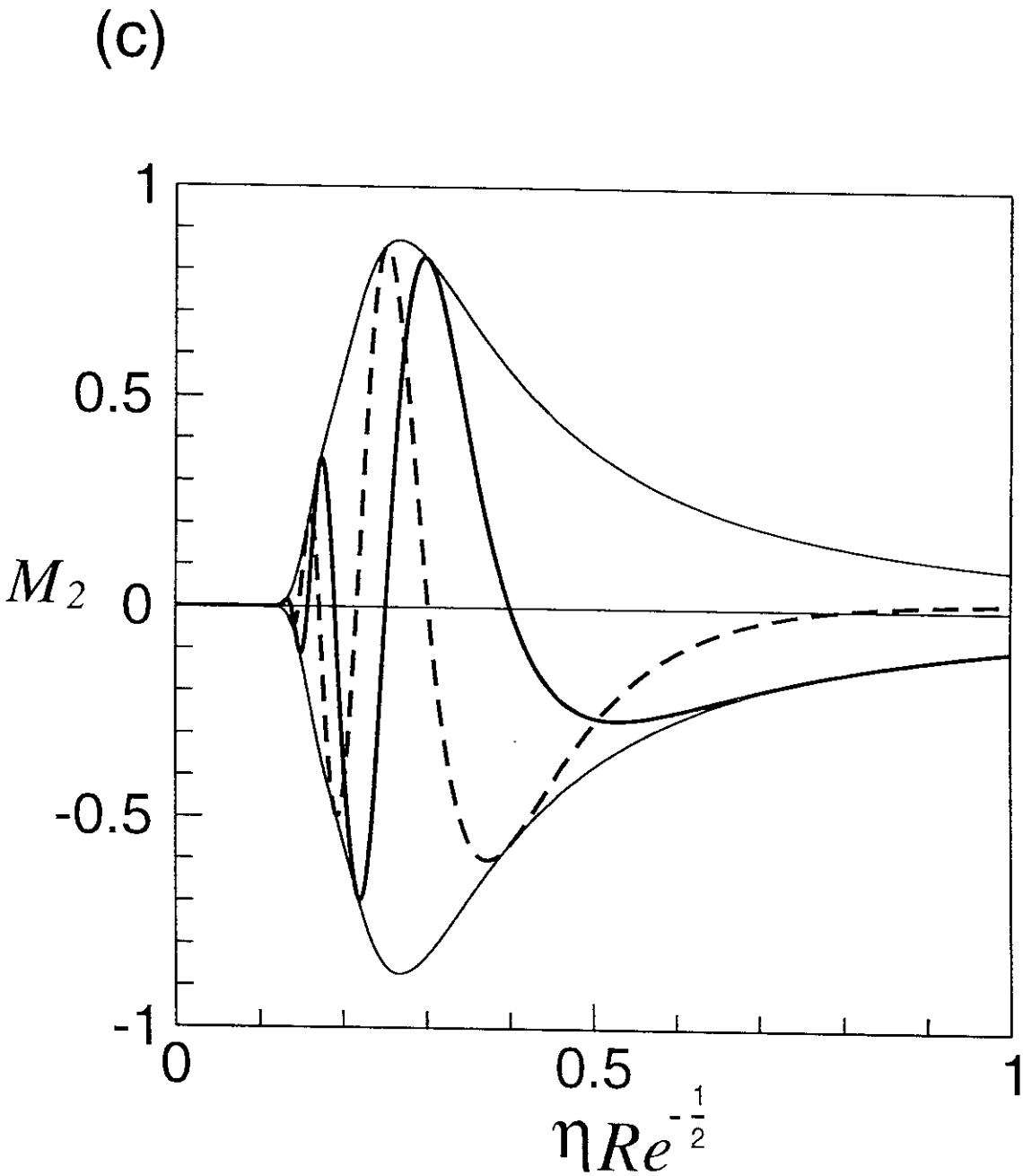

Figure 13(c)

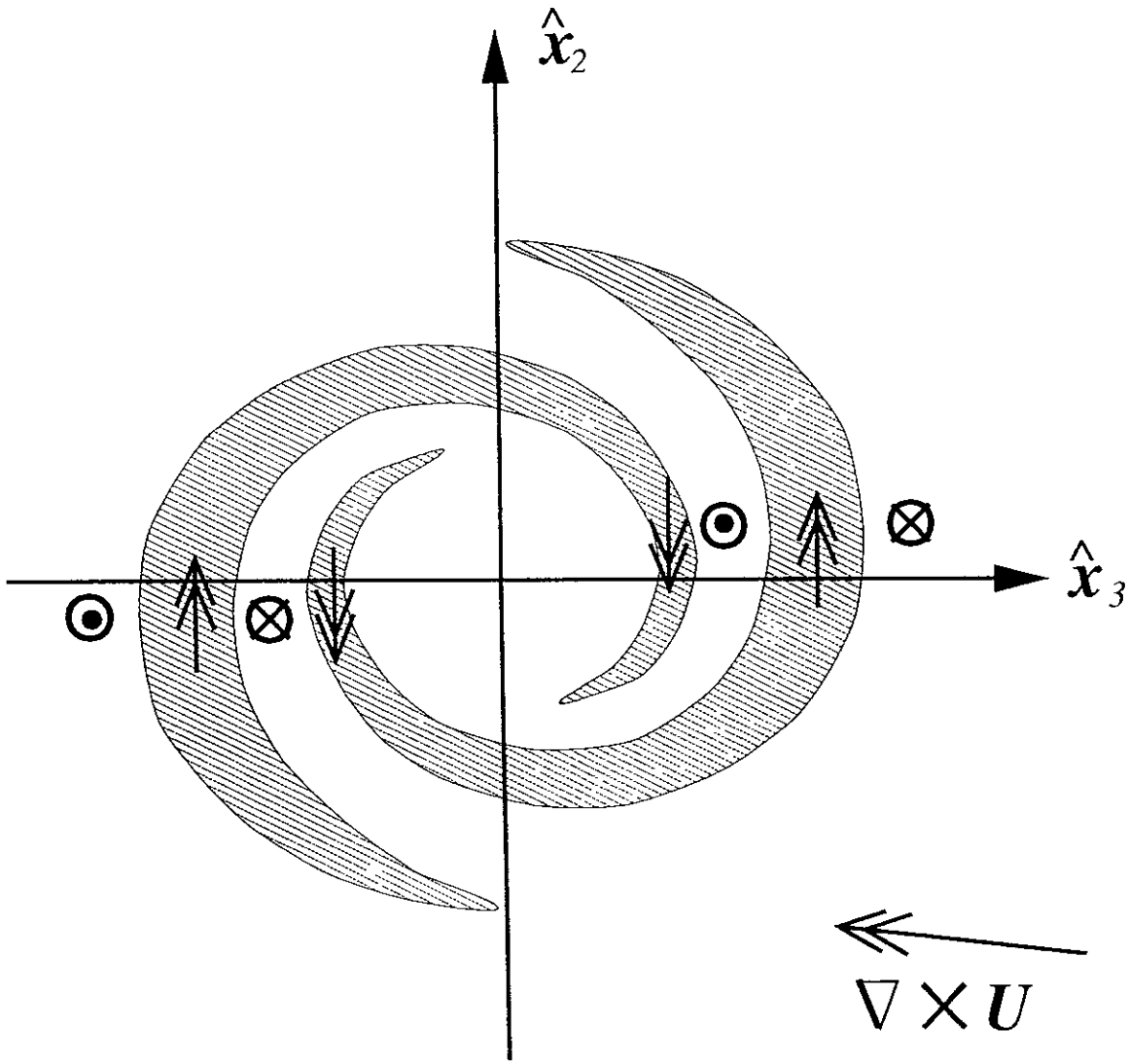

Figure 15

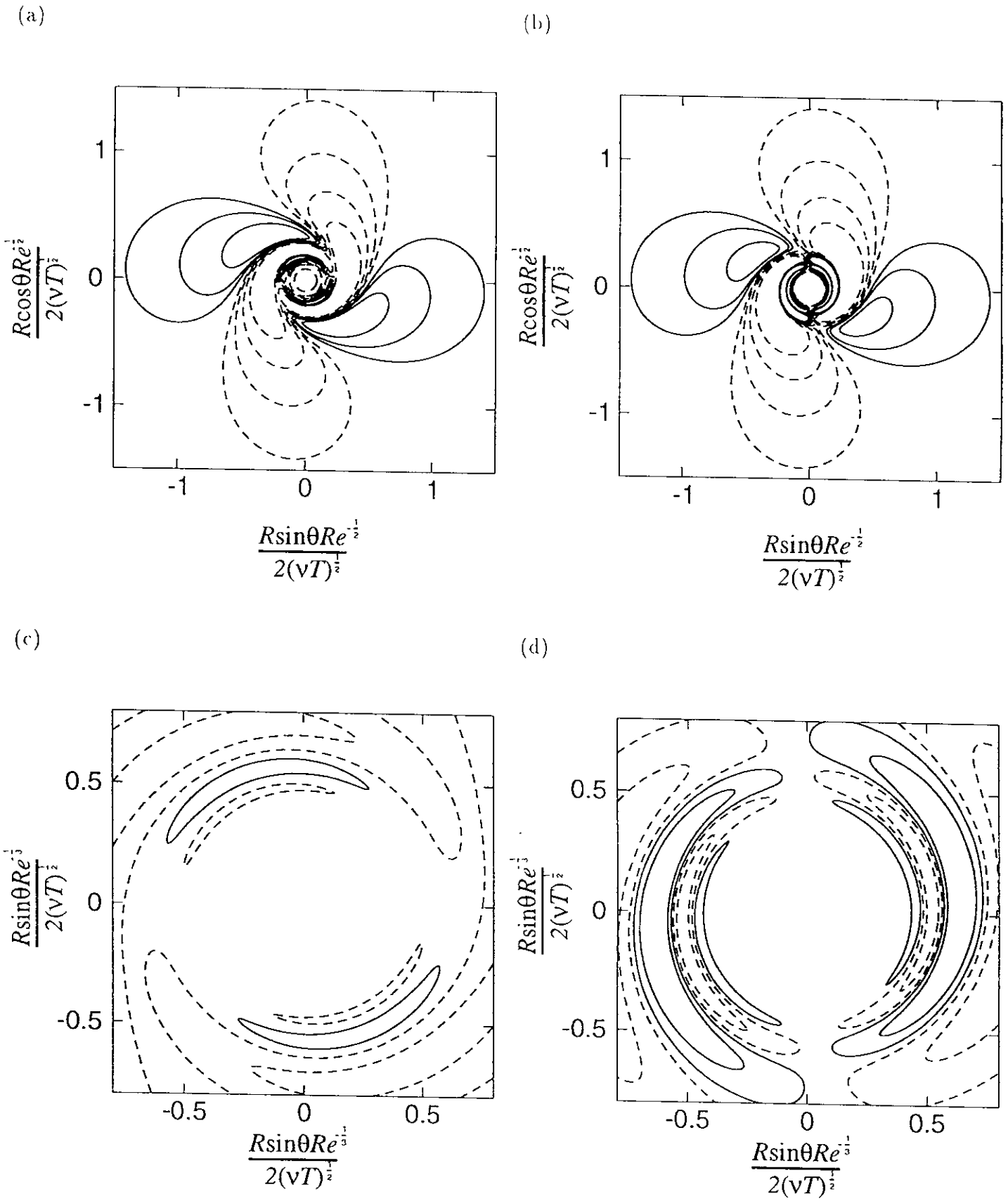
(a)
(b)
(c)
(d)
$\frac{R\cos\theta Re^{\frac{1}{2}}}{2(\nu T)^{\frac{1}{2}}}$
$\frac{R\sin\theta Re^{\frac{1}{2}}}{2(\nu T)^{\frac{1}{2}}}$
$\frac{R\sin\theta Re^{\frac{1}{3}}}{2(\nu T)^{\frac{1}{2}}}$
1
0
-1
0.5
-0.5

Figure 16

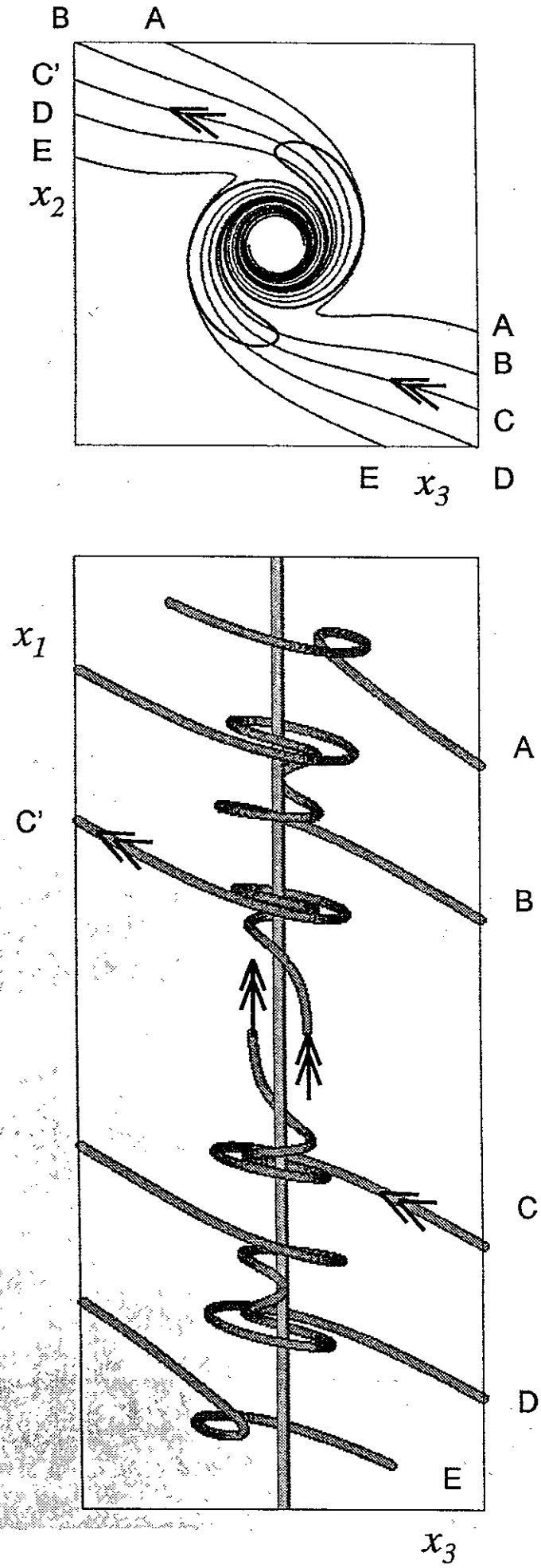

Figure 17(a)

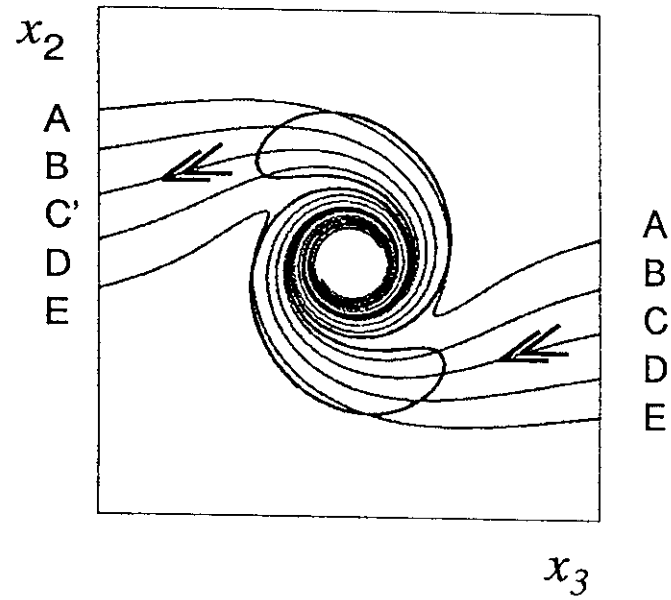

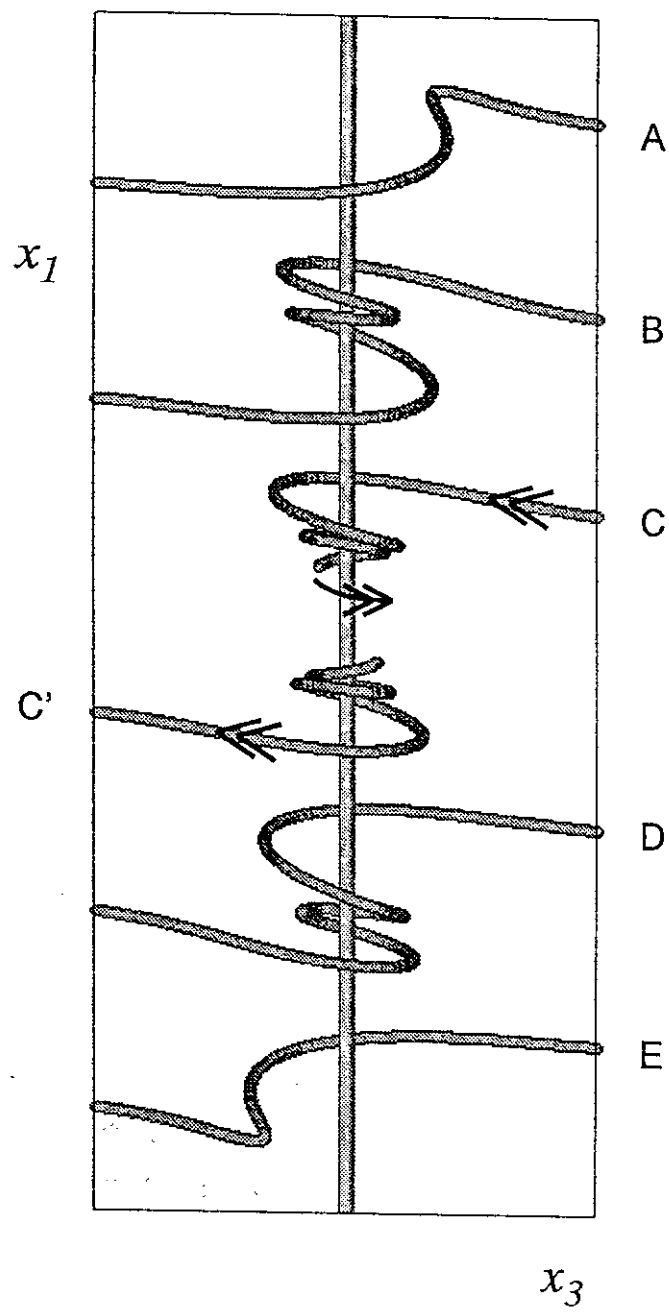

Figure 17(b)

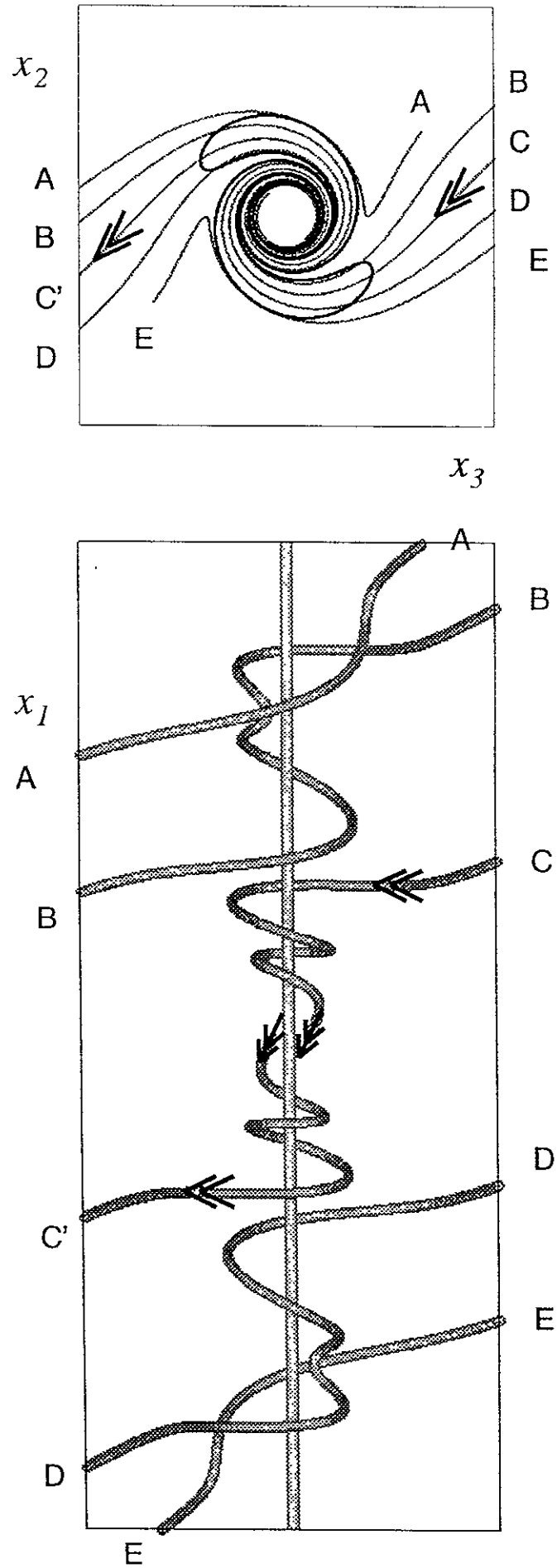

Figure 17(c)

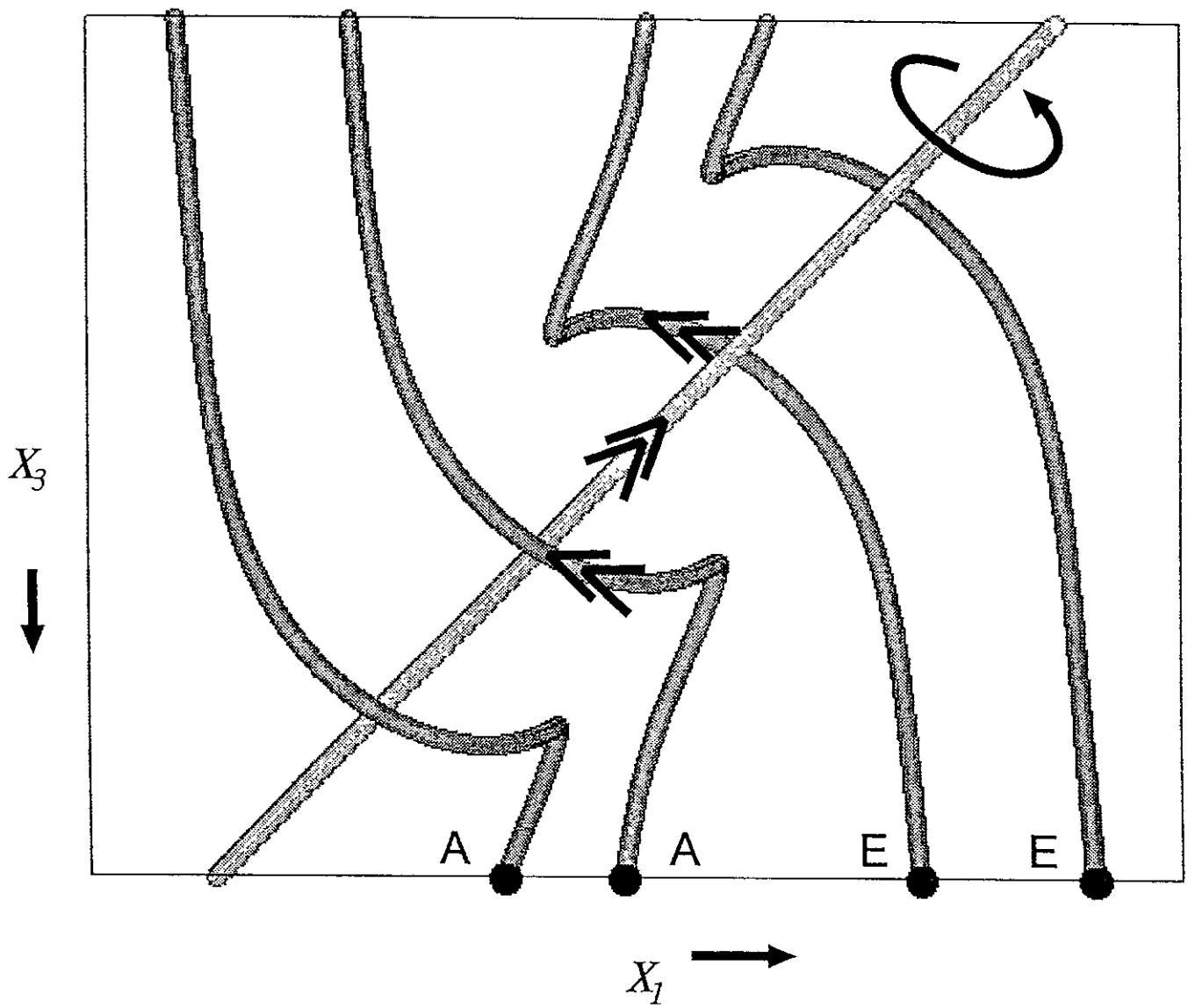

Figure 18

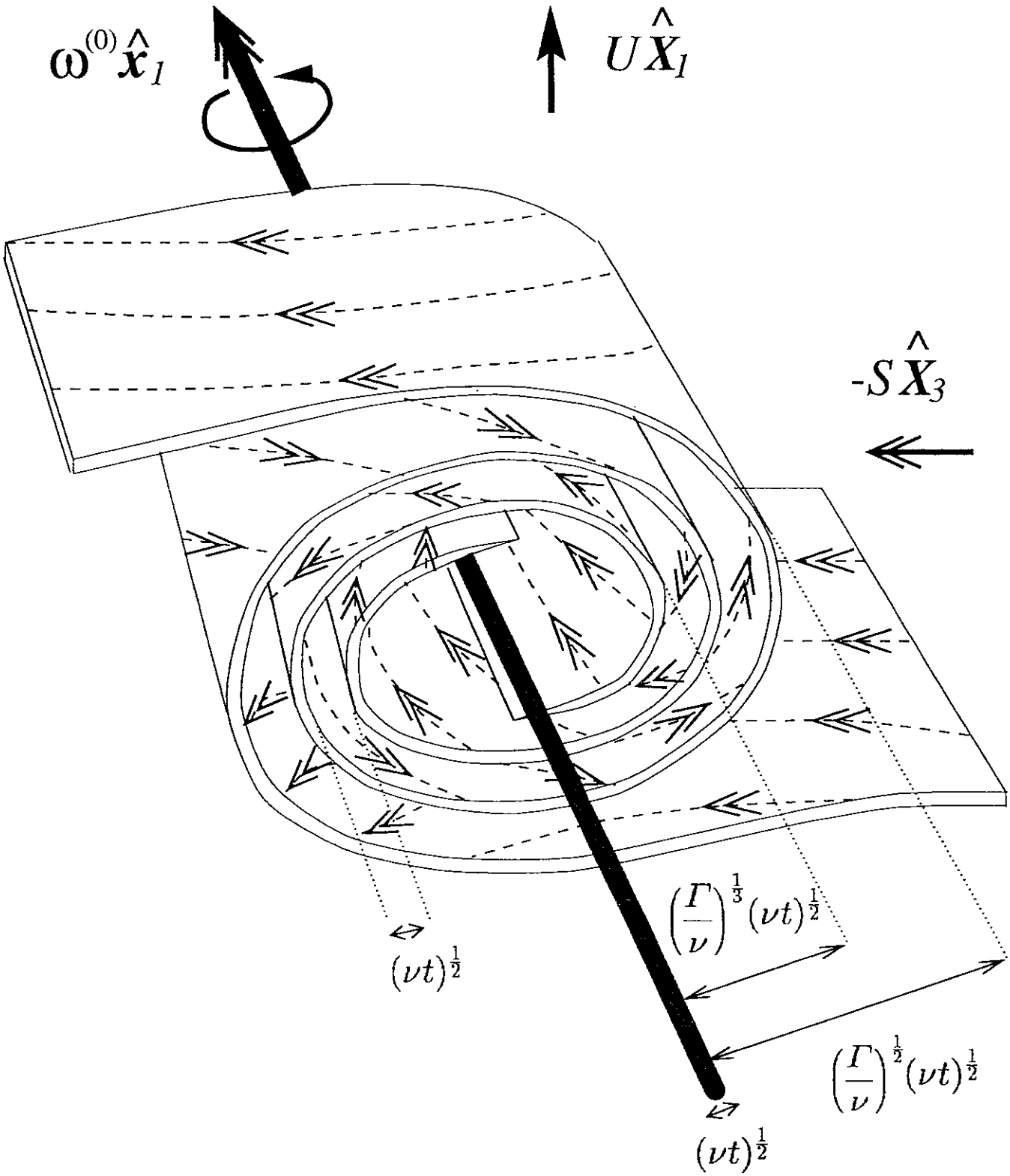
$\omega^{(0)}\hat{x}_1$
$U\hat{X}_1$
$-S\hat{X}_3$
$(\nu t)^{\frac{1}{2}}$
$\left(\frac{\Gamma}{\nu}\right)^{\frac{1}{3}}(\nu t)^{\frac{1}{2}}$
$\left(\frac{\Gamma}{\nu}\right)^{\frac{1}{2}}(\nu t)^{\frac{1}{2}}$
$(\nu t)^{\frac{1}{2}}$

Figure 19

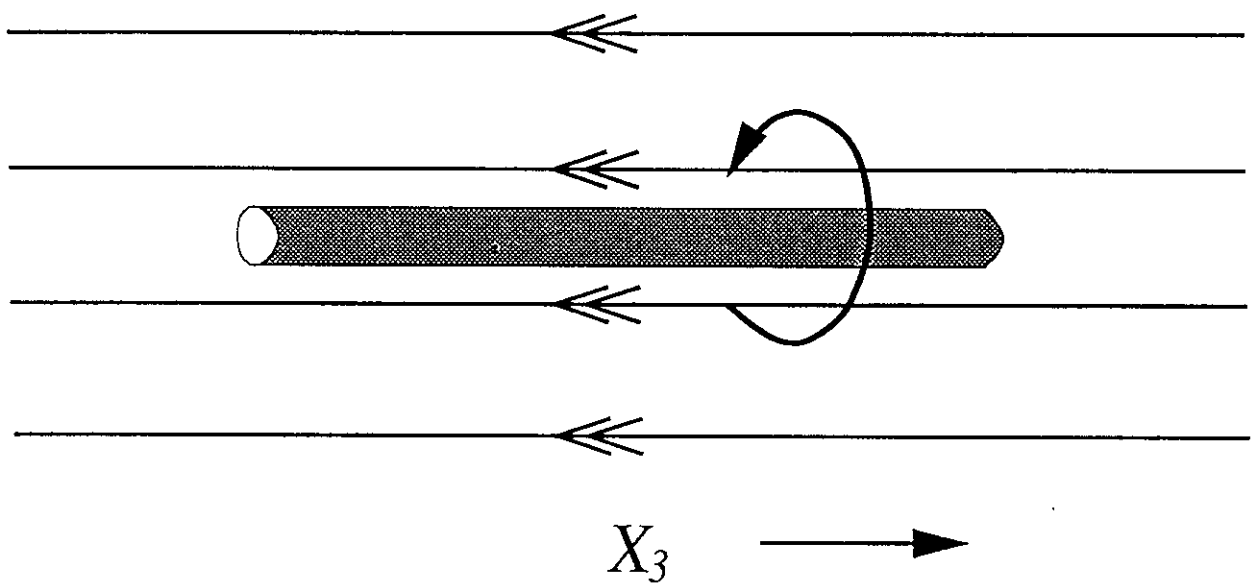

Figure 20(a)

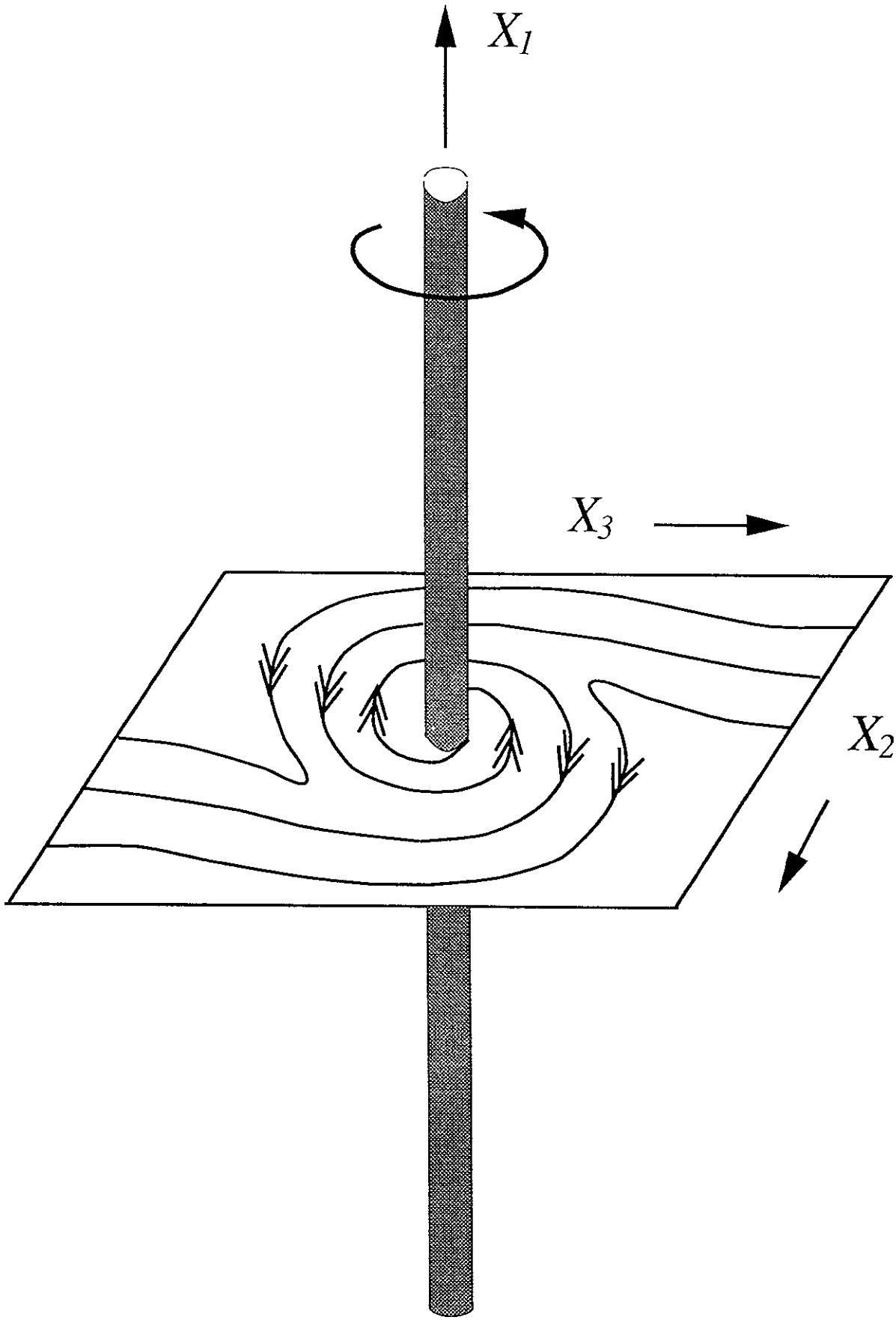

Figure 20(b)

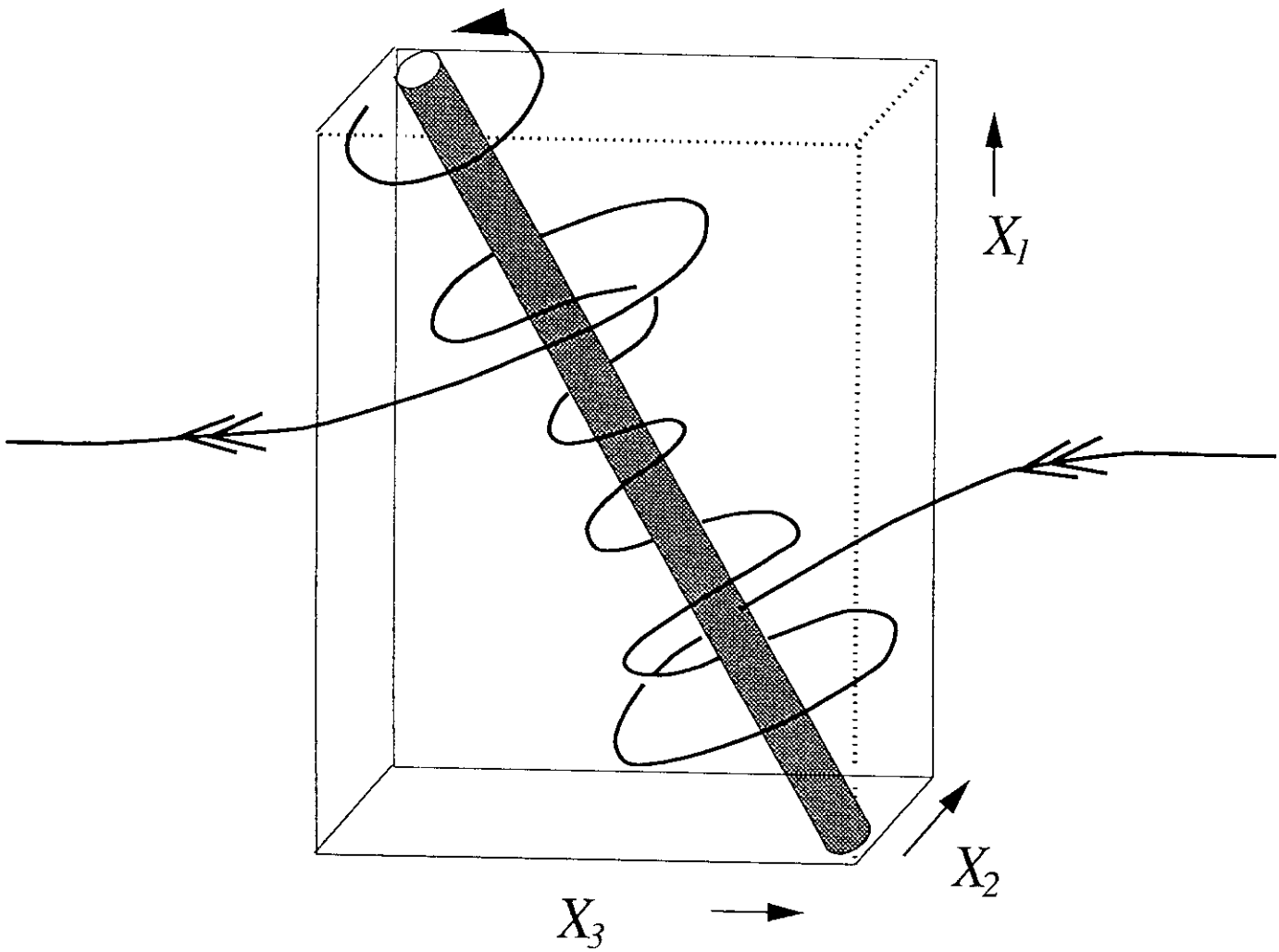

Figure 20(c)

Recent Issues of NIFS Series

NIFS-419 J. Xu, K. Toi, H. Kuramoto, A. Nishizawa, J. Fujita, A. Ejiri, K. Narihara, T. Seki, H. Sakakita, K. Kawahata, K. Ida, K. Adachi, R. Akiyama, Y. Hamada, S. Hirokura, Y. Kawasumi, M. Kojima, I. Nomura, S. Ohdachi, K.N. Sato
Measurement of Internal Magnetic Field with Motional Stark Polarimetry in Current Ramp-Up Experiments of JIPP T-IIU; June 1996

NIFS-420 Y.N. Nejoh,
Arbitrary Amplitude Ion-acoustic Waves in a Relativistic Electron-beam Plasma System; July 1996

NIFS-421 K. Kondo, K. Ida, C. Christou, V.Yu.Sergeev, K.V.Khlopenkov, S.Sudo, F. Sano, H. Zushi, T. Mizuuchi, S. Besshou, H. Okada, K. Nagasaki, K. Sakamoto, Y. Kurimoto, H. Funaba, T. Hamada, T. Kinoshita, S. Kado, Y. Kanda, T. Okamoto, M. Wakatani and T. Obiki,
Behavior of Pellet Injected Li Ions into Heliotron E Plasmas; July 1996

NIFS-422 Y. Kondoh, M. Yamaguchi and K. Yokozuka,
Simulations of Toroidal Current Drive without External Magnetic Helicity Injection; July 1996

NIFS-423 Joong-San Koog,
Development of an Imaging VUV Monochromator in Normal Incidence Region; July 1996

NIFS-424 K. Orito,
A New Technique Based on the Transformation of Variables for Nonlinear Drift and Rossby Vortices; July 1996

NIFS-425 A. Fujisawa, H. Iguchi, S. Lee, T.P. Crowley, Y. Hamada, H. Sanuki, K. Itoh, S. Kubo, H. Idei, T. Minami, K. Tanaka, K. Ida, S. Nishimura, S. Hidekuma, M. Kojima, C. Takahashi, S. Okamura and K. Matsuoka,
Direct Observation of Potential Profiles with a 200keV Heavy Ion Beam Probe and Evaluation of Loss Cone Structure in Toroidal Helical Plasmas on the Compact Helical System; July 1996

NIFS-426 H. Kitauchi, K. Araki and S. Kida,
Flow Structure of Thermal Convection in a Rotating Spherical Shell; July 1996

NIFS-427 S. Kida and S. Goto,
Lagrangian Direct-interaction Approximation for Homogeneous Isotropic Turbulence; July 1996

NIFS-428 V.Yu. Sergeev, K.V. Khlopenkov, B.V. Kuteev, S. Sudo, K. Kondo, F. Sano, H. Zushi, H. Okada, S. Besshou, T. Mizuuchi, K. Nagasaki, Y. Kurimoto and T. Obiki,

Recent Experiments on Li Pellet Injection into Heliotron E; Aug. 1996

NIFS-429 N. Noda, V. Philipps and R. Neu,
A Review of Recent Experiments on W and High Z Materials as Plasma-Facing Components in Magnetic Fusion Devices; Aug. 1996

NIFS-430 R.L. Tobler, A. Nishimura and J. Yamamoto,
Design-Relevant Mechanical Properties of 316-Type Stainless Steels for Superconducting Magnets; Aug. 1996

NIFS-431 K. Tsuzuki, M. Natsir, N. Inoue, A. Sagara, N. Noda, O. Motojima, T. Mochizuki, T. Hino and T. Yamashina,
Hydrogen Absorption Behavior into Boron Films by Glow Discharges in Hydrogen and Helium; Aug. 1996

NIFS-432 T.-H. Watanabe, T. Sato and T. Hayashi,
Magnetohydrodynamic Simulation on Co- and Counter-helicity Merging of Spheromaks and Driven Magnetic Reconnection; Aug. 1996

NIFS-433 R. Horiuchi and T. Sato,
Particle Simulation Study of Collisionless Driven Reconnection in a Sheared Magnetic Field; Aug. 1996

NIFS-434 Y. Suzuki, K. Kusano and K. Nishikawa,
Three-Dimensional Simulation Study of the Magnetohydrodynamic Relaxation Process in the Solar Corona. II.; Aug. 1996

NIFS-435 H. Sugama and W. Horton,
Transport Processes and Entropy Production in Toroidally Rotating Plasmas with Electrostatic Turbulence; Aug. 1996

NIFS-436 T. Kato, E. Rachlew-Källne, P. Hörling and K.-D Zastrow,
Observations and Modelling of Line Intensity Ratios of OV Multiplet Lines for 2s3s 3S1 - 2s3p 3Pj; Aug. 1996

NIFS-437 T. Morisaki, A. Komori, R. Akiyama, H. Idei, H. Iguchi, N. Inoue, Y. Kawai, S. Kubo, S. Masuzaki, K. Matsuoka, T. Minami, S. Morita, N. Noda, N. Ohyabu, S. Okamura, M. Osakabe, H. Suzuki, K. Tanaka, C. Takahashi, H. Yamada, I. Yamada and O. Motojima,
Experimental Study of Edge Plasma Structure in Various Discharges on Compact Helical System; Aug. 1996

NIFS-438 A. Komori, N. Ohyabu, S. Masuzaki, T. Morisaki, H. Suzuki, C. Takahashi, S. Sakakibara, K. Watanabe, T. Watanabe, T. Minami, S. Morita, K. Tanaka, S. Ohdachi, S. Kubo, N. Inoue, H. Yamada, K. Nishimura, S. Okamura, K. Matsuoka, O. Motojima, M. Fujiwara, A. Iiyoshi, C. C. Klepper, J.F. Lyon, A.C. England, D.E. Greenwood, D.K. Lee, D.R. Overbey, J.A. Rome, D.E. Schechter and C.T. Wilson,
Edge Plasma Control by a Local Island Divertor in the Compact Helical

System; Sep. 1996 (IAEA-CN-64/C1-2)

NIFS-439 K. Ida, K. Kondo, K. Nagaski T. Hamada, H. Zushi, S. Hidekuma, F. Sano, T Mizuuchi, H. Okada, S. Besshou, H. Funaba, Y. Kurimoto, K. Watanabe and T. Obiki,
Dynamics of Ion Temperature in Heliotron-E; Sep. 1996 (IAEA-CN-64/CP-5)

NIFS-440 S. Morita, H. Idei, H. Iguchi, S. Kubo, K. Matsuoka, T. Minami, S. Okamura, T. Ozaki, K. Tanaka, K. Toi, R. Akiyama, A. Ejiri, A. Fujisawa, M. Fujiwara, M. Goto, K. Ida, N. Inoue, A. Komori, R. Kumazawa, S. Masuzaki, T. Morisaki, S. Muto, K. Narihara, K. Nishimura, I. Nomura, S. Ohdachi, M.. Osakabe, A. Sagara, Y. Shirai, H. Suzuki, C. Takahashi, K. Tsumori, T. Watari, H. Yamada and I. Yamada,
A Study on Density Profile and Density Limit of NBI Plasmas in CHS; Sep. 1996 (IAEA-CN-64/CP-3)

NIFS-441 O. Kaneko, Y. Takeiri, K. Tsumori, Y. Oka, M. Osakabe, R. Akiyama, T. Kawamoto, E. Asano and T. Kuroda,
Development of Negative-Ion-Based Neutral Beam Injector for the Large Helical Device; Sep. 1996 (IAEA-CN-64/GP-9)

NIFS-442 K. Toi, K.N. Sato, Y. Hamada, S. Ohdachi, H. Sakakita, A. Nishizawa, A. Ejiri, K. Narihara, H. Kuramoto, Y. Kawasumi, S. Kubo, T. Seki, K. Kitachi, J. Xu, K. Ida, K. Kawahata, I. Nomura, K. Adachi, R. Akiyama, A. Fujisawa, J. Fujita, N. Hiraki, S. Hidekuma, S. Hirokura, H. Idei, T. Ido, H. Iguchi, K. Iwasaki, M. Isobe, O. Kaneko, Y. Kano, M. Kojima, J. Koog, R. Kumazawa, T. Kuroda, J. Li, R. Liang, T. Minami, S. Morita, K. Ohkubo, Y. Oka, S. Okajima, M. Osakabe, Y. Sakawa, M. Sasao, K. Sato, T. Shimpo, T. Shoji, H. Sugai, T. Watari, I. Yamada and K. Yamauti,
Studies of Perturbative Plasma Transport, Ice Pellet Ablation and Sawtooth Phenomena in the JIPP T-IIU Tokamak; Sep. 1996 (IAEA-CN-64/A6-5)

NIFS-443 Y. Todo, T. Sato and The Complexity Simulation Group,
Vlasov-MHD and Particle-MHD Simulations of the Toroidal Alfvén Eigenmode; Sep. 1996 (IAEA-CN-64/D2-3)

NIFS-444 A. Fujisawa, S. Kubo, H. Iguchi, H. Idei, T. Minami, H. Sanuki, K. Itoh, S. Okamura, K. Matsuoka, K. Tanaka, S. Lee, M. Kojima, T.P. Crowley, Y. Hamada, M. Iwase, H. Nagasaki, H. Suzuki, N. Inoue, R. Akiyama, M. Osakabe, S. Morita, C. Takahashi, S. Muto, A. Ejiri, K. Ida, S. Nishimura, K. Narihara, I. Yamada, K. Toi, S. Ohdachi, T. Ozaki, A. Komori, K. Nishimura, S. Hidekuma, K. Ohkubo, D.A. Rasmussen, J.B. Wilgen, M. Murakami, T. Watari and M. Fujiwara,
An Experimental Study of Plasma Confinement and Heating Efficiency through the Potential Profile Measurements with a Heavy Ion Beam Probe in the Compact Helical System; Sep. 1996 (IAEA-CN-64/C1-5)

NIFS-445 O. Motojima, N. Yanagi, S. Imagawa, K. Takahata, S. Yamada, A. Iwamoto, H. Chikaraishi, S. Kitagawa, R. Maekawa, S. Masuzaki, T. Mito, T. Morisaki, A.

Nishimura, S. Sakakibara, S. Satoh, T. Satow, H. Tamura, S. Tanahashi, K. Watanabe, S. Yamaguchi, J. Yamamoto, M.Fujiwara and A. Iiyoshi, *Superconducting Magnet Design and Construction of LHD*; Sep. 1996 (IAEA-CN-64/G2-4)

NIFS-446 S. Murakami, N. Nakajima, S. Okamura, M. Okamoto and U. Gasparino, Orbit Effects of Energetic Particles on the Reachable β–Value and the Radial Electric Field in NBI and ECR Heated Heliotron Plasmas; Sep. 1996 (IAEA-CN-64/CP -6) Sep. 1996

NIFS-447 K. Yamazaki, A. Sagara, O. Motojima, M. Fujiwara, T. Amano, H. Chikaraishi, S. Imagawa, T. Muroga, N. Noda, N. Ohyabu, T. Satow, J.F. Wang, K.Y. Watanabe, J. Yamamoto , H. Yamanishi, A. Kohyama, H. Matsui, O. Mitarai, T. Noda, A.A. Shishkin, S. Tanaka and T. Terai
Design Assessment of Heliotron Reactor; Sep. 1996 (IAEA-CN-64/G1-5)

NIFS-448 M. Ozaki, T. Sato and the Complexity Simulation Group,
Interactions of Convecting Magnetic Loops and Arcades; Sep. 1996

NIFS-449 T. Aoki,
Interpolated Differential Operator (IDO) Scheme for Solving Partial Differential Equations; Sep. 1996

NIFS-450 D. Biskamp and T. Sato,
Partial Reconnection in the Sawtooth Collapse; Sep. 1996

NIFS-451 J. Li, X. Gong, L. Luo, F.X. Yin, N. Noda, B. Wan, W. Xu, X. Gao, F. Yin, J.G. Jiang, Z. Wu., J.Y. Zhao, M. Wu, S. Liu and Y. Han,
Effects of High Z Probe on Plasma Behavior in HT-6M Tokamak; Sep. 1996

NIFS-452 N. Nakajima, K. Ichiguchi, M. Okamoto and R.L. Dewar,
Ballooning Modes in Heliotrons/Torsatrons; Sep. 1996 (IAEA-CN-64/D3-6)

NIFS-453 A. Iiyoshi,
Overview of Helical Systems; Sep. 1996 (IAEA-CN-64/O1-7)

NIFS-454 S. Saito. Y. Nomura, K. Hirose and Y.H. Ichikawa,
Separatrix Reconnection and Periodic Orbit Annihilation in the Harper Map; Oct. 1996

NIFS-455 K. Ichiguchi, N. Nakajima and M. Okamoto,
Topics on MHD Equilibrium and Stability in Heliotron / Torsatron; Oct. 1996

NIFS-456 G. Kawahara, S. Kida, M. Tanaka and S. Yanase,
Wrap, Tilt and Stretch of Vorticity Lines around a Strong Straight Vortex Tube in a Simple Shear Flow; Oct. 1996